5-2011

MULTI-SCALE MODELING OF THE FONTAN CIRCULATION USING A MOCK CIRCULATORY SYSTEM

John Chiulli
Clemson University, john.chiulli@gmail.com

MULTI-SCALE MODELING OF THE FONTAN CIRCULATION USING A MOCK CIRCULATORY SYSTEM

A Thesis
Presented to
the Graduate School of
Clemson University

In Partial Fulfillment
of the Requirements for the Degree
Master of Science
Mechanical Engineering

---

by
John Andrew Chiulli
May 2011

Accepted by:
Dr. Richard Figliola, Committee Chair
Dr. Donald Beasley
Dr. Yong Huang

ABSTRACT

The Fontan circulation is the result of a series of operations performed to save the lives of children born with univentricular circulations. The Fontan procedure achieves venous return to the pulmonary circulation without a ventricular power source. The load on the heart is reduced to normal, and these patients can lead a normal life into adulthood, although late complications continue to prevent normal lifespan. A unique feature of the Fontan circulation is the dependency of inferior vena cava flow on respiration. The Fontan circulation has been modeled experimentally using an adjustable mock circulatory system, which for the first time includes the influence of respiration. A multi-scale model based on a realistic, 3D patient-specific test section coupled with a lumped parameter model tuned to patient-specific parameters is used to simulate the pressure and flow found in the Fontan circulation. For the first time, the clinically observed respiratory effects in TCPC venous physiology were successfully simulated in an experimental model, where venous flow increased during inspiration and decreased during expiration. Clinically observed hepatic vein flow reversal was also seen in the model. This reverse flow was accentuated when the pulmonary vascular resistance was increased on the venous side.

ACKNOWLEDGMENTS

I would like to gratefully acknowledge support from the Leducq Foundation and NIH Grant HL083975, who funded this research. I am also very grateful for the guidance of Dr. Figliola, Dr. Beasley, and Dr. Huang on this project. I would especially like to acknowledge Dr. Figliola for his knowledge and wisdom, and his willingness to help. He was an invaluable resource to me during this project. I also want to thank Dr. Figliola for seeking funding for such an interesting project, for choosing me to work on it, and for giving me the opportunity to be a research assistant. I want to thank Dr. Tim Conover, who was always there to answer my questions, to help me troubleshoot my system, and to give me further insight into my own project. I gratefully acknowledge research team members John Porcher, Sharmad Joshi, Tiffany Camp, Yan Zhao, Zhenyu Xue, and maybe even Ben Grier for their help to me during this project. I want to also thank Michael Justice, Jamie Cole, and Stephen Bass for their tremendous help in building this system.

The work presented here would not have been possible without the love and support of my family. Specifically, I want to thank my parents Rick and Kathy for their continuous encouragement and advice to me on this project. I would not have made it this far without them. I would like to thank my fiancée Nicole Griffin for her love and encouragement during my time here. Her positive energy and outlook helped sustain me countless times and I thank her sincerely for that. I would like to thank my brother and sister Stephanie and Michael for the love they demonstrated towards me during my time

here. I want to thank Stephanie for her guidance and wisdom, and Michael for his encouragement and support. I want to thank Ginger and Zoe also for their self-assured, if not dogmatic, inputs to my research. I love each of you dearly.

TABLE OF CONTENTS

Page

Table of Contents (Continued) Page

LIST OF TABLES

LIST OF FIGURES

List of Figures (Continued)

List of Figures (Continued)

CHAPTER ONE

INTRODUCTION

Background on the Fontan Circulation

As early as the 18th century, efforts have been made on the part of scientists to understand the workings of the mechanism inside each of us that delivers oxygen to our cells and keeps us breathing: the human circulatory system. It goes without saying that the main supply of energy to the system is the heart, which pumps our blood through the arteries and veins throughout the body. However, achieving a more detailed description of this system has been the subject of scientific and medical research for the past two centuries.

A major early contributor to these efforts was Reverend Stephen Hales, who emphasized the property of elasticity within the cardiovascular system – namely the vascular tree (Slife et al., 1990). He believed that the arterial system would distend under pressure waves from the heart, and that the arterial system behaved like a large, distensible reservoir. This reservoir would exhibit elasticity, or compliance, within the arterial tree. Later, German literature began calling these reservoirs "windkessels", meaning "air chambers" (Slife et al., 1990). There are numerous reasons why this continues to be a region of emphasis in engineering research, including a better understanding of the effects of congenital heart defects and of the surgical options that exist to extend and improve the quality of the lives of patients.

In a normal human biventricular circulation, the systemic (body serving) and pulmonary (lung serving) circulations are connected in a series configuration (Gewillig et al., 2005). The red blood, rich in oxygen, is pumped from the left ventricle and through the aorta. The aorta branches many times into smaller and smaller arteries until the arteries reach cellular size. At this stage, oxygen is delivered to the cells in the capillary beds. The deoxygenated blue blood exits through similarly small veins, which then converge into larger veins. These veins continue to converge until only two great veins, the superior vena cava and inferior vena cava, remain. The superior vena cava carries deoxygenated blood from the upper body, accounting for 30% of the total blood flow in adults with much higher ratios in small children. The inferior vena cava carries deoxygenated blood from the lower body, accounting for the remaining 70% in adults, with lower proportions in small children. In a biventricular circulation, this blood will enter the right atrium, pass through the tricuspid valve, and enter into the right ventricle. From the right ventricle, the blood is pumped through the pulmonary valve and into the pulmonary artery, which delivers the deoxygenated blood into the lungs. The pulmonary artery divides into a left and right artery, with each serving a lung. At this stage, oxygen is delivered to the blood through another capillary system and the blood is returned via two pulmonary veins. The blood, now red and oxygenated, flows back towards the heart and into the left atrium. From this point, the blood flows through the mitral valve and into the left ventricle where the process is repeated. The typical biventricular human circulation has been studied and is well understood at this point. What is not as well

understood is the atypical univentricular circulation: one in which only one functional ventricle exists.

A small fraction of infants are born with defects that result in a univentricular circulation, where only one functional ventricle exists in the heart to act as a pump. These defects are different from case-to-case but all imply that one ventricle must pump blood to both the systemic and pulmonary circulations (de Leval et al., 2005). In this case, the systemic and pulmonary circulations are connected in parallel, rather than in series. This has major disadvantages, including arterial desaturation of the blood, and chronic volume overload to the single ventricle (Gewillig et al., 2005). The desaturation is a result of the blue blood from the systemic veins mixing with the red blood from the pulmonary veins. Lower oxygen content in the blood results, requiring more work output by the heart to deliver the same amount of oxygen to the body. Chronic volume overload to the single ventricle results from fact that the ventricle must pump to two circulations, rather than one. This chronic volume overload can be tolerated initially, but will eventually impair ventricular function by the time the patient reaches his/her 30's.

As early as the 1940's, it was observed that the arterial pressure in fish, amphibians, reptiles, birds, and most importantly to us, mammals, was sufficiently great enough such that the force to supply blood to the lungs could be adequately provided by residual venous pressure (de Leval et al., 2005). In 1971, Francis Fontan performed a new operation to re-route the blood flow of the vena cavae to the pulmonary circulation directly in patients with tricuspid atresia (Fontan et al., 1971). This in turn, would bypass the right atrium and return only oxygenated blood to the left heart. A major result of the

Fontan operation is that the pulmonary and systemic circulations are once again connected in series. This has some advantages, including better oxygen saturation and decreased load on the ventricle. Also, the post-capillary mechanical energy is not wasted, but instead used to drive the flow through the pulmonary circulation. There are downsides to this arrangement, however. The chief negative result of the Fontan operation is chronic hypertension in the systemic veins (Gewillig et al., 2005). Typical caval pressures in a biventricular circulation are less than 10 mmHg, this can be much higher in the Fontan circulation (de Leval et al., 2005). The lack of a pump downstream of the systemic veins elevates these pressures. This decreases cardiac output, as the ventricle must now pump against both the systemic and pulmonary resistances in series. Lower pulmonary venous pressure impairs ventricular filling, also reducing cardiac output.

When a patient is being considered for the Fontan operation, there are several criteria taken into account. In 1978, Choussat and Fontan described their recommendations for candidates of the Fontan operation: the patient must have good cardiac output at an acceptable systemic venous pressure (Gewillig et al., 2005). These rules have since been expanded upon, as further insight has been gained. The ideal candidate for the Fontan operation has unobstructed ventricular flow, and good ventricular function. There must be good-sized pulmonary arteries such that the resistance is not too high in the pulmonary circuit. There must also not be any obstruction to the pulmonary venous return (Gewillig et al., 2005).

As soon as these children are born and identified as having a univentricular circulation, the Fontan operation cannot be performed immediately. The veins are small, and thus resistance is still very high (Gewillig et al., 2005). This makes implementing the Fontan circulation a virtual impossibility in newborns. A staged approach is preferred, as it will allow the body to gradually make adjustments to the different hemodynamic conditions that the Fontan operation will introduce. Even at birth, however, there are things that doctors can do to help better the chances of survival.

All steps are taken at this stage to ensure that proper balance of blood flow exists between the lungs and the body. Any obstructions to flow in the systemic circulation are relieved, if they exist. Enough pulmonary blood flow must exist to ensure adequate oxygen supply for tissue growth (Sandeep et al., 2008). However, pulmonary blood flow needs to be low enough to ensure that pulmonary vascular resistance (PVR) is kept down, and the ventricle is not overloaded. This is done with a systemic-pulmonary shunt, usually a 3-4 mm synthetic conduit. This conduit is used to connect a major systemic central artery (usually the aorta) and a proximal pulmonary artery to divert more flow towards the lungs. In patients with hypoplastic left heart syndrome, a conduit is placed between the right ventricle and left pulmonary artery (Sandeep et al., 2008). This provides parallel flow of pulmonary to systemic blood flows from the right ventricle. This operation is referred to as the Stage 1 Fontan operation. A successful Stage 1 operation alleviates desaturation, but the chronic volume overload to the heart remains. At this early stage, this can actually be good for the development of the heart, as long as

it is not allowed to exist indefinitely (Gewillig et al., 2005). Over a long period of time this is detrimental to ventricular function.

At 4-12 months of age (depending upon the patient), a superior cavopulmonary connection is made, also called the Glenn shunt or Glenn-type operation (Gewillig et al., 2005). This Stage 2 operation is only performed when pulmonary arteries have grown to sufficient size to allow the low PVR necessary for the circulation. Usually, the shunt from Stage 1 is removed, and cardiopulmonary bypass is used to allow anastomosis of the superior vena cava (SVC) to the proximal right pulmonary artery. The superior vena cava carries the majority of deoxygenated blood in these small children. Blood returning from the upper body now passes directly into the pulmonary circulation, decreasing the load on the ventricle. The inferior vena cava (IVC) still returns deoxygenated blood from the lower half of the body into the single functional ventricle. This deoxygenated blood mixes with the oxygenated blood returning from the pulmonary veins before being pumped out through the aorta. This mixing results in the patient being slightly cyanotic, but is not severe enough to be threatening to the patient. Oxygen saturations after the Stage 2 operation remain roughly 80-85% of normal values (Gewillig et al., 2005).

Once the patient reaches 1-5 years of age, depending upon growth of vascular structures and cyanosis at rest and during exercise, the patient is ready for the completion of the Fontan circuit via the Stage 3 operation (Sandeep et al., 2008). In this operation, the inferior vena cava is also connected to the pulmonary artery. The two primary methods of achieving this are the atriopulmonary connection (APC) and the total cavopulmonary connection (TCPC). In the APC, the right atrium acts as a valveless

contractile chamber interposed between the great systemic veins and the pulmonary artery (de Leval et al., 2005). The problem with this method is that it operates at a much higher pressure than normal, as there is no ventricle to supply power. In vitro experiments have shown that placing a compliant atrial chamber between systemic veins and pulmonary arteries causes a loss of mechanical energy due to the generation of turbulence (de Leval et al., 2005). The APC has proven to be an inefficient method of the Stage 3 Fontan procedure, as it can lead to chronic atrial distension and supraventricular arrhythmias (de Leval et al., 2005). The Stage 3 operation has undergone many modifications since its inception, but the TCPC has emerged as the superior method over the APC (de Leval et al., 1988). In the TCPC, the superior and inferior vena cavae are connected directly to the pulmonary artery, bypassing the right heart entirely. There are two distinct methods for connecting the inferior vena cava.

The first of these methods is the lateral tunnel method. Developed during the 1980's, the lateral tunnel provides a channel between the inferior vena cava and the pulmonary artery via a prosthetic baffle and a portion of the lateral atrial wall. This is the preferred method for use in patients on the younger end of the spectrum, as this connection can grow with the patient (Gewillig et al., 2005). It results in only a small amount of atrial tissue being exposed to high pressure, which over a long period of time can lead to arrhythmias. The other method, first performed in 1990, is known as the extra cardiac conduit (Marcelletti et al., 1990). In the extra cardiac conduit, a tube graft is placed between the end of the inferior vena cava and the pulmonary artery. The entire right atrium is left at a low pressure, as the right heart is bypassed entirely (Gewillig et

al., 2005). This method is offered only to patients who have grown large enough to accept the graft adequate for the inferior vena cava flow, as it has no growth potential (Gewillig et al., 2005). Candidates for the extra cardiac conduit must have high enough pulmonary vascular compliance (PVC) (Yun et al., 2009). If this condition is not met, there is increased risk of pleural effusion (fluid buildup around the lungs) and protein-losing enteropathy (Yun et al., 2009).

Problems with the Fontan Circulation

Once the Fontan operation is completed, the patients will usually live two or three decades of a semi-normal life until side effects of the procedure lead to congestive heart failure. The primary reasons for these complications are the elevated systemic venous pressure and reduced cardiac output (de Leval et al., 2005). The univentricular heart is known to become dilated, hypocontractile, and hypertrophic over time (Gewillig et al., 2005). These all result from the chronic volume overload facing the heart in single ventricle anatomy. Also, the elevated systemic venous pressures are known to cause protein-losing enteropathy, plastic bronchitis, and liver failure (de Leval et al., 2005). The elevated systemic venous pressures result in increased lymph production, and there is eventual impairment in lymphatic resorption, also leading to protein-losing enteropathy (de Leval et al., 2005). In addition, these patients will experience a reduced exercise tolerance. The pulmonary compliance gradually decreases over time, attributed to the lack of flow pulsatility in the pulmonary circulation due to lack of a ventricle (de Leval et al., 2005). The pulsatile pressure waveforms from the heart are damped out in the

systemic capillary beds, and thus the flow in the systemic veins and into the pulmonary circulation is less pulsatile in nature. This lack of pulsatility in the pulmonary circuit leads to increased stiffness from the lack of dilation (de Leval et al., 2005). This increased stiffness eventually leads to higher pulmonary vascular resistance, meaning even higher systemic venous pressures, even lower cardiac output, etc. Unfortunately, many of these negative symptoms feed back and make the causes even worse as time moves forward. Gravity has a worse effect on Fontan patients than on biventricular subjects. Hsia et al. (2000) has shown that gravity reduces forward venous flow in Fontan patients.

A study on the failing Fontan operation was done by Cavalcanti et al. (2001) retrospectively on patients to determine what factors of the operation correlated with a failing Fontan circulation. It was hypothesized that the anastomosis sites of the Fontan operation are critical to the success or failure of the operation. When examining patient data retrospectively, patients were lumped into one of two categories: a group with no symptomatic signs of Fontan failure, and a group with symptomatic Fontan failure. The differences between systemic arterial and pulmonary artery pressures between the two groups were not statistically significant. In contrast to this, the pressure at the end of the pulmonary vein was significantly higher in the group with the failing Fontan. Mean cardiac output was 36% lower in the failing Fontan group. Pressure in the superior vena cava was 5.4 mmHg higher in the failing Fontan group, and 6.8 mmHg higher in the inferior vena cava. Even though the cardiac output was lower in the group with the failing Fontan, the total pressure losses over the cavopulmonary connections were still

higher in the group with the failing Fontan. The total pressure loss over the cavopulmonary connections were much higher in the failing Fontan group, and this increase was more significant over the inferior vena cava connection. Also studied was the total energy loss across these cavopulmonary connections in both the non-failing and failing Fontan circulations. The energy loss in the inferior vena cava connection was significantly higher in the patients with the failing Fontan circulation. The energy loss study in the superior vena cava did not reach statistical significance. These increased resistances exacerbate the already existing problem of elevated systemic venous pressures in these Fontan patients. Minimizing energy loss and resistance within the TCPC reduces the possibilities of these elevated pressure drops across the connections that are known to be directly related to a failing Fontan circulation (Cavalcanti et al., 2001).

Review of Relevant Previous Work

Many studies have been carried out over the years to enable a better understanding of the Fontan circulation. Research today focuses on improving this circulation to relieve these symptoms and to give Fontan patients a better chance for a normal life. A primary focus of research in this field is the TCPC itself, since it is the aspect of this circulation over which some amount of control can be exercised. How the caval veins are connected, where they are connected, and with what material can all have large effects upon the behaviors of these systems. Three primary methods for studying the Fontan circulation have emerged: in vivo studies, in vitro studies, and numerical/analytical modeling. In vivo tests involve examining patients with these

circulations to collect data of all types. These tests give the best data but are invasive in nature. In vitro studies involve construction of a physical model that resembles the in vivo system. This has advantages in that parameters can be changed without worrying about harm to an individual, but has disadvantages in that it cannot always predict to body's response to certain conditions. Modeling implies the use mathematical models (usually numeric) to simulate pressures, flow rates, resistances, and compliances to better understand the effects of certain parameters on each other.

A study by Itatani et. al (2009) examined the optimum size for the conduit used in the extra cardiac conduit Stage 3 procedure. It is desirable to determine this optimum size to balance the risk factors of energy loss, flow stagnation, and thrombosis. With a smaller conduit diameter, there is less likelihood for flow stagnation, as the flow will have to move faster given the small cross sectional area. However, a smaller conduit size provides more resistance, and hence energy loss. In the Fontan circulation, energy is at a premium and any resistance that can be avoided will alleviate some of the higher systemic venous pressures that can ultimately lead to the congestive heart failure later in life. A conduit should be sufficiently large enough such that the energy loss across it is not too great. However, with too large of a conduit, there is an increased likelihood of flow stagnation. It is important to avoid flow stagnation at all times because of the clotting nature of blood. A blood clot in such an area due to flow stagnation could have catastrophic consequences for a patient. This presents a tradeoff between energy loss and flow stagnation, both of which will harm the patient. It is known that with the non-pulsatile nature of the flow, most of the variations in flow are driven by respiration.

Measuring stagnation volume and energy loss at rest and at exercise for different conduit sizes, it was found that the most stagnation occurred during respiratory expiration (Itatani et al., 2009). In fact, reverse flow was even measured with the larger conduit sizes. With systemic venous hypertension already a problem for these patients, reverse flow is very undesirable. Stagnation was found to decrease during exercise as the overall flow rate experienced an increase. It was found that for children of 2-3 years of age, the optimum diameter for the extra cardiac conduit lies in the range of 16 to 18mm. Anything with a larger diameter was said to have redundant space, and could increase the risk of flow stagnation and thrombosis. Smaller diameters could result in unnecessary energy loss (Itatani et al., 2009).

The non-pulsatility of the flow in the systemic veins represents an eventual problem for the pulmonary circulation. This non-pulsatility refers to the lack of systolic-diastolic pressure waveforms because of the omission of a right ventricle in the circulation. This is known to reduce the compliance (PVC) and increase resistance (PVR) in this region over time. Respiration has been shown to serve as a type of driving force for flow and pressure variations in the pulmonary circulation, and in the TCPC itself (Hsia et al., 2007 and Itatani et al., 2009).

Penny et al. (1991) examined the role of the lungs after the Fontan operation in patients in which a sub-pulmonary atrium was still connected to the pulmonary circulation. The study examines the role of the right atrium as an energy supply in relation to the energy provided by respiration to the pulmonary blood flow. During expiration, the right atrial contribution to forward flow was found to be 51.4% with a

standard deviation of 8.8%. The total forward flow during inspiration was 63.6% higher than during expiration, with a standard deviation of 35%. This is to be expected, as during inspiration the pressure inside the thoracic cavity drops below atmosphere pressure, drawing flow into the lungs. The right atrial contribution to forward flow during inspiration was 52% during inspiration with a standard deviation of 10%, so roughly the same as during expiration. During right atrial systole, inspiration increased the maximum forward flow velocity from 39.8 cm/s to 51.4 cm/s. The study did not gather hard evidence of the likelihood of flow reversal, however it is believed that backflow would appear more likely during expiration than during inspiration (Penny et al., 1991).

Hsia et al. (2000) studied the effects of respiration and gravity upon flow in the systemic veins in patients with both normal biventricular (as a control) and Fontan circulations. Of the 48 Fontan patients, 15 underwent the APC operation while 33 underwent the TCPC operation. Of the patients who had the TCPC, 27 were done via the lateral tunnel method, while the remaining 6 had the extra cardiac conduit. The flow in the primary vein returning from the liver, the hepatic vein, was studied and found to fluctuate most significantly in patients with the TCPC. The effect of respiration was most significant also in patients with the TCPC, as the average ratio of inspiratory to expiratory flow rates was 3.4, compared to 1.6 for APC patients and 1.7 for the control group. In the portal vein, the flow was higher during expiration in normal patients, but this was not found to be the case in the Fontan patients. The inspiratory to expiratory flow rates in the portal vein were 0.8 in normal patients, 1.0 in TCPC patients, and 1.1 in

APC patients. So, in contrast to the control group, flow in patients with the APC was higher during inspiration. The effects of respiration on the subhepatic inferior vena cava were similar for all patients. Also the effect of gravity was studied. Gravity had no significant effect on either net forward flow or retrograde flow in patients with a normal circulation in the subhepatic inferior vena cava. For both the APC and TCPC patients, gravity had the effect of decreasing the net forward flow and increasing retrograde flow in the subhepatic inferior vena cava. Gravity also reduced the net forward flow in the hepatic vein for control subjects. However, the reduction in hepatic vein flow due to gravity was much greater in the Fontan patients, especially in those with the APC. Also, TCPC patients having the lateral tunnel showed similar results in all cases to those having the extra cardiac conduit (Hsia et al., 2000).

Redington et al. (1990) first studied the effect of respiration in the pulmonary artery in patients with a total cavopulmonary shunt. This study was done on patients who have the right heart completely bypassed: only the venous blood from the coronary sinus and liver were returned to the right atrium. Using doppler echocardiography, flow measurements were made in the pulmonary artery. Blood flow was observed to increase during inspiration and decrease during expiration in the pulmonary artery. Also studied were the effects of the Valsalva manoeuvre (filling lungs with air and holding), and the Mueller manoeuvre (trying to breathe in with airways closed). The Valsalva and Mueller manoevres create prolonged positive and negative pressures in the thoracic cavity, respectively. During a brief Valsalva manoeuvre, there was flow away from the lungs. With a sustained Valsalva manoeuvre the flow initially moved away from the lungs, but

after 2-5 seconds there was normal flow again into the lungs. During a brief Mueller manoeuvre, there was an increase of flow towards the lungs in all patients. With the sustained Mueller manoeuvre there was an initial surge of flow into the lungs, followed by normal flow again after a few seconds. Since the flow to the lungs is attenuated considerably when there is positive pressure inside the thoracic cavity, it is necessary to keep the airway pressures as low as possible in patients to keep the pulmonary blood flow at a sufficient level. This study proposes that negative pressure ventilation may provide a better alternative to the current method of positive pressure ventilation because it would augment the pulmonary blood flow in the patients (Redington et al., 1990).

Hjortdal et al. (2003) examined the relationship between blood flow and respiration during rest and exercise in 11 Fontan patients with the TCPC. Flows were monitored in the IVC and SVC using real-time magnetic resonance imaging (MRI). In patients at rest, the SVC flow was not significantly affected by respiration. The mean inspiratory to expiratory flow rate ratio was 1.0 with standard deviation of 0.2. Exercise did not change these ratios significantly. The IVC flow was much more respiration dependent, however. In patients at rest, the mean ratio was 1.9 with a standard deviation of 0.5. This implies nearly twice as much flow occurring in the IVC during inspiration, a significant reliance on inspiration. This ratio decreased during exercise, as more flow appears to be driven by ventricular activity. Reverse flow ratios of 0-1% were seen in the SVC at both rest and exercise. In the IVC, a mean reverse flow ratio of 10.5% was seen at rest; this decreased to 2.9% during exercise (Hjortdal et al., 2003). These results

demonstrate a respiration dependency of IVC flow during rest. This dependency is somewhat diminished during exercise, however.

Hsia et al. (2007) studied the effect of diaphragm plication, a surgery done to relieve symptoms of diaphragm paralysis, on both normal and Fontan patients. Flows in the hepatic vein, portal vein, and subhepatic inferior vena cava were evaluated using doppler ultrasound. All of the Fontan patients under the study had the TCPC operation. In the control group of biventricular circulations and normal diaphragms, hepatic venous flow during inspiration was 2.4 times greater than during expiration in the upright position. However, in these patients with diaphragm plication this ratio reduced to 1.4, showing that the full effect of respiration was diminished. Also in the biventricular patients there were no significant differences in portal and subhepatic inferior vena caval flows depending upon whether there was normal diaphragm function or if there was diaphragm plication. The portal vein experienced slightly higher forward flow during expiration in these cases. Moving to the case of the Fontan patients, there was an inspiratory to expiratory hepatic vein flow ratio of 3.2 in the supine position for normal diaphragm operation. This reduced to 2.3 for diaphragm plication, again in the supine position. In the upright position, the hepatic flow ratio was 2.5 for normal diaphragm operation and 1.7 in the patients with diaphragm plication. In the portal vein, flow remained relatively independent of respiration in patients with normal diaphragm operation, but patients with plication experienced an inspiration/expiration forward flow ratio of 1.6 and 1.7 for supine and upright positions, respectively. The subhepatic inferior vena cava study in Fontan patients did not reach statistical significance. Also studied was

the effect of gravity upon these patients. Gravity had a reduction of portal venous flow in Fontan patients, with an upright-to-supine flow ratio of 0.7, but diaphragm plication did nothing to change this. Fontan patients experienced an upright-to-supine flow ratio of 0.6 with normal diaphragm operation, this ratio evened out to 0.8 for patients with the diaphragm plication. In the subhepatic inferior vena cava, the upright-to-supine flow ratio in Fontan patients was 0.7 for normal diaphragm operation and 0.8 for patients with the plication. In summary, the diaphragm plication operation does not fully restore operation to the diaphragm, as all effects of respiration are muted somewhat in patients with the diaphragm plication. In Fontan patients, the effects of respiration on the systemic venous flows are of utmost important, and this effect is lost somewhat in patients with a diaphragm plication. It is for this reason that phrenic nerve injury should be avoided if at all possible in patients who have received, or will receive, the Fontan operation (Hsia et al., 2007).

Ovroutski et al. (2007) studied the effect of the Fontan operation upon exercise and oxygen capacity. They hypothesized that one of the most important factors in the success of these patients was the age at which the operation is performed. Earlier separation of the blood circuit preserves the function of the ventricle because long-term volume overload is avoided, along with cyanosis. Patients who had the TCPC Fontan procedure either as adults or children were studied. Patients were monitored during exercise in early and late postoperative tests. The mean early cardiopulmonary oxygen capacity was higher in children: 27.9 ml/min per kg body weight in children, and 22.9 in adults. This small difference was magnified in the late postoperative tests, as oxygen

capacity was 30.1 in children and 16.9 in adults. For all adolescent and adults, the cardiopulmonary oxygen capacity showed reduction between early and late postoperative testing. Overall, the study showed that the timing of the Fontan operation has a major impact on the effect the operation has upon cardiopulmonary oxygen capacity. Adults showed the most significant loss in oxygen capacity, while adolescents lost only slight oxygen capacity. Small children showed stable or even improved levels of oxygen capacity between post-operative tests. The exercise capacity was also better in children postoperatively than in adults. The median exercise capacity in children was 2.2 W/kg, as opposed to a median of 1.9 in adults early postoperatively. In the late postoperative tests, the median exercise capacity of children was 2.2 compared with 1.9 in adults. In the overall patient group, a decrease in exercise capacity from 2.1 to 1.8 was seen from the early to late postoperative tests. Lastly, the peak heart rate was observed in these patients during testing. The median peak HR was 136 beats per minute in children and 112 in adults in early postoperative tests. There was no difference in maximum heart rate between early and late postoperative tests at the peak of exercise (Ovroutski et al., 2007).

Models of the Human Circulation

Snyder and Rideout developed a mathematical model of the human cardiovascular system for NASA (Snyder et al., 1969). This model included a lumped parameter approach for modeling the certain characteristics of each branch of the circulatory system (Snyder et al., 1969). In a lumped parameter model, each branch of the circulatory system is given characteristic impedance, much like an electric circuit (Manoliu et al.,

2009). These lumped parameter models account for the effects of resistance, compliance, and inertance. Resistance represents real impedance, while inertance and compliance are complex impedances. In this study, the pulmonary system was modeled using three resistance-compliance elements, based on average pressures and flows (Snyder et al., 1969). The effects of gravity and of respiration are included into this model. Gravity was modeled through use of additional pressure generators, and respiration was modeled by grounding relevant compliances to either intrathoracic or abdominal pressure. The model is broken up into four main sections: head, thoracic cavity (pulmonary circuit), abdominal cavity, and legs (Snyder et al., 1969).

In most cases, the human circulatory system can be modeled using a lumped parameter model. This takes data from each branch of the circulatory system and characterizes it as resistance, compliance, or inertance. This can be viewed in the same manner as an electric circuit with resistance, capacitance, and inductance. In modeling the Fontan circulation, it is important that data from patients with a Fontan circulation is utilized, as it has different properties. Fontan patients will have different systemic venous pressures, different pulmonary compliance, and different flow characteristics in the pulmonary circulation.

A study by Manoliu et al. (2009) used windkessels to model the cardiovascular system. A two-element windkessel includes one resistor and one capacitor in a parallel circuit. A three-element windkessel includes two resistors and one capacitor. One of these resistors appears in series with the capacitor, and one appears in parallel. These capacitors (or “compliance elements” in fluid mechanics) model the distension that

occurs in the arteries and veins due to changes in pressure (Manoliu et al., 2009). The best example of this is in the aorta, which will distend outward during each systolic period of the cardiac cycle as a response to the increase in arterial pressure. In fluid mechanics, compliance is defined as the change in volume per unit change in pressure (Kulakowski et al., 2007). Windkessel theory helps to explain why pressure variations in the aorta have less amplitude than in the left ventricle. In this theory, the aorta is represented by an elastic chamber and peripheral blood vessels are represented by a rigid tube: meaning that they will exhibit constant resistance. Total arterial compliance and peripheral resistance seem to be the only two important parameters when looking at the pulse pressure in the aorta. The four-element windkessel also includes inertance effects (Manoliu et al., 2009). Inertance is proportional to density and length, and inversely proportional to cross-sectional area (Kulakowski et al., 2007). Both compliance and inertance are opposite complex impedances, thus both of these can be modeled as one net effect. In the case of modeling the cardiovascular system, the net complex impedance can be modeled with a compliance element. This demonstrates that a three-element windkessel is sufficient for modeling branches of the human circulation (Manoliu et al., 2009).

A study by Kilner et al. (2008) studied pulmonary regurgitation and the effects of different parameters upon the magnitude of regurgitation in the pulmonary circulation. This study was not done on a Fontan circulation, but some of the results are still relevant. This study was done using a mathematical model of pulmonary regurgitation. Pulmonary regurgitation is the "backflow" that occurs back into the right ventricle from the

pulmonary artery. This occurs in patients having a poorly functioning pulmonary valve, or no valve at all. The effects of resistance both near and far from the compliance, and of the compliance itself upon the regurgitation were studied. With free regurgitation (no valve), about 30% regurgitation was found, which is similar to what is found in patients without a pulmonary valve. There was no reverse flow in the small capillaries, only in large arteries (Kilner et al., 2008). Raising the resistance far from the compliance (far from the pulmonary valve) raised regurgitation to 46% (Kilner et al., 2008). This makes intuitive sense because during diastole when the heart expands, the path of least resistance for the blood was simply back into the heart. When the resistance was raised close to the compliance, the regurgitation was lowered to only 10%. In this case the path of least resistance for the blood during diastole was mostly forward. Doubling the proximal compliance increased the regurgitation from 30% to 35%, an halving the compliance lowered it to 23% (Kilner et al., 2008). It should be noted that pulmonary regurgitation can be tolerated by the circulatory system for several decades but eventually leads to fatal arrhythmias (Camp et al., 2007). Arteries that are dilated due to higher flows have a higher compliance, such as during exercise. Arteries that are distended due to hypertension will exhibit a lower compliance. This is because these arteries are already being stretched and are at the limit of their elastic range (Kilner et al., 2008). Because of this, they are stiffer and will not distend as much due to cardiac variations, thus they have a lower compliance (Kilner et al., 2008).

Cardis et al. (2006) examined the compliance and elastic properties of a reconstructed aorta in patients with hypoplastic left heart syndrome (Cardis et al., 2006).

The study was not done specifically on Fontan patients, however candidates for the Fontan operation can include patients with this disorder (Sandeep et al., 2008). Hypoplastic left heart syndrome (HLHS) is a condition in which children are born with a small and underdeveloped left side of the heart. Coarction of the aorta is a narrowing of the aorta between the upper body and lower body branches, causing high blood pressure in the upper body and low blood pressure in the lower body. The goal of the study was to examine the elastic properties of reconstructed aortic arches in patients with HLHS in comparison to patients with other forms of single ventricle and simple shunt lesions as the control group. They found the distensibility index was significantly less and stiffness index was higher in the reconstructed arch of HLHS patients than in the single and double ventricle patients (Cardis et al., 2006). Also found was that the compliance decrease had the effect of increasing the cost of "cardiac ejection"; that is, it makes the heart work harder. This confirms the idea that lower compliance can reduce cardiac output in Fontan patients (de Leval et al., 2005). The reason for using these stiff materials for aortic reconstruction has always been to avoid aneurysms, but currently there are new methods being explored that could reduce the amount of reconstructive material needed. This would help to retain some of the original elastic properties of the aorta, while at the same time reducing the risk of an aneurysm (Cardis et al., 2006). These findings are significant to Fontan patients, as the Stage 1 operation can involve a reconstruction of the aorta.

Goals of this Study

An article by DeGroff et al. (2007) outlines a brief history of the Fontan operation, highlights some of the progress that has been made in the previous decades, and emphasizes the areas where research can and should continue. Unfortunately, the long-term outlook for most Fontan patients is still troublesome. The "4th stage" of the Fontan operation is a heart transplant, as this circulation eventually fails as discussed previously. Most research has been centered on developing the "ideal Fontan circuit" where turbulence, recirculation, regurgitation, vortices, and stagnation points are minimized to increase energy efficiency and to reduce the likelihood of thrombosis. Most studies and models created to study the Fontan circulation contain large simplifications: DeGroff challenges that these simplifications have compromised the validity of some of the results that have been published. Some of these simplifications include: non-compliant blood vessels, effects of respiration, and the steady flow assumption (DeGroff et al., 2007). In addition to these simplifications, the parameters used usually are from 5-7 year olds at rest: this doesn't include any exercise effects or help in understanding why the Fontan circulation fails when patients reach their 20's and 30's. In future research, DeGroff recommends that as many of the following as possible should be included: vessel diameters and flow rates that are representative of the range seen in the patient group including rest and exercise states, appropriately matched vessel size and flow, compliant vessels, better modeling of surgical anastomosis sites, effects of respiration, non-steady (pulsatile) flow and correctly shaped vessels (DeGroff et al.,

2007). It is a goal of this study to model the Fontan circulation with several of these goals in mind.

In this research, the Stage 3 Fontan circulation is experimentally modeled with an attempt to include as much of DeGroff's criteria as is achievable. In this study, an in vitro, multi-scale model of the Stage 3 Fontan circulation is fabricated and validated against clinical patient data. The multi-scale model approach is used in order for the mock circulatory system to demonstrate equivalent characteristics to the actual patient's circulation. In this approach, clinical data is acquired from the patient and it is reduced to form an equivalent lumped parameter (LP) circuit using complex impedances and a reasonable number of branches. An anatomically accurate, three-dimensional (3D) model of the surgical construction of the TCPC is used for realistic flow modeling. Hence, a multiscale model couples the local hydrodynamics of the circulation, using an accurate, a 3D model of the local anatomy, with the rest of the circulation, using a lower order model.

One goal of the model is to accurately portray the surgical anastomosis sites. Great care is taken such that the total cavopulmonary connection (TCPC) sites of these patients are as realistic as possible in terms of both geometry and pressure/flow relations. These TCPC "test sections" are fabricated from MR images of patients, and are placed in the mock circulatory system for testing. The flow properties within the TCPC are studied by coupling it to the mock circulatory system that imposes physiologically accurate boundary conditions around it.

In this model, four lumped parameter branches exist: lower body, splanchnic, cranial, and pulmonary. Parameters for these models originate from patient data, from the literature, and from partners in research. The system is built such that it can be tuned to match different patient's data. The effect of respiration upon the Fontan circulation is emphasized within this study. Since the effect of respiration has been studied in vivo, a goal of this study is to replicate this behavior within the mock circulatory system by tuning it to a lumped parameter model. Respiration is modeled by grounding the appropriate compliances to thoracic and abdominal cavity pressures, as was done in the Snyder and Rideout study (Snyder et al., 1969). Figure 1 shows the impedance diagram for the Stage 3 lumped parameter model.

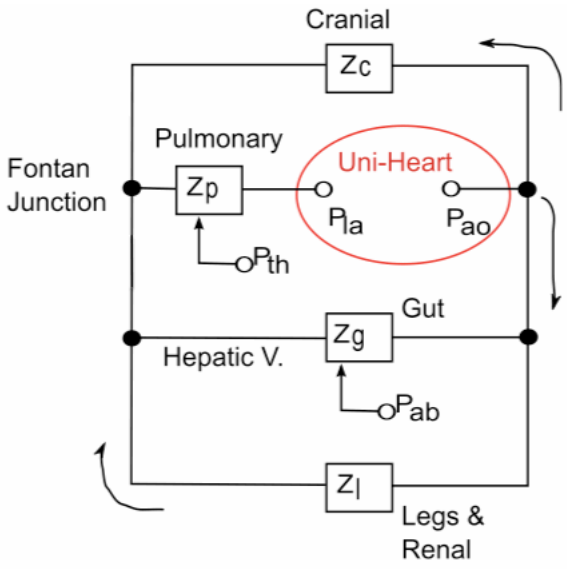

Figure 1: Impedance diagram for Stage 3 model

Three-element windkessels elements are used in each of the systemic branches (Manoliu et al., 2009) to accurately portray the impedance in each branch in accordance with the patient data.

Specific Aim 1: A specific aim of this study is to effectively model the hemodynamics of the Fontan circulation after the Stage 3 operation. We hypothesize that this can be done in a laboratory using a multiscale bench top mock circulatory system that couples a highly accurate localized anatomy with a network characterization of the remaining circulation. We hypothesize that with correct tuning the system can produce clinically realistic results.

Specific Aim 2: A second specific aim of this study is to study the effects of respiration on the Fontan circulation. Hsia (2000) hypothesizes that reducing flow reversal measured in the hepatic vein in Fontan patients will lead to a better long-term outcome. Hence, replicating this behavior in vitro is an essential step towards verifying this hypothesis. The mock circulatory system will provide a means to simulate experimentally the circulation of any Fontan patient, such that potential changes can be studied that may lead to better outcomes for these patients.

CHAPTER TWO

METHODS OF CIRCUIT IMPLEMENTATION

Lumped Parameter Network Model

A multi-scale modeling approach is used as a means for modeling the Fontan circulation. A multi-scale model couples a 0-D lumped parameter model of the circulation with a 3-D test section. The goal is to couple the fluid dynamic behavior within the test section to the dynamics of the circulation. This is achieved by inserting a physiologically realistic model of a TCPC into a mock circuit that is tuned to match parameters in a Fontan patient based on clinical measurements. Corsini et al. (2010) developed a lumped parameter model of the Fontan circulation based on four main branches: upper body, thoracic cavity, abdominal cavity, and legs. Each of these branches contains several resistive and capacitive elements to most accurately portray the characteristics of the circulation. A simplified model based upon the Corsini model is used extensively throughout this study.

The hydrodynamic parameters studied include the systemic arterial pressure, the flow rates in arterial and venous branches, the pressures and flow rates at the location of the Fontan connection, and the pressure at the end of the system in the atrium. Each branch of the simplified model contains circuit elements that correspond with a device in the mock circuit that serves as a physical realization of that parameter. These include resistance and compliance elements, which are analogous to resistance and capacitance in an electric circuit.

The potential for flow to occur in the mock circulatory system is provided by a static pressure differential. Setting the inlet and outlet pressures to the system imposes the pressure differential. Resistance in the system controls the flow rate that can occur for a given pressure differential. The confined tube through which the fluid passes provides some resistance, but additional resistance is provided to the system by valves or laminar flow elements. Resistance in a fluid circuit is defined as (Waite et al., 2007):

$$R = \frac{\Delta P}{Q} \tag{2.1}$$

where R is the value of resistance, ΔP is the pressure differential across the resistance section, and Q is the volumetric flow rate through the resistance section. In this way, fluid resistance is analogous to electrical resistance relating voltage potential drop with current flow.

In biofluid flows, the capacitance is referred to as compliance, and refers to the energy storage of an element given a change in pressure in the time domain. Compliance describes volume change per unit pressure change, and is given by (Kulakowski et al., 2007):

$$C = \frac{\Delta \forall}{\Delta P} \tag{2.2}$$

where C is the compliance, $\Delta\forall$ is volume change and ΔP is pressure change. Compliance has no effect on the behavior of a steady system. Compliance and damping

are critical in accurately modeling the effects of respiration upon the mock circulatory system, as they dictate pressure-volume relationships within the circuit. The concept of compliance is completely analogous to capacitance in electrical circuits.

Inductors, like capacitors, affect only non-steady systems. In fluids, inertance is defined as the pressure gradient required to accelerate a flow. Fluid inertance describes how quickly pressure changes will affect flows in the system. The fluid inertance in a circular tube with parabolic velocity profile is (Kulakowski et al., 2007):

$$L = \frac{2\rho x}{A} \tag{2.3}$$

where L is inertance, ρ is the density of the fluid, x is the length of tubing, and A is the cross-sectional area of the tube. The fluid inertance is analogous to electrical inductance.

The three impedance elements (R,L,C) define the damping and natural frequency of the system. The damping ratio of a series RLC-circuit is (Hambley, 2008):

$$\zeta = \frac{R}{2}\sqrt{\frac{C}{L}} \tag{2.4}$$

where ζ is the damping ratio, R is resistance, C is compliance, and L is inertance. The natural frequency ω_n of the same system is (Hambley, 2008):

$$\omega_n = \frac{1}{\sqrt{LC}} \tag{2.5}$$

The human circulatory system can be effectively modeled using these impedances and source pressures. Pulsatility from the cardiac cycle contributes significantly to hemodynamic behavior on the arterial side, but the arterial tree and capillary system contain large resistances and compliances. The primary source of resistance in the body is the branching of blood vessels down to capillary networks. The elasticity of these vessels and surrounding tissue provide the compliance. These networks act as low pass filters, and effectively dampen out most of the pulsatility in the blood flow by the time it reaches the venous side and TCPC. The Fontan circulation is especially less pulsatile on the venous side due to the absence of the ventricle. For the purposes of this study, the remaining pulsatility from the cardiac cycle is not modeled, such that the respiration effect can be isolated. The systemic arterial and atrial pressures are modeled using constant head tanks.

In a lumped parameter model, a complex system is reduced to a mathematically equivalent circuit that can be reasonably analyzed. Clinical measurements lead to assignment of impedance values in each branch. The lumped parameter model used in this study derived from the full lumped parameter model of Corsini et al. (2010) and is shown in Figure 2.

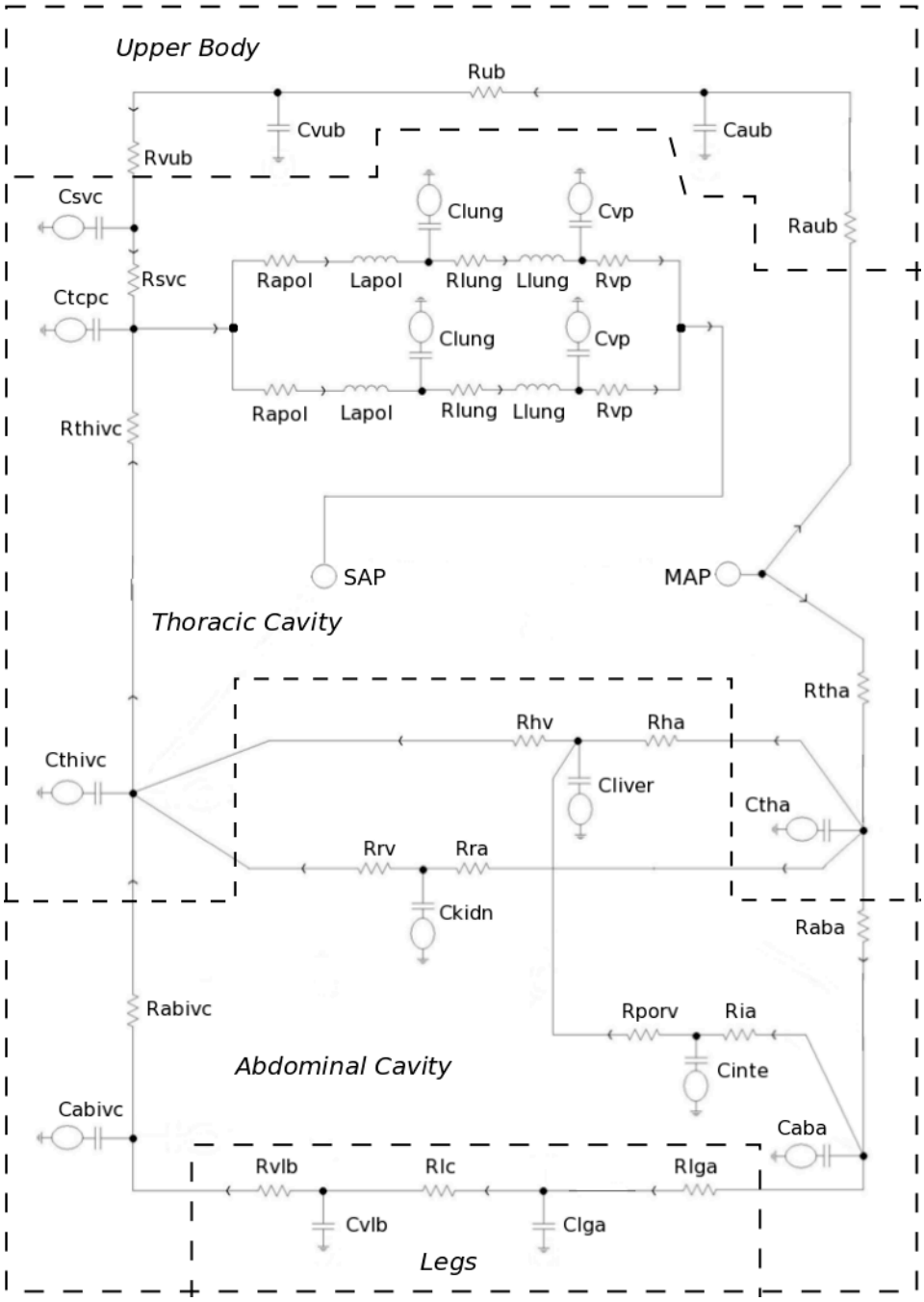

Figure 2: Full lumped parameter model of the Fontan circulation (Corsini et al., 2010)

The full lumped parameter model shown in Figure 2 is not practical in a laboratory bench top realization. The number of elements requiring connectors and tubing would create too much inertance. Tuning such a system in a real analog circuit would be difficult. In order to create a more practical system, the full lumped parameter model is reduced to branch circuits of equivalent impedance. The model in Figure 2 is broken up into four regions: upper body, thoracic cavity, abdominal cavity, and legs. The legs branch in the full model is already an equivalent circuit of two identical legs (Corsini et al. 2010). Each of these regions is reduced down into an equivalent impedance branch with two resistances and one compliance. Each systemic branch includes one artery and one vein, and the pulmonary branch includes two arteries and two veins to account for a left and right lung.

Each branch of the full lumped parameter model (Figure 2) is characterized by an impedance spectrum, with imaginary and real components that vary as a function of frequency. This spectrum is calculated using a Thevenin equivalent circuit to Figure 2. The resistance in each branch at steady flow represents the purely real component of the impedance. This value is already determined by the flow rates passing through each branch, and is derived from clinical data. The sum of the venous and arterial resistances is held to this value, enabling the correct flow rate in each branch. The proportion of the two resistances in the simplified model, however, can be varied to find a closest match to the impedance spectrum of the full model. The venous resistances are varied in the systemic branches, while the arterial resistances are varied in the pulmonary branch. These resistances, along with the compliance in each branch, are varied until a least-

squares fit is found to the impedance spectrum of the full model. Frequencies in the 0-2.5 Hz band are considered for the least-squares analysis. There is competition between splanchnic and lower body branches, reducing the splanchnic Thevenin-equivalent source pressure. In simplification, systemic arterial pressure was set equal to the lower splanchnic source pressure, for maximum fidelity in the splanchnic branch. Cranial and lower body arterial resistances were reduced to preserve the mean flow rates. Thus, the systemic arterial pressure in the model is lower than the biological mean aortic pressure.

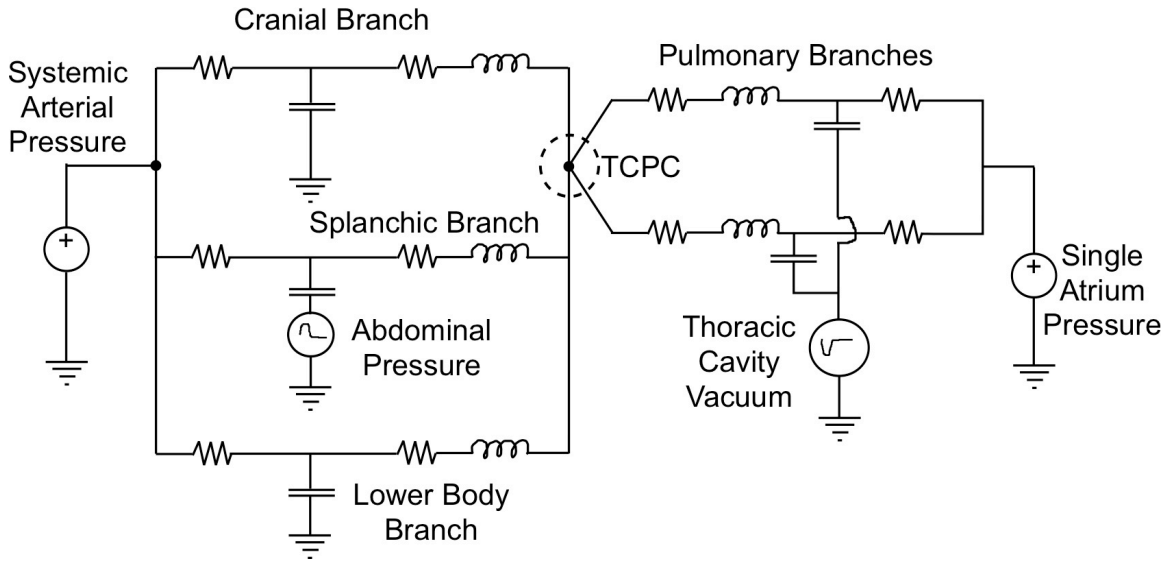

Figure 3: Simplified lumped parameter network model equivalent to Figure 2

The simplified lumped parameter network model shown in Figure 3 is the resulting simplified equivalent circuit to that of Figure 2 and is used as the basis for the mock circulatory system design. The branches in the simplified lumped parameter model are: lower body, splanchnic, cranial, and pulmonary. The lower body branch is

sometimes referred to as the legs/renal branch. The splanchnic branch models the portal circulation the body and contains the hepatic vein of interest (sometimes referred to as hepatic branch). Figure 3 is used as a design basis for the mock circulatory system, as each component in this network model is physically implemented into the mock circulatory system. The remainder of this chapter discusses how each element in Figure 3 is physically implemented into the system.

Systemic Arterial and Single Atrium Pressures

The systemic arterial and single atrium pressures set the pressure differential across the entire circuit, creating the potential for flow to occur in the system. The systemic arterial pressure is the primary energy source for the system, and is achieved in the mock circulatory system using hydrostatic pressure. A column of fluid exerting force upon a point provides hydrostatic pressure. Assuming that the fluid is incompressible, this becomes the product of the density of the fluid ρ, the gravitational constant g, and the height of the column of fluid above the point of interest z. (White, 2003). Here, z_2-z_1 are the relative hydrostatic pressure of the systemic arterial and single atrial pressures.

$$P(z) = \int_1^2 g \cdot \rho(z)\, dz = \rho\, g\, (z_2 - z_1) \tag{2.6}$$

The systemic arterial pressure is set via an adjustable head tank at the front of the system. A sliding rail system is used to set the height of the tank, and an elevated

draining mechanism assures that the height of the surface of the fluid remains constant throughout operation. This setup is shown in Figure 4.

Figure 4: The systemic arterial pressure head tank of adjustable height

This source pressure is connected to the front end of all three systemic branches and is used to tune resistances in each of these branches.

The other set pressure in mock circulatory system is the single atrium pressure. This is the pressure at the conclusion of the pulmonary veins in the mock circulatory system. This pressure is created by another head tank that is placed at the end of the system. The single atrium pressure is adjusted by moving the head tank up and down on a rod. Single atrium pressure is set relative to a reference height used in the system. From the single atrium head tank, the flow is drained down to a reservoir where it is then pumped back up to the systemic arterial pressure head tank.

Resistance

The system resistance controls the pressure drop that will occur in each branch, and the flow rate that will take place across this pressure drop. In this study, there are two primary methods for tuning resistance: ball valves and laminar flow elements. Each of these two methods has advantages and disadvantages in the physical system.

The easiest way to achieve resistance is to place a valve in the branch. Throttling the valve varies the resistance. Head loss across a valve is proportional to the velocity head of a fluid (White, 2003) as:

$$\Delta h = K \frac{\overline{V}^2}{g} \tag{2.7}$$

where Δh is head loss, K is the loss coefficient, $\overline{V}$ is the average velocity of the fluid, and g is the gravitational constant. K is dictated by the position of the valve. From Equation 2.7, head loss is proportional to the square of velocity. Pressure head itself is given by the Bernoulli equation is the sum of the pressure head and the elevation of the fluid (White, 2003).

$$h = \frac{P}{\rho g} + z \tag{2.8}$$

In Equation 2.8, P is the gage pressure, ρ is the density of the fluid, g is the gravitational constant, and z is the height of the fluid. Flow rate is related to average velocity in the pipe (White, 2003),

$$Q = \overline{V} A \tag{2.9}$$

where $\overline{V}$ is velocity and A is cross-sectional area of the pipe. Combining Equations 2.7, 2.8, and 2.9, pressure loss in a valve is related to the square of flow rate:

$$\Delta P = \frac{4 \rho K Q^2}{\pi d^2} \tag{2.10}$$

where d is the inner diameter of the pipe. This is not consistent with resistances in the lumped parameter model, as all resistances in the lumped parameter models are supposedly linear resistances. The problem goes beyond the valves, however. Much resistance in the system is caused by these minor losses, as the fluid travels through fittings, hose barbs, pipe elbows, tees, etc. An unavoidable consequence of using a mock circulatory system is the presence of square-law resistances in the system, but the resistances themselves can still be made correct during steady flow.

The other method used to achieve resistance in this study is the laminar flow element. The laminar flow element separates one flow into several smaller flows. This

separation and reconnection of flows brings about a pressure loss in the system that can be used as a resistance. Small coffee stirrers (thin walled, open diameter tubes) were placed in parallel and inside a larger size tube to create these elements. A number of the stirrer tubes in each element were plugged using silicone sealant. The actual number of plugged coffee stirrers present controlled the resistance: more resistance was offered with more plugged stirrers. If all coffee stirrers are plugged, then the flow can only pass through the cracks and spaces in between the straws. A clamp was applied to the exterior for fine adjustment of resistance, as seen in Figure 5.

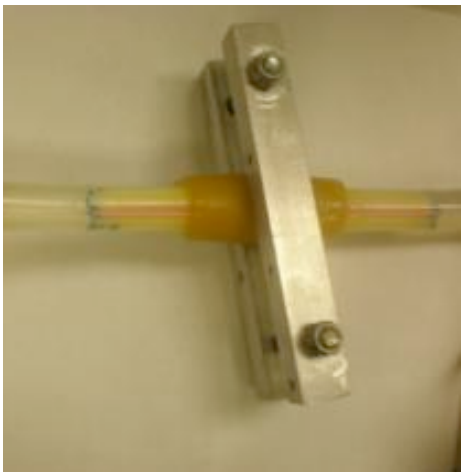

Figure 5: Laminar flow element used for resistance

The resistance offered by the laminar flow element results from the fluid having to pass through a much smaller diameter tube. The pressure drop due to flow through a long cylindrical pipe is given by the Hagen-Poiseuille equation (White, 2003),

$$\Delta P = \frac{8\mu LQ}{\pi r^4} = \frac{128\mu LQ}{\pi d^4} \qquad (2.11)$$

where μ is the dynamic viscosity, L is length of pipe, Q is volumetric flow rate, and d is the diameter of the pipe. Equation 2.11 shows that the pressure loss due to a long cylindrical pipe is linearly related to the volumetric flow rate Q. Therefore, it is a linear resistance.

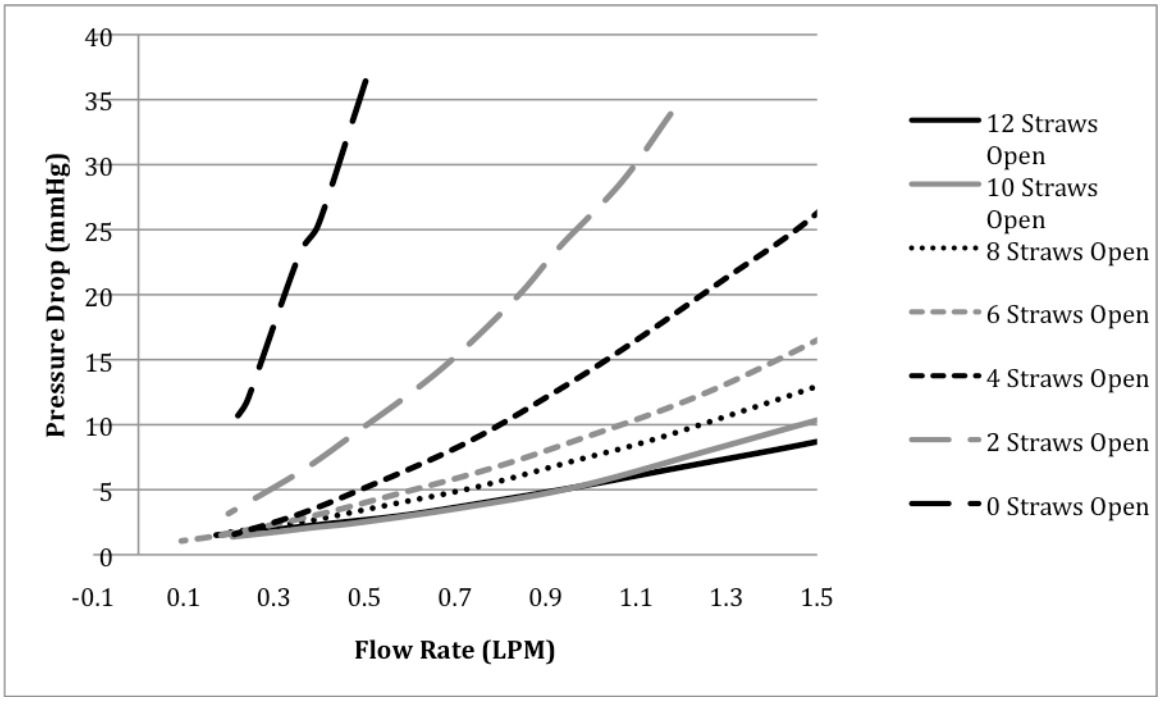

Figure 6: Laminar flow element resistance curves

Figure 6 shows pressure drop vs. flow rate for several laminar flow elements. In each case there are 12 total coffee stirrers (2.16 mm inner diameter, 3.05 mm outer diameter) inside the tube (12 mm inner diameter), but the number of "open" straws is listed. For example, in the "10 Straws Open" case there are 10 straws not plugged and 2

that are. No clamping is done here. In most cases, a pressure loss value that is desired will be in between two lines shown here. The arrangement with less resistance is taken and then clamped until it reaches the desired resistance value. There is some non-linearity to the curves shown in Figure 6, with a maximum linear error of 2.78 mmHg occurring at the highest flow rate with 6 open straws. Nonlinearity is due to the small parasitic/minor losses in the arrangement that behave as a square-law resistance.

Windkessels

Compliance simulates elasticity in the blood vessels, and plays a large role in cardiovascular function. High compliance allows for more expansion, resulting in smaller pressure oscillations. The behavior of the system as it responds to respiration is largely dictated by the compliance. For this reason, it is imperative that a reliable system for controlling circuit compliance is in place.

All compliances in the system are either grounded to atmospheric pressure or to some respiration pressure. The pressure to which the compliance is grounded refers to the pressure on the other side of the compliant boundary that interacts with the system. The compliances grounded to atmospheric pressure simply respond to conditions in the branch to which they are connected. These compliances are passive, and dampen out pressure oscillations. They are located in regions of the body where the respiration pressures do not forcibly act upon the flows. These branches include the cranial and lower body branch. Windkessels provide these compliances, and are essentially air

chambers inserted into the system (the word “windkessel” literally means “air chamber” in German). Figure 7 shows a windkessel attached to the system.

Figure 7: Windkessel connected to a branch tube

The compressibility of air in the chamber is used as an elastic reservoir for the system, and acts as a spring. The compliance provided by this air is a function of its volume. The windkessel’s compliance is calculated with Equation 2.12 and assumes isentropic compression of air,

$$C = \frac{\forall}{k P} \tag{2.12}$$

where C is the compliance, $\forall$ is the volume of air, k is the heat capacity ratio of the trapped gas, and P is the absolute mean pressure of the gas. The heat capacity ratio of standard air is k =1.4. The volume of air is adjusted to control compliance in the system, as the pressure is a function of resistance and cannot be varied.

Abdominal Respiration

Compliance elements not grounded to atmospheric pressure are necessary for correctly implementing the respiration effect to the mock circulatory system. The splanchnic branch, located in the abdominal cavity, is the only systemic compliance grounded to a respiration pressure. In the body's abdominal cavity, the diaphragm pushes downward during inspiration, causing a rise in pressure here. This compliance dictates the relationship between the branch and abdominal cavity pressures, with higher compliance allowing for more interaction. The compliance in the splanchnic branch is provided by a hydraulic accumulator, which couples the branch to the abdominal pressure. A schematic diagram of the hydraulic accumulator is shown in Figure 8.

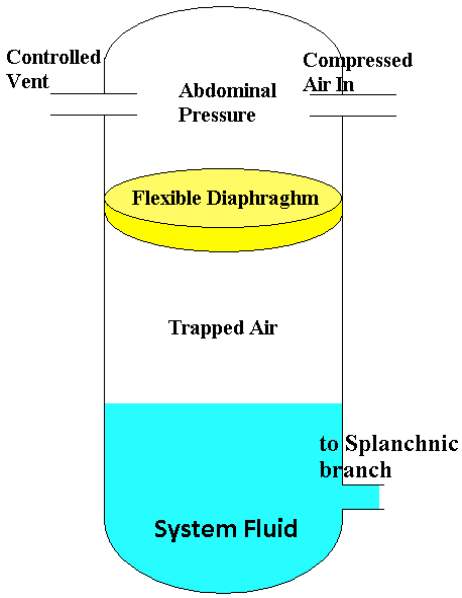

Figure 8: Splanchnic accumulator used for compliance

The accumulator shown in Figure 8 is attached directly to the splanchnic branch at its base. It is comprised of two chambers that are partitioned by a diaphragm. The splanchnic branch dictates the pressure in the lower chamber, and the upper chamber contains the time-dependent abdominal cavity pressure. A system has been installed to achieve realistic pressure waveforms in the abdominal cavity. A schematic of this system is shown in Figure 9.

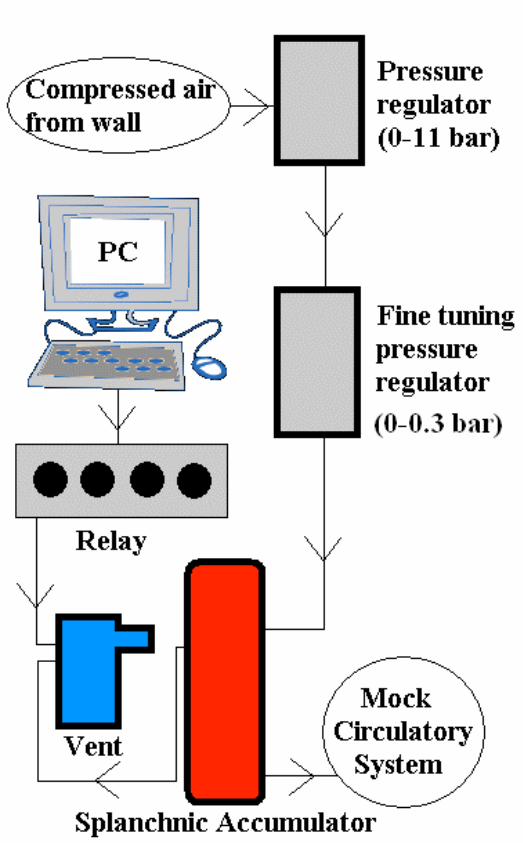

Figure 9: Abdominal cavity pressure system

The compressed air line in the laboratory is turned to a low pressure setting with a pressure regulator. Since the pressures in the abdominal cavity are extremely small relative to the range of the air pressures provided by this regulator, a series of regulators are used to step down the pressure. The final regulator enables for fine-tuning of the abdominal pressure amplitudes. An electronic solenoid valve is used to control the timing of the respiration. For the majority of the respiration cycle, the lungs and diaphragm are at rest in the body. During this time, air simply flows through the accumulator and is allowed to exit freely. The pressure inside the upper chamber remains near zero. At inspiration, a step voltage is outputted from the National Instruments NI

USB-6211 card and the solenoid valve closes. The abdominal pressure rises, and the diaphragm exerts downward force upon the splanchnic branch. The volume displaced by the diaphragm is the product of the abdominal pressure and the compliance of the diaphragm. The size and flexibility of the diaphragm is changed to vary the compliance. The solenoid valve opens to start expiration, and the pressure returns to near zero.

Figure 10: Small splanchnic accumulator

Figure 11: Large splanchnic accumulator

Figure 10 and Figure 11 show two of the accumulators used, depending upon the value of compliance needed for the lumped parameter model circuit. The smaller accumulator is used for compliances 0-4 mL/mmHg and typical of a child. The larger accumulator is used for higher compliance values; models of older patients need the larger accumulator, as this compliance increases with body size.

Thoracic Respiration

The other compliance in the mock circulatory system that is not grounded to atmospheric pressure is the pulmonary compliance. Not surprisingly, the most significant effects from respiration occur in the thoracic cavity where the lungs are located. The

interaction between the thoracic cavity and pulmonary branch pressures is modeled by the pulmonary compliance.

The two pulmonary arteries (left and right) run parallel through an airtight chamber that models the thoracic chamber. It is composed of a piece of clear PVC pipe held together by two acrylic endplates and threaded rods. The tubes enter via Swagelok fittings through the first end and exit though NPT barbs that are threaded into both sides of the plate. Two thoracic chambers were built in this study for different tubing sizes and are shown in Figure 12.

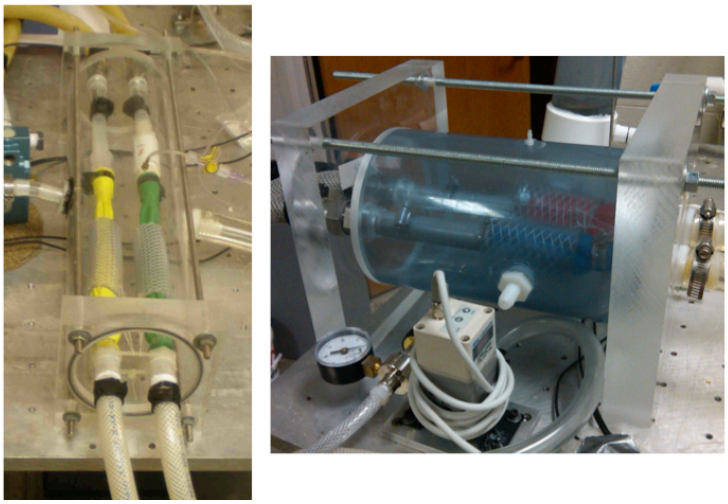

Figure 12: Thoracic chambers used for respiration

Flow enters the chamber through tubing that is connected to the balloons. The balloons have both ends cut off so that flow can pass through them. These serve as a compliant boundary between the pulmonary branch and thoracic cavity.

In the body, the diaphragm muscle pushes downward and expands the volume of the thoracic cavity during inspiration, creating a vacuum. The magnitude of this vacuum pressure is largely dependant upon age and activity level, but typically range from 0 to 4-10mmHg. The effects of exercise are not examined in this study, but they may significantly change the behavior in the TCPC (Hjortdal, 2003).

A system has been constructed to provide the thoracic chamber pressure, and is shown in Figure 13. The primary source of vacuum is the pump. The air receiver is used to keep the vacuum supply at a constant level, and serves as a reservoir.

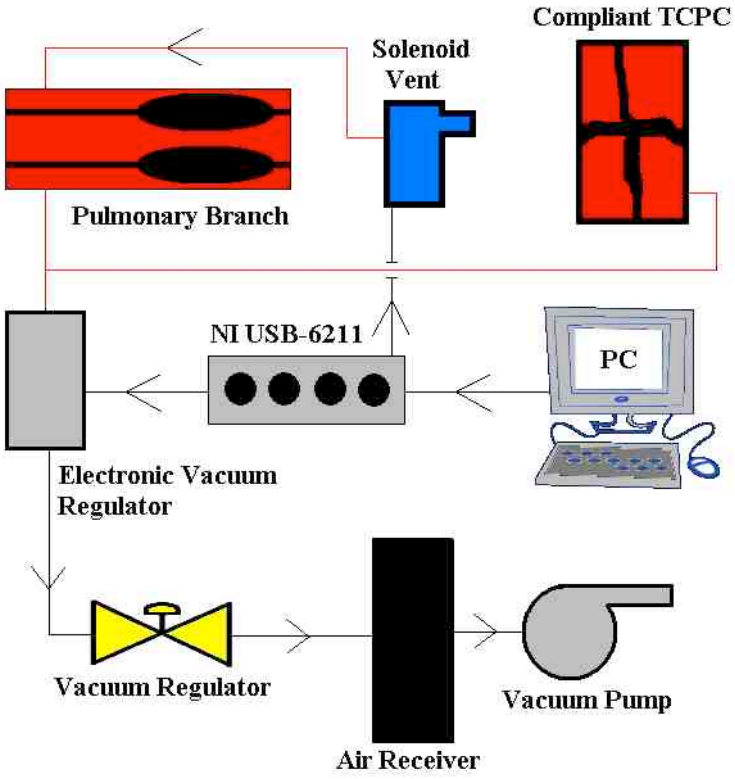

Figure 13: Thoracic cavity pressure system

A manual vacuum regulator controls the vacuum supply to the SMC electronic vacuum regulator. It is placed between the air receiver and electronic regulator. A buffered analog output signal from the DAQ system is used to help control the shape of the respiration curve. The SMC regulator is attached to its own power supply, and receives the signal. The amplitude of this signal can be adjusted for fine-tuning of the curve, along with the frequency. The breathing rate was kept between 18-25 breaths per minute. On the other end of the electronic vacuum regulator is the thoracic chamber. When inspiration begins, the vacuum regulator receives the signal and pulls vacuum on the chamber.

To achieve better waveforms, more venting is required than what is given by the electronic vacuum regulator. For this reason, a solenoid valve was used as a supplementary vent to the thoracic chamber. This solenoid valve opens at the end of the respiration cycle, and remains closed during inspiration. The chamber can return to atmospheric pressure at a faster rate with the additional vent. The output of the electronic vacuum regulator is connected to the thoracic chamber, but thoracic chamber pressure can also be imposed upon a compliant TCPC. If a rigid TCPC is used, the thoracic chamber pressure is only used to ground the pulmonary compliances.

In addition to the thoracic cavity pressure waveform, the pulmonary compliance must be adequately controlled. Placing a tube over the balloons restricts their expansion and controls the compliance. The size and location of the tube is adjusted to achieve the correct compliance.

Once the flow has passed through the thoracic chamber and pulmonary compliance elements, only the pulmonary resistance remains before exiting at the single atrium pressure. Most resistance in the pulmonary branch is in the arterioles. This mostly isolates the compliance of the capillaries from contributing to the input impedance. The resistance provided by the arterioles, capillaries, and veins get lumped together into the distal resistance. The distal pulmonary resistance is applied in the pulmonary veins of the system, as most of the compliance lies in the arteries.

Ideally, there would be a venous and arterial resistance in each branch that was tuned. It is deemed sufficient in this study to have the correct overall resistance and compliance in each branch of the system. The system is already greatly simplified as a lumped parameter model, so the original scope of the project must be kept in mind when considering the construction of this model.

TCPC Model

Each TCPC has a unique geometry based on the patient and circumstances during surgery. The geometry of the TCPC has a significant effect upon flow behavior; thus having a realistic geometry at the junction is essential to modeling the Fontan circulation correctly.

Using computer-aided design (CAD) and 3D solid modeling tools in conjunction with magnetic resonance (MR) images from Fontan patients, a digital file of the TCPC is created and used for a Rapid Prototyping (RP) process. Magnetic resonance imaging (MRI) is used to carry out magnetic resonance angiography (MRA), which allows for

non-invasive imaging of blood vessels. This results in a series of images contained in a digital DICOM (Digital Imaging and Communications in Medicine) format (Armillotta et al., 2007). An MR image of a TCPC taken from a Great Ormond Street Hospital Fontan patient is shown on the left side of Figure 14.

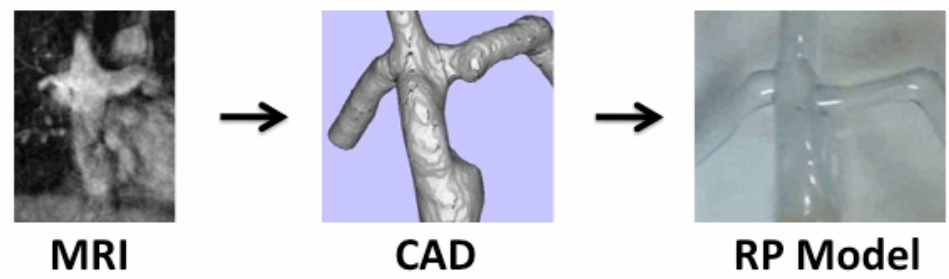

Figure 14: TCPC reconstruction method from MRI

One inherent difficulty lies in the fact that individual MR images are 2-D in nature, and are taken in slices about 5 mm apart (Chiulli, 2011). This limitation is overcome using adaptive control grid interpolation between images in the stack (Zélicourt et al., 2005), and reconstructing the image as a virtual 3-D model in MIMICS (Materialise Inc. Ann Arbor, MI). MIMICS is used to smooth the virtual model, which is then converted to an STL file. The triangular meshes that define surfaces within an STL file are overlaid with a series of nurbs patches in Geomatic Studio. An STL file representation of the TCPC is shown in the middle of Figure 14. The virtual 3-D model is then saved as an IGS file, which can be opened in SolidWorks, Pro/Engineer, or other solid modeling software packages (Zélicourt et al., 2005). From here, the models can be modified for connection or scaling purposes before they are fabricated.

Two fabrication approaches are taken. Semi-transparent compliant models are created using the PolyJet RP technique with FullCure930 TangoPlus material. This material can experience elongation up to 218% and has a Scale A hardness of 27. An example of a compliant TCPC model of this material is shown in Figure 15. This model exhibits a compliance of approximately 0.2 mmHg/mL. Rigid, transparent, water-resistant test sections were also created using stereolithography and the material DSM Somos WaterShed XC 11122. This material is strong and has a modulus of elasticity of over 2,000 MPa. It does not exhibit significant compliance, but its transparency is suitable for optical flow measurements.

Biologically, the TCPC lies within the thoracic cavity. If a compliant TCPC (shown in Figure 15) is being tested, thoracic chamber pressure is connected to an airtight box containing the TCPC in addition to the usual thoracic chamber in the pulmonary branch. Otherwise, the rigid TCPC is placed into an acrylic box that is built around it. The box contains an open top and aluminum rods that are threaded for fine adjustment through threaded holes that are tapped at the appropriate angles. A rigid, transparent TCPC and surrounding box are shown in Figure 16.

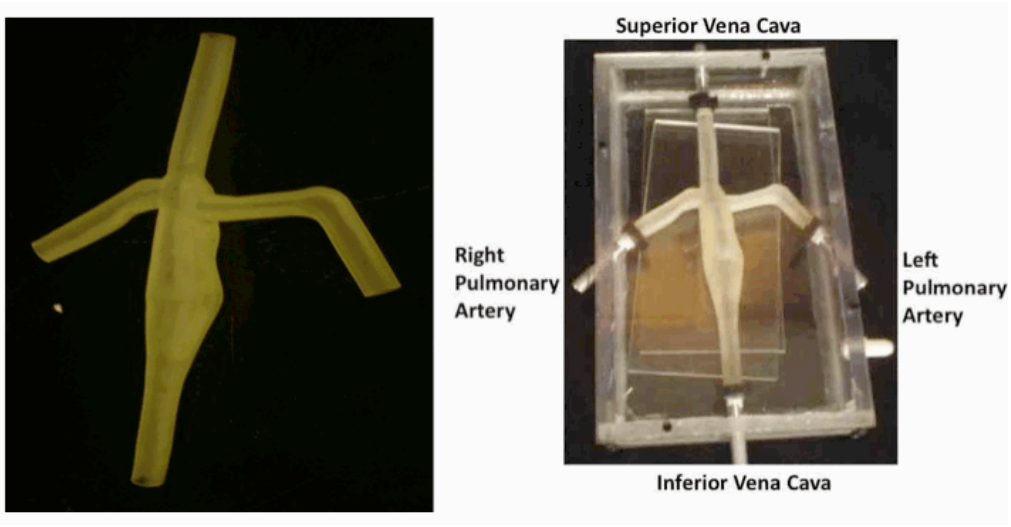

Figure 15: Compliant TCPC model and model mounted within an airtight box

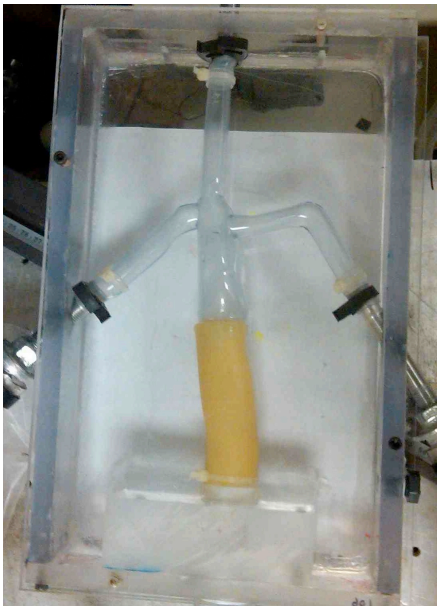

Figure 16: Transparent, rigid TCPC model mounted within an open box

Particle Image Velocimetry (PIV) Considerations

Certain aspects of the system were designed with the knowledge that particle image velocimetry (PIV) would be carried out. PIV is a method by which flow fields can be mapped experimentally within transparent structures. The fluid is seeded with tiny (10μm diameter) silver-coated hollow glass spheres. An Nd:YAG laser is used with a cylindrical lens to create a two-dimensional laser sheet. These spheres appear as tiny dots when illuminated by a laser sheet, which is directed to illuminate the plane of interest. The particle size is chosen such that it occupies several pixels. Two pictures are taken in rapid succession by a high-speed camera, and the location of dots can be correlated between the two images to map out the flow field.

In order to correct for image distortion due to refractive index mismatch between test section, surrounding air, and fluid:

- The TCPC test section is placed within a transparent box filled with a liquid with identical refractive index properties as the test section
- A test fluid blood analog having a matching refractive index is used. Two fluids, diethyl phthalate (DEP) and saturated sodium iodide (NaI) have been used with success.

The TCPC is submerged into a fluid of correct refractive index on the outside, in addition to the working fluid on the inside. For this reason, the TCPC is mounted within an open box and submerged within an index of refraction matching liquid. The angles of the pulmonary arteries in the TCPC require the laser to be brought in from the SVC side. Mirrors were used to direct the laser into the TCPC from the SVC-RPA side. For this

reason, a pentagonal box was constructed with an angled surface between the SVC and RPA connections to minimize light scattering. The laser beam is expanded into a sheet with a concave lens, and the laser slit is adjusted to control sheet thickness. The camera is mounted directly above the TCPC. The PIV setup is shown in Figure 17.

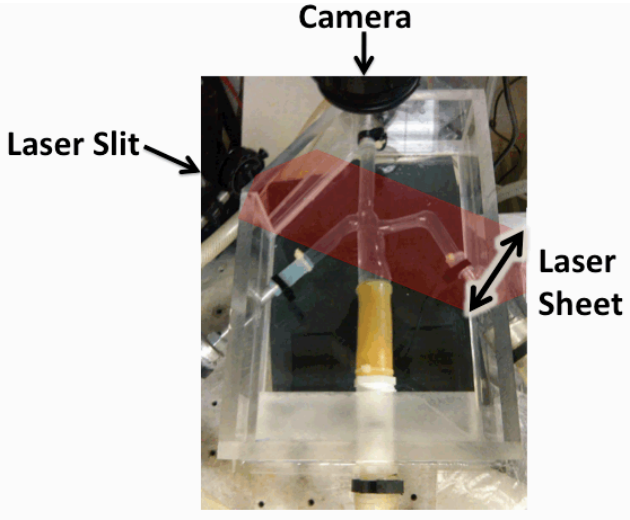

Figure 17: Particle image velocimetry (PIV) setup for TCPC model

The refractive index of the transparent TCPC ranges from 1.521-1.525, which was matched using a saturated solution of sodium iodide and water. A 64.8% by weight solution of sodium iodide at 25 degrees Celsius was used to achieve a refractive index of 1.501. Also tried was a solution of diethyl phthalate (DEP). The DEP worked well, and had a density closer to that of blood. Preliminary measurements using DEP were superior to that of sodium iodide. The DEP was not totally compatible with all system components, and would have required material changes in the system. So the NaI solution was used herein. This provided a near match, which could be improved with

higher solubility. If it were feasible to maintain the solution at 70 degrees Celsius, a 74.6% by weight solution would have created an exact match. Refractive index matching results in less surface deflection and image distortion. The resulting density of the fluid was 1.89 g/cm^3, and the particle density was 1.4 g/cm^3. Particles were added to the solution until there were an average of 5 particles within a typical interrogation window.

Mock Circuit Overview

The complete mock circulatory system is shown in Figures 18-20. Figure 18 shows the head tank that supplies the systemic arterial pressure to the system. The flow enters through the manifold and into the three systemic branches. Figure 19 shows the majority of the mock circulatory system. Included are all three systemic branches with their respective compliance elements, the TCPC and its connections, the pulmonary arteries, and the thoracic chamber. The balloons inside the thoracic chamber are the pulmonary compliance elements. The accumulator pressure supply and vent are also shown. Figure 20 shows the thoracic chamber and the pulmonary veins. The pulmonary resistance is controlled with the valves located in the pulmonary veins. The exit pressure for the system is controlled with the single atrial pressure head tank. The fluid is drained to a reservoir where it is then pumped back to the systemic arterial pressure head tank.

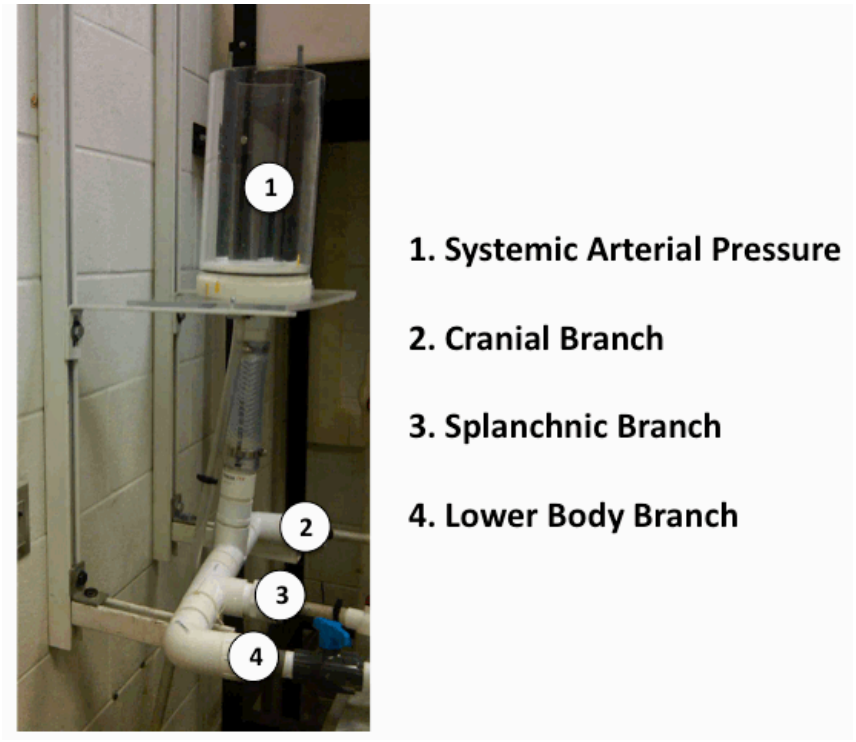

Figure 18: Front end of mock circulatory system

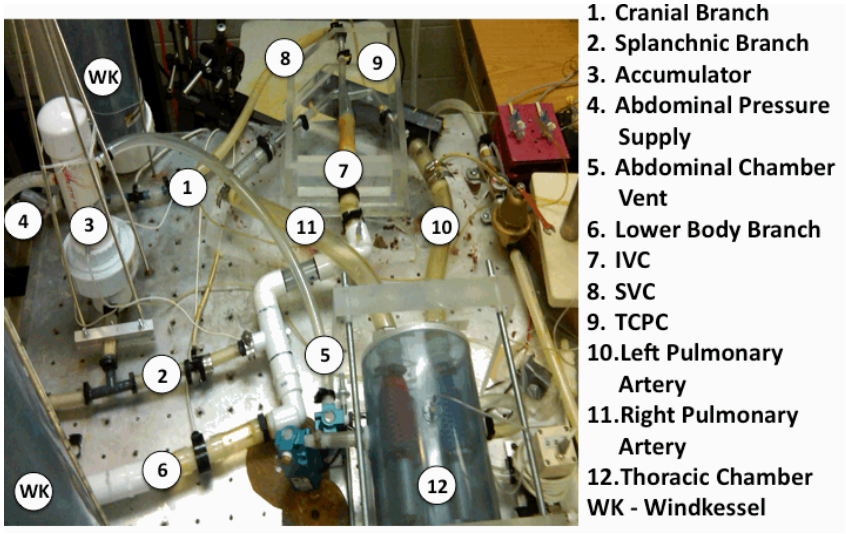

Figure 19: Center of mock circulatory system

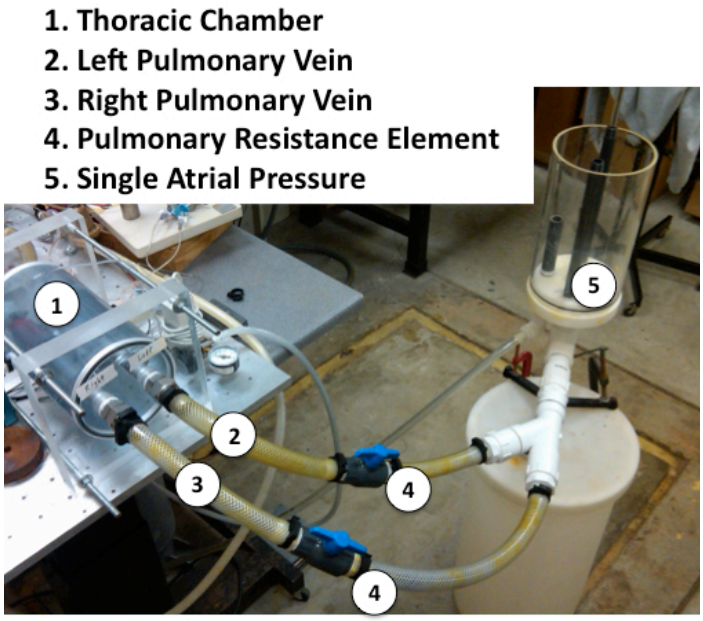

Figure 20: Back end of mock circulatory system

The mock circulatory system is based upon a lumped parameter model of the Fontan circulation and a patient specific 3-D test section. The lumped parameter models can be adjusted to match the circulation of any Fontan patient, and the test section can be made from clinical images of the patient. As such, the mock circulatory system is a physical realization that can be tuned to match the Fontan circulation of any patient.

CHAPTER THREE

METHODS OF SYSTEM TUNING

Introduction

Each parameter in the network model has a specified value that is determined by clinical measurements. These values are physically realized in the mock circulatory system through various components. The key to achieving realistic results within the mock circulatory system is accurate tuning of these individual components within the system. Inaccuracy of one component can be responsible for incorrect behavior throughout the entire system. Much care is taken to tune these individual components within the system.

There are many different methods by which resistance and compliance can be measured. However, it is important to be sure that the method used to tune a particular element makes assumptions that are valid when this element is operating within the mock circulatory system. This assures that a measurement made during the tuning stages can be trusted during system operation.

Measurement Systems

Pressure measurements are made using BD DTX-Plus pressure transducers attached to tube pressure taps and connected through fluid-filled lines. The transducers are mounted at a zero reference height assigned and used for all system height measurements. The frequency response of these transducers includes undamped frequencies up to 10 Hz, which is sufficient for this study. The range includes pressures up to 110 mmHg. Liquid-side pressure measurements are made in the following locations: in the IVC and SVC just upstream of the TCPC, and in the RPA and LPA just downstream of the TCPC. Air-side pressure measurements are made in the thoracic chamber and in the upper chamber of the accumulator, which houses the abdominal chamber pressure. Each pressure is measured by a wall tap and is connected to the system by fluid-filled catheter lines.

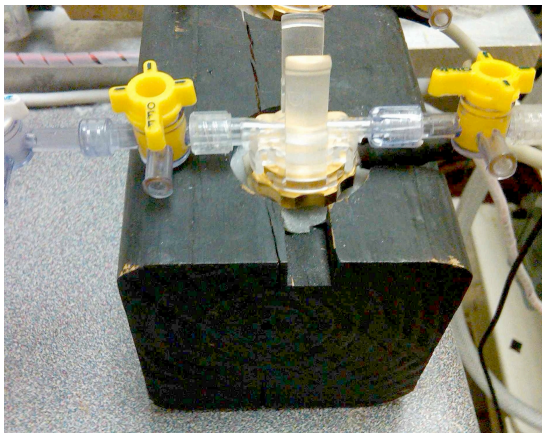

Figure 21: Pressure transducers with mount at zero-datum height

The transducers are fastened down by Velcro pads and are connected to catheter lines that attach to 2 mm diameter wall mounted pressure taps, as shown in Figure 21. Liquid-side transducers are bled of all air within the lines using a syringe.

Each transducer signal is passed through a Measurements Group 2120A millivolt direct-through amplifier for null zero adjustment and gain. The DC offset is adjusted periodically to maintain zero output at zero gauge pressure, as the electronics have a tendency to drift when not in use. The pressure transducers are calibrated by varying the fluid elevation within the catheter tubing and recording the output signal. Each signal is measured using a National Instruments Model NI-USB-6211 analog measurement channel. Additional gain is applied in the LabView 2010 virtual instrument, and is adjusted to give output units of millimeters of mercury (mmHg). A low-pass filter with a cutoff frequency of 8 Hz is also applied in LabView for noise reduction.

All flow measurements are made with Carolina Medical EP-series electromagnetic flow probes, such as in Figure 22. The flow probes are connected to a Carolina Medical FM501 Square-Wave Electromagnetic flow meter, shown in Figure 23. Output signals from the flow meters are measured using an analog measurement channel of a National Instruments USB-6211 data acquisition module. The sizes of probes depend upon where they are being used. For this experiment, EP640 and EP680 probes are used for ½" (12 mm) and 1" (25 mm) inner diameter tubes, respectively. The cranial and splanchnic branches use ½" (12 mm) tubing, while the lower body branch uses 1" (25 mm) tubing. These probes require use of a conductive fluid, so salt is added to the working fluid.

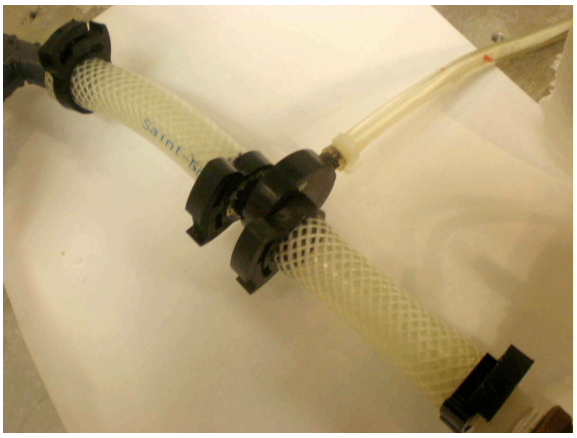

Figure 22: EP640 Electromagnetic flow probe

These flow probes require a ground to complete the circuit, and must also be in contact with the fluid. Since there is typically three flow probes throughout the system – one in each systemic branch – multiple grounds are used. The grounds must be close enough to the flow probe, usually within centimeters.

Figure 23: FM501 Electromagnetic flow meter

Only one flow probe is monitored at a time. A low-pass filter with a cutoff frequency of 10 Hz is used to eliminate unnecessary noise in the flow signal. Each flow probe has a "Probe factor" included from the factory, a gain which is set on the FM501.

Before use in the system, the flow probes are individually calibrated with a catch-and-weigh method. The gain adjustments relative to the provided probe factors are very small; the calibrations were merely a fine-tuning. The additional calibration is probably not necessary in basic applications of flow measurement, where a high degree of accuracy is not necessary. In this application, it was an additional step taken to ensure the best possible tuning of the system.

All signals are acquired and stored using a LabView 2010 virtual instrument designed for the mock circulatory system. Signals are acquired at a rate of 80 Hz with a resolution of $1x10^{-5}$ units. The output units, depending on the measurement, are liters per minute (LPM), millimeters of mercury (mmHg), or volts.

Systemic Arterial and Single Atrium Pressures

The first element of the mock circulatory system is the systemic arterial pressure, which drives the flow through the system relative to the atrial pressure. The tank height is adjusted by loosening the fastening screws along the support rails for the head tank. The reference height used throughout this study is about 10 cm above the table. Based upon the systemic arterial pressure given in the lumped parameter model that is being used, the height of the head tank is adjusted to the appropriate height based upon the conversion factor between millimeters of mercury and inches of water.

To show some setups used, three simplified lumped parameter models are chosen as examples. Each lumped parameter model contains a systemic arterial pressure that is used as the source pressure to drive the system. The corresponding elevation of the head tank above the reference height is also shown. The small child and adolescent simplified lumped parameter models are based upon the Corsini model (Corsini et al., 2010), and the young adult model is based upon clinical data from a 17-year old patient from Great Ormond Street Hospital. The small child and adolescent models are based on body surfaces areas of 0.67 m^2 and 1.38 m^2, respectively. The measured body surface area of the young adult patient was 1.74 m^2. These models are shown in Table 1 and are referenced throughout the study.

Table 1: Systemic arterial pressures

Lumped Parameter Model	Systemic Arterial Pressure (mmHg)	Tank Elevation Above Reference Height (in.)
Small Child	44.6	23.87 (606.29 mm)
Adolescent	45.2	24.19 (614.43 mm)
Young Adult	41.0	21.94 (557.27 mm)

These simplified models used for the laboratory system are representative samples of three different age groups. The difference in head tank heights (systemic arterial pressure and single atrium pressure) creates the potential for flow to occur throughout the system. A higher head tank here will provide higher potential for flow. The single atrium pressure is 6.4 mmHg for all models, and is provided by the lower head tank at the end of the system.

Resistance

The most important elements that are tuned in the system are the cranial, splanchnic, lower body, and pulmonary branch resistances. Each branch contains an arterial and venous resistance. The systemic resistance elements are placed on the arterial side in the systemic branches. This is reasonable as the systemic venous resistances are very small compared to the arterial resistance. The pressure drop (mmHg) per flow rate (mL/s) gives a resistance with units of (mmHg*s/mL); this is used throughout this study. There are many sources of resistance within a branch other than the valve and/or laminar flow element. These sources can be lumped together by tuning the resistance across the entire branch, even though the valve and/or laminar flow element will contribute most of it.

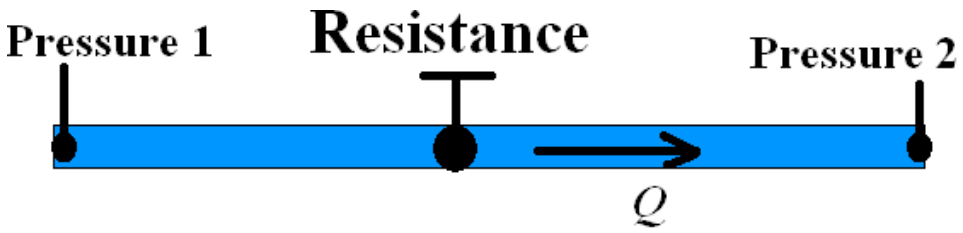

Figure 24:Measuring resistance within a branch

One branch is tuned at a time, and two pressures and one flow rate are required to measure resistance (shown in Figure 24). When tuning the systemic resistances, the upstream pressure is assumed to be constant at the systemic arterial pressure.

Increasing resistance within a branch (closing the valve) decreases flow rate and downstream pressure. The upstream (of the systemic branches) pressure is held constant by the drain in the head tank. The downstream pressure measured is one of the TCPC

pressures. If one of the IVC-feeding branches is being tuned, the pressure on the IVC side of the TCPC is used. If the cranial branch is being tuned, then the pressure on the SVC side of the TCPC is used as the downstream pressure.

There are three branches in parallel, which results in more complex behavior. Opening a valve increases flow and pressure downstream, which in effect decreases the flows in the other branches. For this reason, the TCPC pressure target must be known before any tuning takes place. For correct resistance tuning, the flow rate in a single branch must be achieved at the same time as the correct downstream pressure. The upstream pressure does not change.

The correct TCPC pressure is calculated from circuit analysis. The entire circuit is reduced to one equivalent resistance in order to determine the cardiac output, or the total system flow rate. From here the flow rates through each pulmonary artery are determined by the ratio of their resistances. Based on their resistances, the pressure drops across the pulmonary arteries are determined. From knowing the single atrium pressure from the lumped parameter model, this pressure drop is used to determine the correct TCPC operating pressure.

When the resistances are tuned, the pulmonary resistance is the last thing to be set. This is because the pulmonary resistance elements are used to vary the pressure in the TCPC to achieve the correct tuning in the other branches. Since one branch is tuned at a time, there is only one combination of systemic and pulmonary resistance that will simultaneously give the correct flow rate through the branch and the correct TCPC pressure. Once a branch is tuned, the flow in that branch should remain the same as long

as the TCPC pressure is correct. This is how multiple branches can be tuned. Table 2 gives a guide used on how the resistance is iterated based upon whether the flows and pressures are too high or too low.

Table 2: Resistance Tuning Procedures

	TCPC Pressure Too High	**TCPC Pressure Too Low**
Flow Rate Too High	Increase Systemic Resistance	Increase Pulmonary Resistance
Flow Rate Too Low	Decrease Pulmonary Resistance	Decrease Systemic Resistance

Tuning of the resistances is an iterative process. The adjustments are made until either the TCPC pressure or flow rate becomes correct. It is either a matter of taste or of which item happens to become correct first. Assuming either the TCPC pressure or the flow rate is correct, the actions in Table 3 are carried out based upon the conditions present.

Table 3: Resistance Tuning Procedures (continued)

	Other Quantity Too High	**Other Quantity Too Low**
TCPC Pressure Correct	Increase Systemic Resistance	Decrease Systemic Resistance
Flow Rate Correct	Increase Systemic Resistance	Decrease Systemic Resistance

Either resistance could be adjusted, but it is better to adjust the systemic resistance since it is the parameter being tuned here. The pulmonary resistance is actually not being tuned during this process; it is simply being manipulated to achieve the correct TCPC pressure as more branches are brought online.

Once the systemic branches are tuned, attention can be turned to making sure the TCPC pressure is always correct. As long as the TCPC pressure is correct, then the pulmonary resistance is correct by default. When the system is taken down or drained, the only tuning required is to reassure that the TCPC pressure is correct. Unless something is adjusted, the systemic branches can be trusted to have the correct flow rates. The tuning is deemed sufficient once the pressures are within 0.1 mmHg, and the flow rates are within 0.02 LPM of the expected values. Table 4 gives system resistances (mmHg•s/mL) in several simplified lumped parameter models.

Table 4: Resistance values (mmHg•s/mL)

	Small Child	**Adolescent**	**Young Adult**
Lower Body Arterial	3.79	1.26	0.380
Lower Body Venous	0.108	0.032	0.010
Splanchnic Arterial	9.135	4.716	1.425
Splanchnic Venous	0.094	0.0486	0.015
Cranial Arterial	1.75	1.266	1.059
Cranial Venous	0.108	0.006	0.049
Pulmonary Arterial	0.077	0.042	0.038
Pulmonary Venous	0.163	0.074	0.067

Table 4 shows three different simplified lumped parameter models. The resistances decrease with age, attributed to larger vessel and body size. The magnitude of blood flowing to the brain remains relatively constant from birth into adulthood, compared to the other branches. The splanchnic and lower body branches experience large increases in blood flow, reflected in the models as a large reduction in resistance.

Windkessels

The resistances dictate the steady flow behavior. However, the compliance and inertance dictate the transient behavior. The compliance is the primary element used in this study to model the transient flows and pressures resulting from respiration. Inertance is simply reduced to a manageable level in the system so that it does not significantly dampen the flows or accentuate the pressures differentials.

Each of the systemic branches has one compliance element per branch, while the pulmonary branch has two. The cranial and lower body branch compliances are grounded to atmospheric pressure, and this is provided by windkessels. Adjusting the volume of air in the windkessel controls the amount of compliance provided.

Figure 25: Windkessel compliance element

Figure 25 shows a windkessel connected to the system. The air volume is adjusted by moving either the test ball or fluid level. Venting the windkessel with a Schrader valve changes the fluid level. The volume of air necessary to achieve certain compliance is calculated using Equation 2.12. The gage pressure within the windkessel is estimated by leaving it open to atmosphere and measuring fluid level. Since absolute pressure is used in Equation 2.12, any error associated with the estimate is relatively small.

The windkessels characterize how the system responds to the disturbances caused by respiration. The manner in which systemic branches respond to respiration is mostly due to the tuning of the compliance elements. A systemic branch with higher compliance will more easily accommodate changes in volume, and thus, of flow rate. A branch with no compliance is limited by the mass balance of what goes in and out of the branch, with no change in volume occurring. Such a branch would exhibit relatively constant flow and more oscillatory pressure. The most exaggerated case is of infinite compliance, or a frictionless piston. Here, the volume of the branch would keep increasing and increasing without change to the pressure. The relationships between the compliances determine where respiration has the greatest effect.

When respiration occurs, the pulmonary compliance elements change volume as a result of the thoracic pressure. This extra volume of fluid must come from somewhere, and the overall systemic compliance plays a large role in determining this. With large systemic compliance, there is a stronger proportion of the extra volume of fluid coming from the upstream systemic branches. Here, the increased flow oscillation relieves some of the pressure oscillations in the TCPC. With lower systemic compliance there tends to

be higher TCPC pressure oscillation. This is because the upstream systemic branches cannot change in volume as easily.

Table 5: Windkessel compliance values (mL/mmHg)

	Small	**Adolescent**	**Young Adult**
Lower Body	1.322	3.76	12.46
Cranial Compliance	2.15	2.75	3.29

Table 5 shows windkessel compliance values (mL/mmHg) from three simplified lumped parameter models used to tune the system. These compliances scale with body surface area, and rise with age. The lower body compliance increases at a much higher rate than that of the cranial branch. The lower body grows much more with age than does the head.

Splanchnic Compliance

The compliance element in the splanchnic branch is grounded to the abdominal cavity pressure. A homemade hydraulic accumulator has two separate chambers partitioned by a flexible membrane to provide this compliance. The compliance of this membrane is critical for two primary reasons. The first reason is that it controls the volume displacement during respiration. Higher compliance within the accumulator will magnify the respiration effect, and vice versa. The second reason is that the accumulator provides compliance after respiration has ended, just as the windkessels do.

The splanchnic compliance is tuned by varying the elasticity of the membrane within the accumulator. A more flexible diaphragm will increase the compliance, as a change in pressure will cause it to distend more.

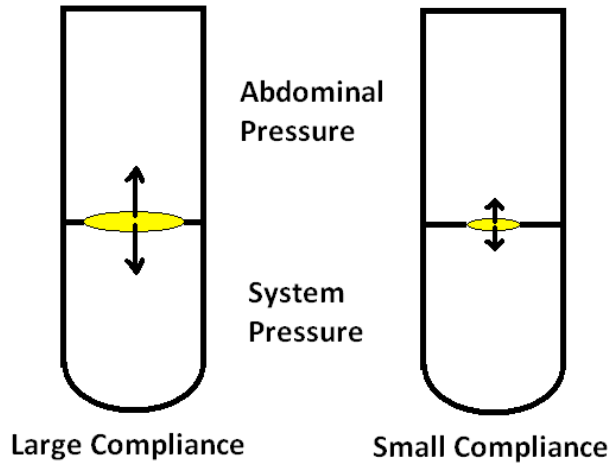

Figure 26: Varying diaphragm diameter in accumulator

Varying the free (unrestricted) diameter and thickness of the membrane changes the elasticity, as shown in Figure 26. A membrane with a larger free diameter will be more elastic and compliant, and one with a smaller free diameter will be less compliant. The range of free diameters used for these latex membranes is roughly 1-4 inches. The smaller of the two accumulators allows for a diameter up to about 1.5 inches, while the larger accumulator allows a diameter up to 4 inches. The latex sheet must be large enough to completely cover the inner diameter of the pipe, or the two chambers will not remain partitioned. The diaphragm motion is restricted by placing a corkboard on either

side of the latex and cutting a hole in the corkboard. The holes in the corkboard are made larger to increase compliance.

If the correct compliance cannot be achieved by varying the free diameter of the diaphragm, the thickness of the latex sheet used is also changed. A thinner sheet provides more compliance than a thick sheet. Latex sheets used for the accumulator compliance vary in thickness from 0.15 to 1 millimeters. Between the thickness of the diaphragm and the opening size in the corkboard, any reasonable compliance value from the simplified lumped parameter model can be iterated. It is important that the compliance is tuned over the same range of pressures that it experiences during system operation. The typical splanchnic branch pressures range from 15-20 mmHg, which pushes the diaphragm upward. If the abdominal pressures are 0-2 mmHg, then the tuning is carried out in the range of 13-20 mmHg to cover the entire spectrum of possible pressure differentials across the membrane. With higher branch pressure, the membrane becomes more stretched, giving it less compliance. This condition is replicated during the tuning of this compliance to achieve the correct parameters.

The tuning procedure for the accumulator involves varying the pressure in the lower chamber and measuring the volume displacement of the diaphragm. The pressure is added to branch chamber because it always has a higher pressure during operation. From the data, a P-V diagram is created. The slope yields the compliance. The compliance of the accumulator is a function of pressure, and may not necessarily be constant. If the slope changes a lot over the range of pressures, then the slope is only taken over the range of operable pressures in the system.

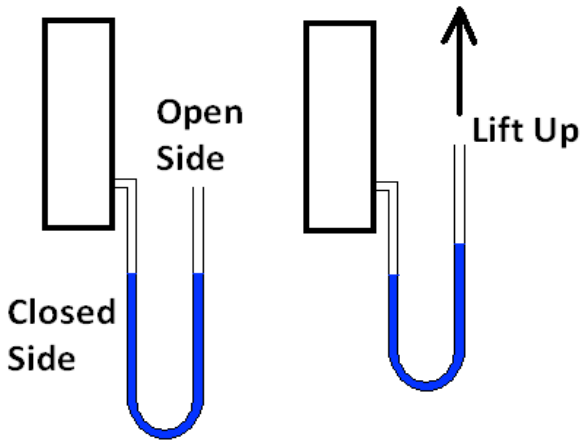

Figure 27: Tuning the splanchnic accumulator

The accumulator is attached to a tube with filled roughly halfway with water. One end of the tube is connected to the lower chamber of the accumulator and the other end is left open to atmosphere. The tube is lowered down below the accumulator and made into a U-shape, creating a manometer. This setup is shown in Figure 27. The initial fluid heights are measured, and should be the same. The free end of the tube is lifted several centimeters. It is important that the tube remains in a U-shape during tuning. This is because volume changes are assumed to only take place at the free surface of the water and in the balloons. Any movement of the tube during the tuning process could invalidate this assumption. Both water heights are measured again. From these two measurements, the pressure and volume change can be determined. The pressure within the accumulator is simply the difference in height between the two water columns: the classic pressure measurement. The change in the fluid's height on the closed side can be used to estimate the change in volume. If the water has moved up 1

centimeter on the closed side, then this implies that a corresponding volume of air has been pushed into the accumulator. An initial volume of 0 mL is taken, as the starting volume is both difficult to determine and not needed for the compliance calculation. Once these measurements are made, the tube can be lifted further to repeat the process. It is repeated until enough measurements are made to have confidence in the slope of the line, and until the numbers over correct range of pressures have been taken.

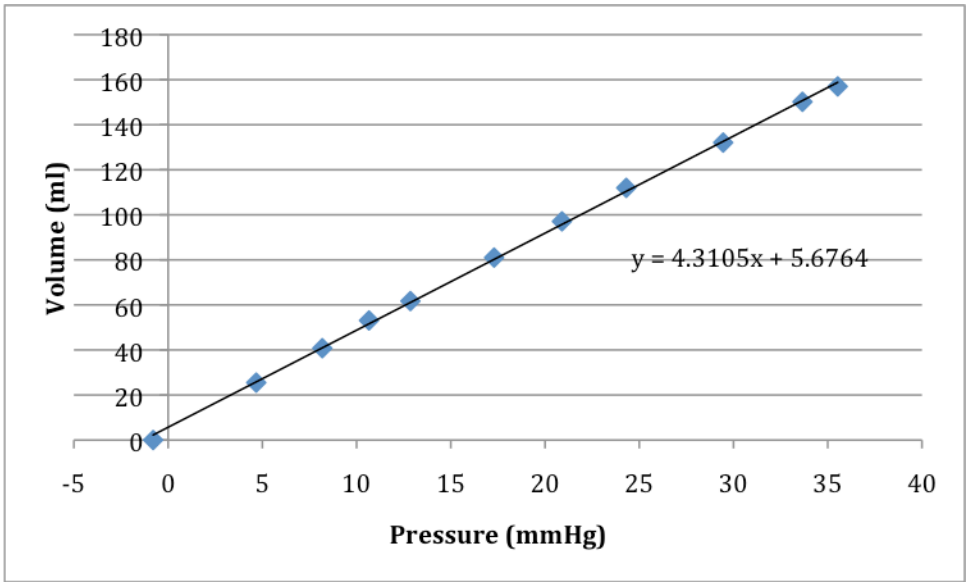

Figure 28: Sample accumulator compliance curve

Figure 28 shows a P-V curve constructed from an iteration of the compliance tuning. In this particular case, the compliance remains relatively constant; that is, the curve is linear. If the compliance resulting from this test is not the desired value, changes are made to the accumulator and another iteration is carried out.

Table 6: Splanchnic compliance values (mL/mmHg)

	Small Child	Adolescent	Young Adult
Splanchnic Compliance	2.168	5.08	16.81

The splanchnic compliances (mL/mmHg) are shown in Table 6 and scale positively with body size. The rate of growth is much higher than the cranial compliance, which is attributed to the fact that the midsection grows at a much higher proportion than the head.

In general, the models used for small children and infants contain very small compliances. These small compliances reduce the damping provided to the system. This can lead to unnecessary oscillations in flow, especially during the resting portion of the respiration cycle. The windkessels are compliances grounded to atmospheric pressure, and serve as a type of low-pass filter to the system. The accumulator is also grounded to atmospheric pressure during the resting period of the respiration cycle, and can also act as a filter. To increase the damping/filtering, resistance can be added between the compliance element and the branch to which it is connected. Figure 29 shows this being accomplished with a clamp.

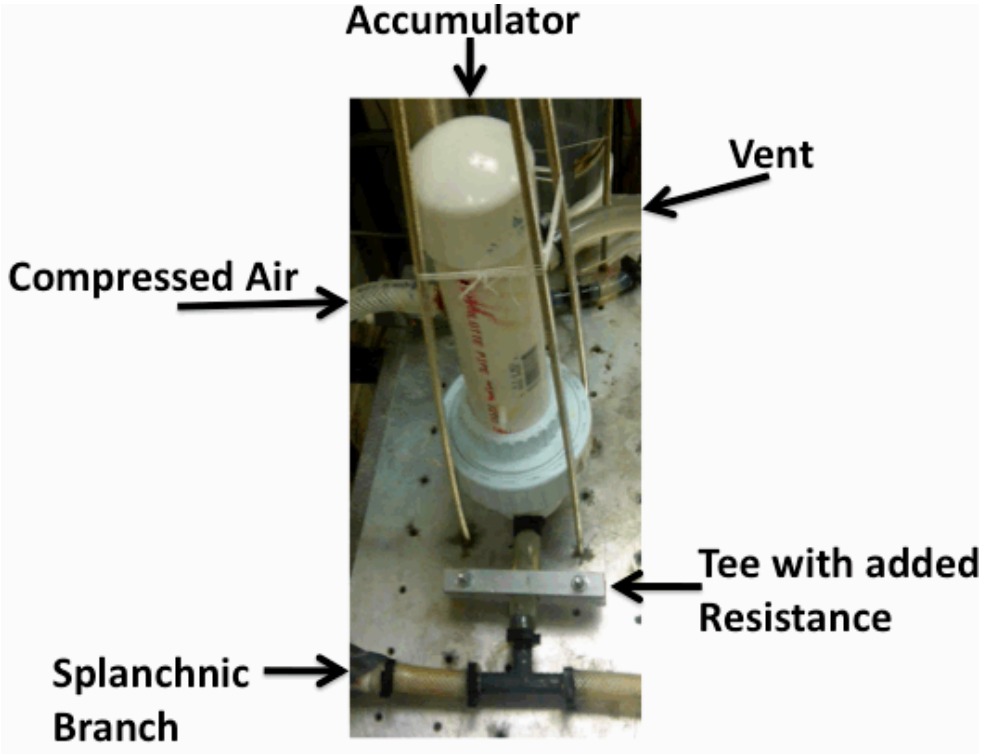

Figure 29: Accumulator with added resistance

This does not change the respiration effect, the compliance, or the resistance within the branch; but it helps to increase damping if the compliances are low in the model.

Pulmonary Compliance

To complete the respiration effect, the pulmonary compliance is grounded to the thoracic cavity pressure. This couples the pulmonary branch and thoracic cavity pressures. This compliance holds the biggest influence over the respiration effects upon the TCPC and systemic venous circulation. Higher pulmonary compliance increases the respiration effect upon the system. All flow in the system passes through the thoracic

cavity. Balloons are used on both of the pulmonary arteries and provide sufficient compliance for any reasonable value within a lumped parameter model. Since there is no reasonable way to vary the thickness of the balloons, the compliance is varied by limiting the extent to which the balloons can expand. This involves placing a rigid object, usually a tube or pipe, around the balloon. A tight-fitting object significantly reduces the compliance, as the balloon cannot expand much.

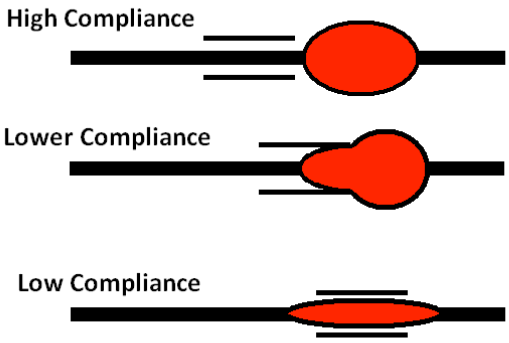

Figure 30: Pulmonary compliance tuning concept

An appropriately sized tube is selected and moved along the axis of the balloon to vary the compliance, shown in Figure 30. By changing the position of the tube, different proportions of the balloon can be left free to expand while the tube restricts the remaining section. A tight fitting tube that covers the entire balloon lowers the compliance to its lower limit, while the upper limit is reached with no restriction. The tubes are held in place by tying them to either a hose clamp or the side of the chamber with a string. Varying the lengths of these strings adjusts the location of the tubes, and hence, the compliance.

The process for tuning the pulmonary compliance begins with taking apart the thoracic chamber entirely, so that a tube can be fitted over the balloon. An initial guess is made for the size and location of the tube. The tubes are placed in their assumed-correct position and tied down to secure them in place.

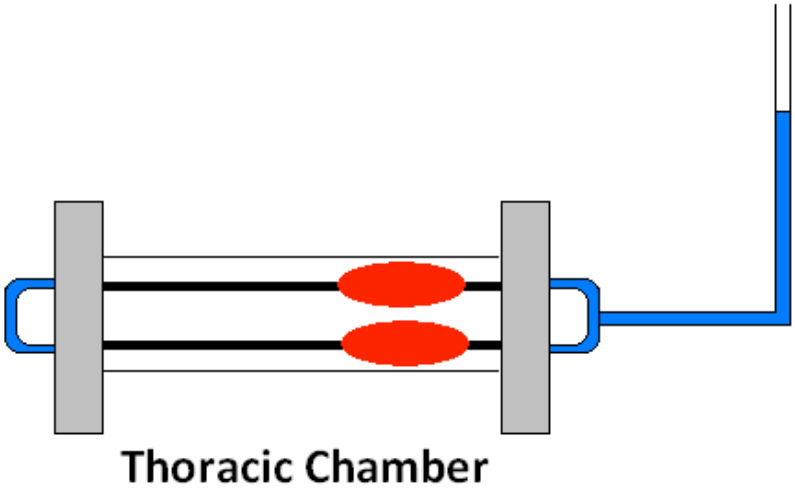

Figure 31: Thoracic chamber and pulmonary compliance tuning

The thoracic chamber is then reassembled and filled with water. There are four ports: right and left pulmonary arteries and veins. One side (either the venous or arterial side) is plugged by simply connecting a tube from the left to right side. At the opposite end of the chamber, the two branches are brought together with a tee and are connected to a single tube. The entire arrangement is filled with water until the water is a desired height above the midsection of the thoracic chamber, shown in Figure 31. The reference elevation is taken at the midpoint of the balloons, as they are side-by-side horizontally. The elevation of the water level is taken, and then 10mL of water is added to the top of

the tube that is above the rest of the chamber. The elevation of the water is taken again and the process repeats until enough points have been taken.

Accurate pressure and volume change measurements are necessary to calculate the compliance. The initial volume could be determined, but it is not needed. It is taken to be 0mL, and the change in volume is taken from there. The change in volume in the compliance element is not as simple as adding 10mL to determine the volume. From knowing the inner diameter of the tube, the change of volume in the balloons can be calculated by measuring the change in height of water after adding the 10mL. If the balloons remained the exact same volume, the water level in the tube would raise a height that corresponded exactly with 10mL of volume (for the given inner diameter of the tube). If the rise of water is less, it is safe to assume the rest of the volume went into the balloons as they expanded. The pressure measurement is simply determined by the inches of water above the center of the balloons in the chamber. This is converted into the standard units (for this study) of mmHg.

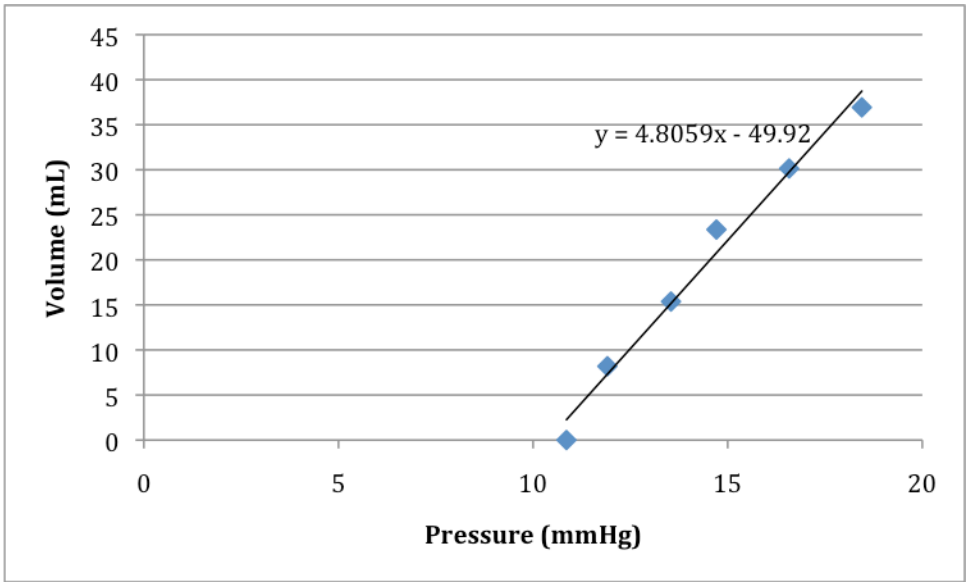

Figure 32: Sample pulmonary compliance curve

Figure 32 shows a P-V diagram, or compliance curve generated while tuning the thoracic chamber compliance. The curve's slope yields the compliance value in units of mL/mmHg. As with the accumulator, it is important that the compliance is tuned over the same range of pressures that are experienced during operation. There is not a pulmonary branch pressure measurement made inside the thoracic chamber during operation of the system, but the pulmonary artery-side TCPC pressure is nearby and can be taken to be close to the pressure. The amplitude of respiration to be used during the operation is also considered. If 4 mmHg vacuum is to be pulled on the thoracic chamber, and the average branch operating pressures are 10-15 mmHg, then the compliances are tuned over the 10-19 mmHg range. This covers all possible pressure differentials across the compliant boundary. The pulmonary compliance elements tend not to have constant compliance over a range of pressures. This makes it necessary to only calculate slope

over the appropriate range. The position of the restricting tubes is iterated until a match is found. Table 7 shows the pulmonary compliance (mL/mmHg) from several simplified lumped parameter models.

Table 7: Pulmonary compliance (mL/mmHg)

	Small Child	**Adolescent**	**Young Adult**
Pulmonary Compliance	1.39	4.60	5.01

The pulmonary compliance rises with increasing age, as the size of the lungs increase as a Fontan patient grows older. In some cases, the left and right pulmonary compliances are specified separately to account for the larger size of the right lung.

Respiration Pressures

The last items tuned within the system are the respiration pressures. These are tuned last because they can be easily adjusted during system operation. The positive pressure used for the abdominal cavity pressure is tuned using a series of pressure regulators. Since the solenoid vent is only a discrete on/off switch, the signal output from the computer cannot be adjusted to change the pressure amplitude. The correct amplitude can be achieved with the regulators. Typically the abdominal pressure amplitude is half that of the thoracic pressure (Corsini et al., 2010). Depending upon the age, this can be from 0-2 mmHg for a small child up to 0-5 mmHg for an adult. The thoracic chamber pressure is tuned via a vacuum pressure regulator that controls the supply vacuum to the electronic vacuum regulator. The electronic vacuum regulator requires a certain level of vacuum supply to operate, so if need be the amplitude of the analog signal sent to the regulator can also be adjusted. This will enable the vacuum supply to be left high enough for it to operate. The amplitudes range from 0-4 mmHg vacuum for a small child to 0-10 mmHg vacuum for an adult.

Having the mock circulatory system tuned to the correct parameters is essential for achieving realistic results. Any of these parameters can be changed to adjust the system to a different patient, or to troubleshoot results. The system has been designed such that it can achieve any realistic value for the resistances and compliances specified in a lumped parameter model.

CHAPTER FOUR

RESULTS AND DISCUSSION

Settings and Inputs

The mock circulatory system contains elements that are physical realizations of parameters in the lumped parameter model. These parameters are tuned to a specific value for a particular patient model. The flow in the system is driven between systemic arterial and atrial pressures. The remaining inputs to the system are the time-dependent respiration curve pressures.

The system was tuned to the small child model with a rigid TCPC (Figure 16) for all results in this chapter, unless otherwise stated. This includes a systemic arterial pressure of 44.6 mmHg (Table 1), and a single atrium pressure of 6.4 mmHg. The resistances used for the small child model are shown in Table 4, and the compliances used are shown in Table 5-Table 7. The respiration settings used in the small child model include abdominal chamber pressures from 0-2 mmHg, and thoracic chamber pressures from 0-4 mmHg vacuum. This corresponds with the amplitudes given in the Corsini model (Corsini et al., 2010). The respiration was set at 25 breaths per minute, or a frequency of 0.417 Hz. This gives a respiration cycle period of 2.4 seconds. Figure 33 shows the respiration inputs to the system, including thoracic (TC) and abdominal chamber (AC) pressures.

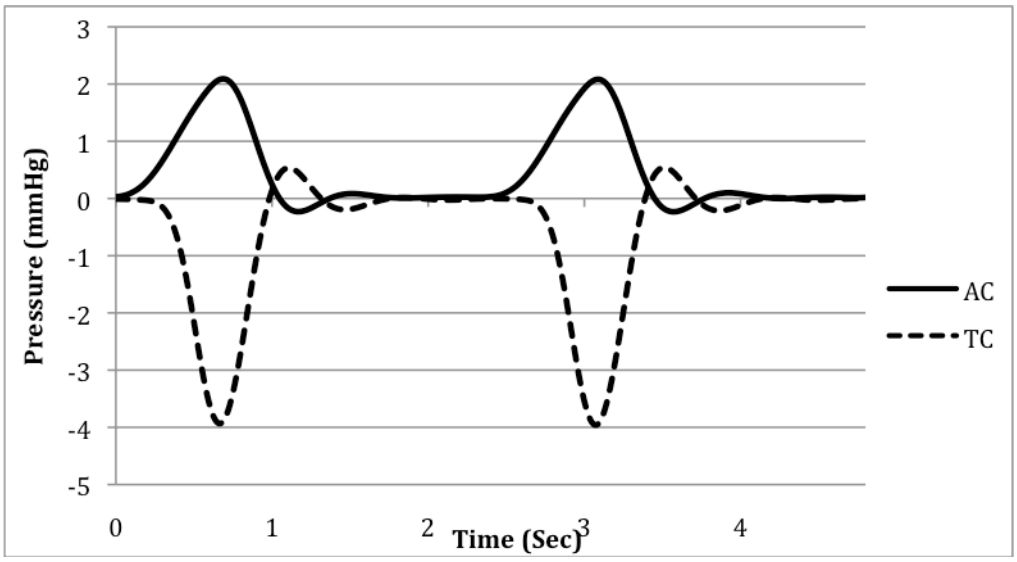

Figure 33: Respiration inputs to system in small child model

Two respiration cycles are shown in Figure 33. The cycle begins with inspiration, marked by a decrease in the thoracic chamber pressure. Abdominal pressure also increases during this time. Expiration begins when the curves reach their maximum or minimum. From this point, the thoracic chamber pressure rises towards atmospheric pressure, while the abdominal pressure falls back towards atmospheric pressure. The two curves are adjusted to be in phase. These pressures act upon their respective compliances, simulating the effects of respiration.

The respiration inputs to the system can be easily adjusted to different amplitudes and waveforms. The young adult model has respiration amplitude of 10 mmHg in the thoracic cavity (Harris et al, 2005). The same ratio between the amplitudes of the thoracic and abdominal pressures is kept in the remaining models (Snyder et al., 1969) (Corsini et al., 2010), so a 5 mmHg amplitude is used in the abdominal chamber. Figure

34 shows the thoracic (TC) and abdominal chamber (AC) pressures for both the nominal child and adult models.

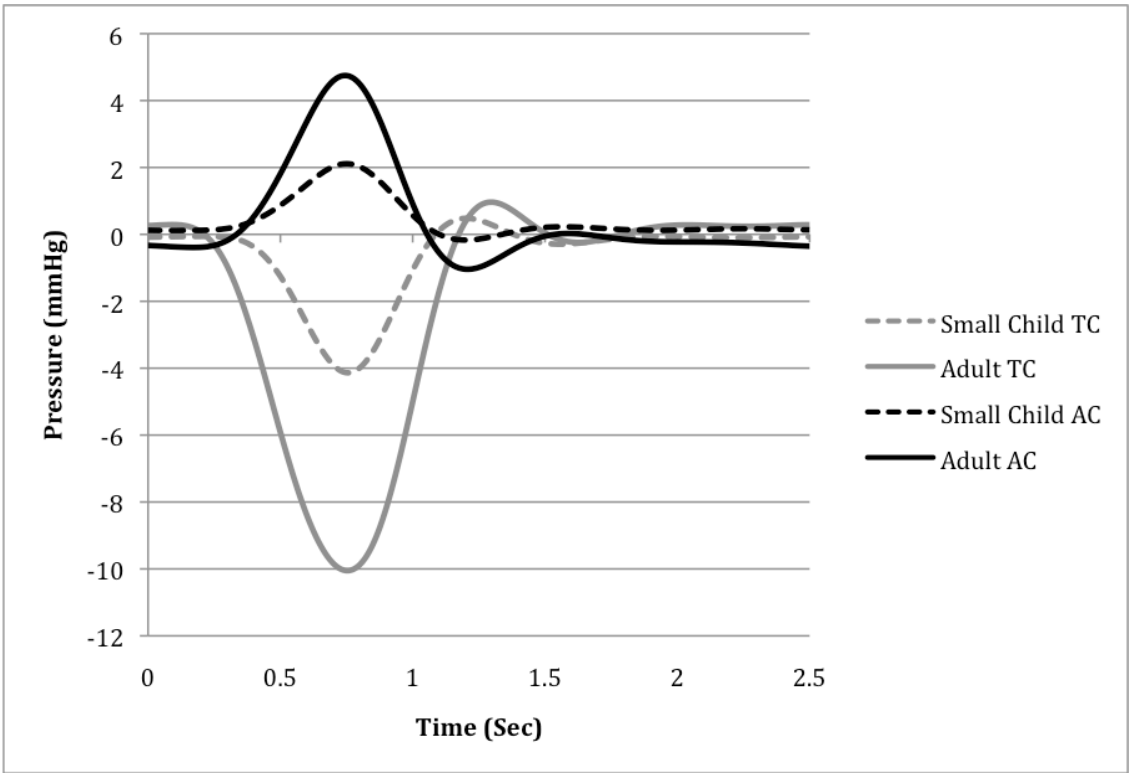

Figure 34: Young adult and small child respiration inputs

The respiration curves are important in that they not only provide the effect to the Fontan circulation to be studied here, but they serve as a reference point for all other measurements in the system. When examining flow and pressure traces within the system, it is important to note when these measurements are in relation to the respiration cycle. The interpretations of other measurements in the system rely upon when they occur in the cycle. For this reason, the results shown in this section are often overlaid with the respiration curves for reference.

TCPC Pressures

For the case with the rigid TCPC model (see Figure 16) and the system tuned to the small child model, the measured pressures on the four sides of the TCPC are shown in Figure 35.

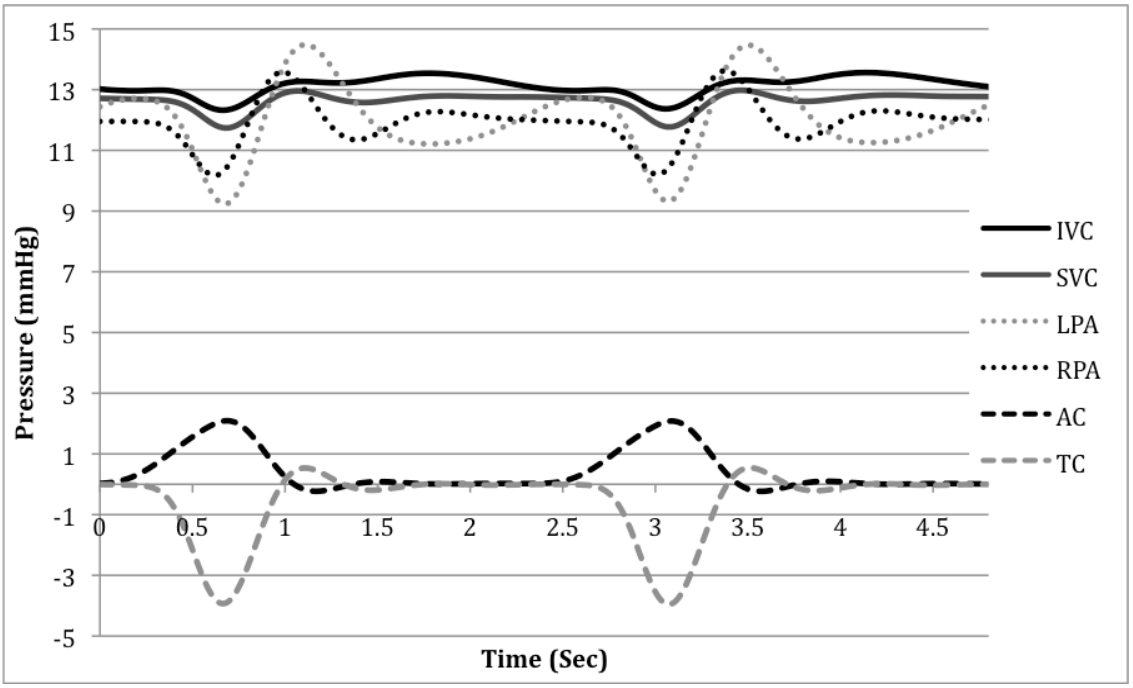

Figure 35: TCPC pressures during two respiration cycles

IVC and *SVC* represent the pressures in the inferior and superior vena cavae, respectively. *LPA* and *RPA* represent the pressures in the left and right pulmonary arteries, respectively. *AC* and *TC* represent the abdominal and thoracic chamber respiration pressures, respectively.

During the resting period of the respiration cycle, the SVC and IVC pressures are higher than the PA pressures. This is a result of the resistance within the TCPC, as forward flow passes from the IVC and SVC into either of the two PA's. At the onset of inspiration, the left and right pulmonary arteries experience a pressure drop down to 9 and 10 mmHg, respectively. The SVC and IVC experience pressure drops also, but with less amplitude. The TCPC resistance isolates the thoracic chamber and PA's somewhat from the rest of the system. Part of this effect is due to placing all of the TCPC compliance into the thoracic chamber, necessary with a rigid, transparent test section. At the end of inspiration, all of the pressures are at their lowest point. The LPA pressure dips the lowest, attributed to a slight stenosis on this side of the TCPC that provides increased resistance. When expiration begins there is a sharp increase in pressures, especially in the pulmonary arteries. The PA's reach pressures higher than both the IVC and SVC at the height of expiration. The adverse pressure gradient signifies the potential for reverse flow towards the veins during expiration. The LPA reaches the highest pressure of all, again attributed to the stenosis. The stenosis on the LPA side of the TCPC results in larger pressure oscillations on that side, since the pressure is measured between the stenosis and the thoracic chamber. There is a small phase difference between the PA's and the vena cavae. The pulmonary arteries are closer to the thoracic chamber than are the vena cavae. Inertance effects create a time-dependency, resulting in this small lag.

During the resting period of the respiration cycle, the signals flatten out and attempt to return to their steady state values. The IVC pressure stays elevated longer than

does the SVC pressure during this resting period. There is more compliance upstream of the IVC than of the SVC. Once expiration has completed, there is more extra volume storage in the IVC-feeding branches. The forward flow increases as a result during this time, and the pressures on the IVC side of the TCPC remain slightly elevated as a result. After expiration, the LPA pressure appears to mirror the RPA pressure, but at a much lower frequency. This can also be attributed to the stenosis, as the resistance increases the length of time over which pressure differentials can be mitigated by flow.

The pressures around the TCPC are depressed during inspiration and elevated during expiration, demonstrating a positive correlation with the thoracic chamber. The effects of respiration also extend to the way in which the fluid flows throughout the mock circulatory system.

System Flows

Flow measurements are made on the venous side of each of the systemic branches within the system. These flows are of primary interest in this study, as one goal is to study the hepatic vein flow behavior documented in clinical measurements (Hsia et al., 2000) (Hsia et al., 2007). The flows on the arterial side of the systemic branches are not measured. Figure 36 shows these flows measured during two respiration cycles.

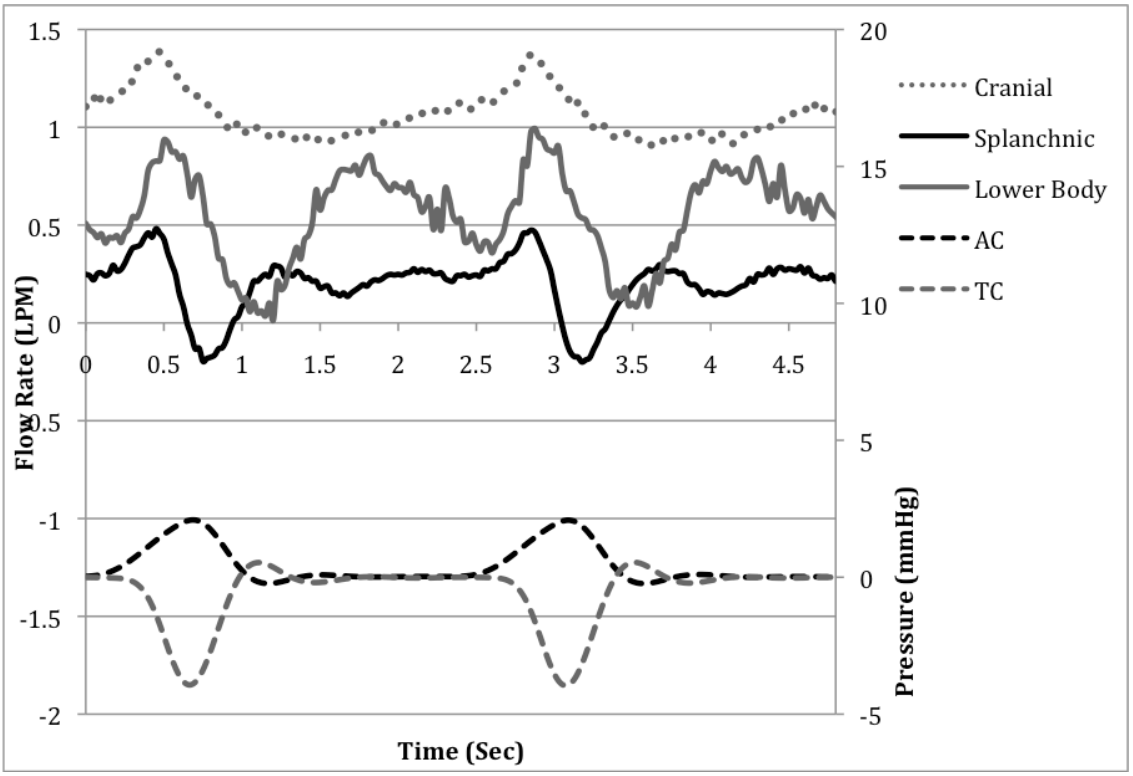

Figure 36: Systemic venous flows in small child model

In a small child, the head receives a much higher proportion of the flow than in an adult. In this model, the steady state flow rate in the cranial branch is 1.01 liters per minute (LPM). Flow rises during inspiration, peaking around 1.4 LPM. The flow rate declines and reaches its lowest flow of about 0.9 LPM during expiration. The flow in the cranial branch does not reverse, a result that is consistent with clinical measurements at rest (Hjortdal et al., 2003). The difference in maximum and minimum forward flow is 0.48 LPM, or about 48% of the total magnitude of the steady-state (ie, non-respiratory) flow rate. The inspiratory to expiratory ratio of flow is 1.2. This means that 1.2 times more flow occurs during inspiration than during expiration. This compares reasonably

with a clinical study that measured this ratio in TCPC patients at rest. This study found that the mean of this ratio was 1.0 with a standard deviation of 0.2 (Hjortdal et al., 2003).

The lower body branch feeds into the IVC, and carries a lower proportion of flow in the small child model. The steady state flow rate in the lower body branch is 0.49 LPM. The lower body branch is unique in that its properties are affected by both respiration sources, but the two respiration sources act in opposition here. The branch is in parallel with the splanchnic branch, where abdominal respiration occurs. These two branches merge together just downstream of their respective flow measurements to form the IVC. During inspiration, the thoracic respiration tends to increase forward flow in the lower body branch, but the abdominal respiration works against this by pushing fluid outward from the splanchnic branch and into the end of the lower body branch.

The lower body branch flow experiences a large increase in forward flow initiated by the onset of inspiration. The flow reaches a maximum of 0.93 LPM at the very end of inspiration. The lower body branch flow peaks about 0.05 seconds after the splanchnic and cranial branch flows. The lower body branch is farthest away from the thoracic chamber in the system setup. This, along with any inertance effects present in a length of tubing, may account for this phase difference.

From the onset of expiration, the flow is reduced considerably. The flow reaches its lowest point of 0.01 LPM at the end of expiration. The lower body branch reaches its minimum value well after the nearby splanchnic branch. This is likely due to the interactions occurring between these two branches. The abdominal chamber, located right in the middle of the branch, primarily drives the splanchnic branch flow. The end of

the splanchnic branch is attached to the IVC: one side of this leads to the lower body branch, and the other leads to the TCPC. As a result, when the splanchnic branch flow reverses, some of this fluid comes from the lower body branch. This elevates the lower body flow. Also of note is when the lower body branch reaches its lowest point, the splanchnic branch sees a small peak in its flow. It is very likely that these two branches are simply experiencing some interacting oscillation back and forth.

The lower body branch has less damping than any of the other branches. This decreases flow oscillation during respiration, but increases it once the flow rate tries to settle back to it steady state value. Some of this is handled by adjusting resistance between the compliance and the branch itself, as discussed for the accumulator. The reduced inertance in the lower body branch is also responsible in part for these oscillations, as flow can accelerate more quickly here. The inertance is lower in this branch because a larger size tube is used. In the splanchnic and cranial branches, ½" (12 mm) inner diameter tube is used, while 1" (25 mm) inner diameter tube is used in the lower body and pulmonary branches. This keeps the resistance down in the system for other models.

The difference between maximum and minimum flow is 0.92 LPM, or 188% of the steady state flow rate. There is 2.12 times more flow occurring during inspiration than expiration, a reasonable result in the context of clinical studies. One clinical study observed a mean ratio of 1.9 in the IVC with a standard deviation of 0.5 (Hjortdal et al., 2003). Another study observed a mean ratio of 1.32 in the IVC with a standard deviation

of 1.31. (Hsia et al., 2000). A final study found a mean ratio of 1.6 with a standard deviation of 1.7 (Hsia et al., 2007).

The branch most significant for this study is the splanchnic branch: the lumped parameter model equivalent of the hepatic vein. The steady-state flow rate in this branch is 0.20 LPM, which is the lowest of any branch. This region of the system is dominated by the abdominal respiration, which occurs within the splanchnic branch.

At the onset of inspiration, the hepatic vein flow experiences an increase. It reaches a maximum of 0.48 LPM near the end of inspiration. During expiration, the flow quickly drops and reverses direction. The reverse flow seen in the splanchnic branch during expiration reaches a value of 0.19 LPM at the lowest point. This reverse flow can be attributed to several factors. Both respiration effects work together at this location in the system. During expiration, the splanchnic compliance element is increasing in volume, while the pulmonary compliance decreases in volume. These two effects push fluid in the same direction at this location in the system, unlike in the lower body branch where they compete. Also, the compliance in the splanchnic branch is the highest of any systemic branch. This encourages higher flow rate oscillation during breathing and less oscillation during the resting portion of the respiration cycle. The difference between the maximum and minimum flow rates in this branch is 0.68 LPM (reverse flow is taken to be negative), which is 340% of the steady-state flow rate. There is 2.02 times more flow occurring during inspiration than expiration. One clinical study measured this ratio in the hepatic vein of TCPC patients, and found a mean ratio of 3.4 with a standard deviation of

1.53 (Hsia et al, 2000). Another study (Hsia et al. 2007) found a mean ratio of 3.2 with a standard deviation of 1.3.

The splanchnic branch flow was also monitored during a study using a compliant TCPC with the system tuned to the same small child model. The thoracic chamber pressure was connected to an airtight box containing the TCPC as shown in Figure 13. This setup resulted in a higher inspiratory to expiratory flow ratio of 3.09. Use of a compliant TCPC increases the respiration effect, as a higher proportion of the thoracic respiration occurs near the veins. The maximum forward flow was 0.46 LPM, while the maximum reverse flow rate was 0.32 LPM. The difference between maximum forward and reverse flow rate is 0.78 LPM, or 382% of the steady state flow rate.

The splanchnic branch flow behavior is consistent with the study by Hsia et al. (2000) demonstrating the hepatic vein flow reversal. Figure 37 shows hepatic vein echocardiogram velocity measurements obtained in a patient plotted with nasal airflow and ECG measurements.

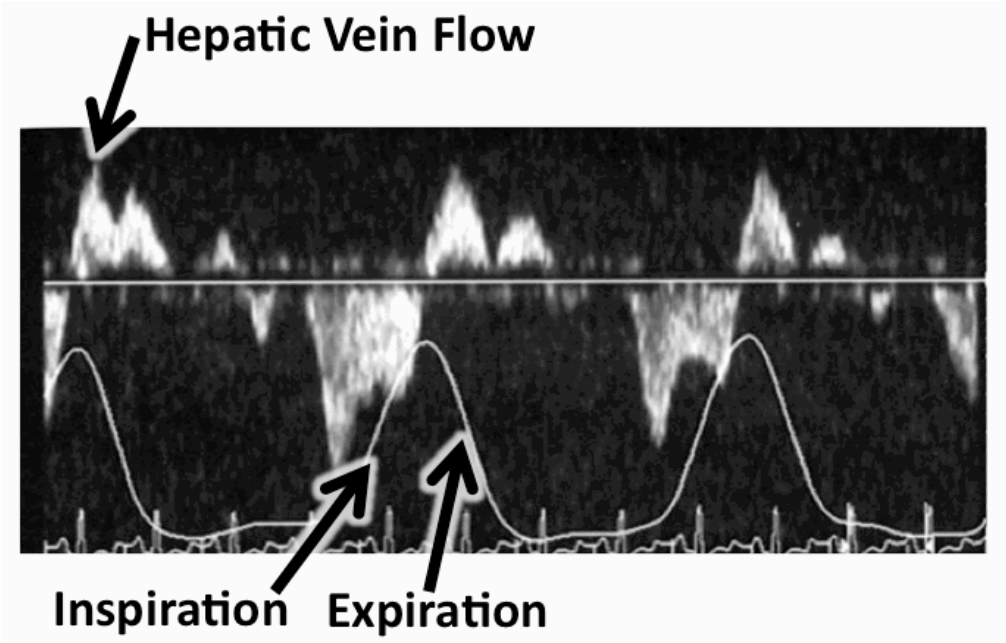

Figure 37: Hepatic vein velocity measurements (Hsia, 2011)

In the case of the nasal flow curves, the upward-sloping portion of the curve signifies inspiration, while the downward-sloping portion signifies expiration. The top of Figure 37 shows the hepatic vein velocity echocardiogram. The assignment of positive and negative velocity in these diagrams depends upon the orientation of the ultrasound sensor. In this particular case, forward flow is shown below the zero line while reverse flow is shown above the line. The hepatic vein shows an increase in forward flow during inspiration, and shows some reverse flow during expiration. This behavior is consistent with splanchnic branch venous flow measurements made in the mock circulatory system.

Hjortdal et al. (2003) and Sondergaard et al. (2000) measured SVC and IVC flows during respiration in Fontan patients at rest. These traces are shown in Figure 38.

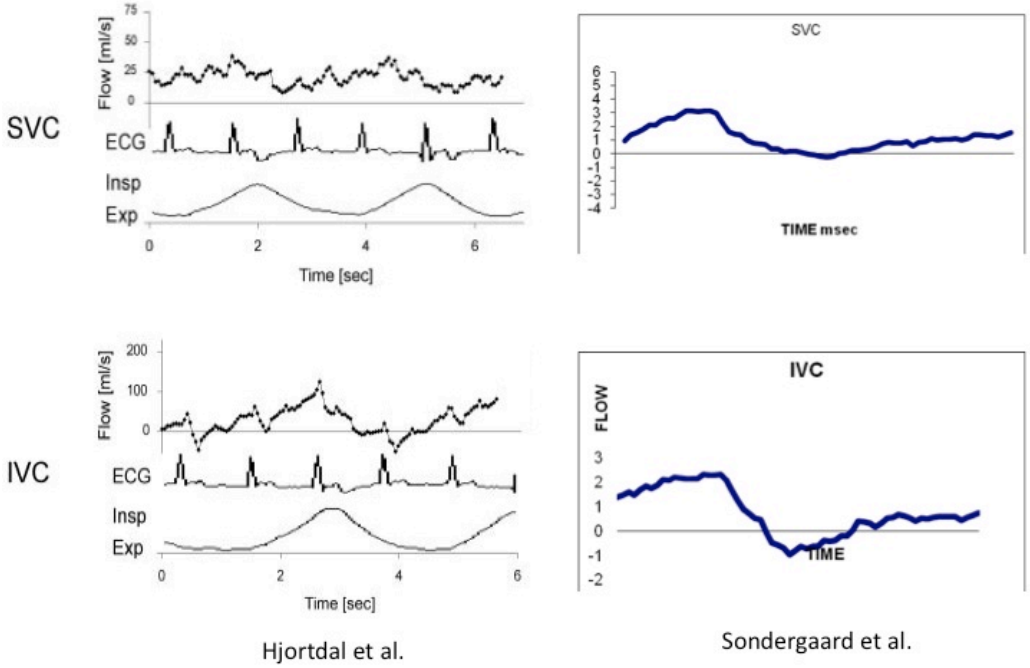

Figure 38: Clinical measurements of SVC and IVC flow (Hjortdal et al., 2003) (Sondergaard et al., 2000)

The Hjortdal et al., (2003) measurements show the flow traces in addition to respiration monitoring. The SVC flow shows a small increase during inspiration and small decrease during expiration. The flow does not reverse in these measurements, a result consistent with mock circulatory system results. The IVC flow appears more dependent upon respiration. The forward flow in the IVC experiences a stronger increase in forward flow during inspiration. The flow reverses during expiration, a result consistent with the splanchnic branch of the mock circulatory system that feeds into the IVC. IVC flow reversal is seen, however, in the forthcoming PIV results (see Figures 42-44).

The flow in the SVC nearly reverses in the Sondergaaard et al. (2000) flow traces. The SVC flow in the mock circulatory system did not come this close, as it is more consistent with the Hjortdal et al., (2000) flow trace. The IVC measurements indicate prominent flow reversal (Sondergaard et al., 2000). There are no flow measurements in the IVC proximal to the TCPC in the mock circulatory system, but IVC flow reversal is seen in the forthcoming PIV results (see Figures 42-44), as well as in the upstream splanchnic branch flow measurements during expiration.

The overall behavior of the flows in the system during respiration can be summarized as follows: forward flow increases during inspiration, and decreases during expiration. In the case of the splanchnic branch, the flow reverses during expiration. Figure 39 shows the total flow going into the TCPC during respiration. The venous flows are summed together to calculate total flow into the TCPC. These in vitro findings are consistent with the clinical measurements and offer verification that the in vitro system is functioning correctly. This behavior has never before been modeled and documented within a mock circuit.

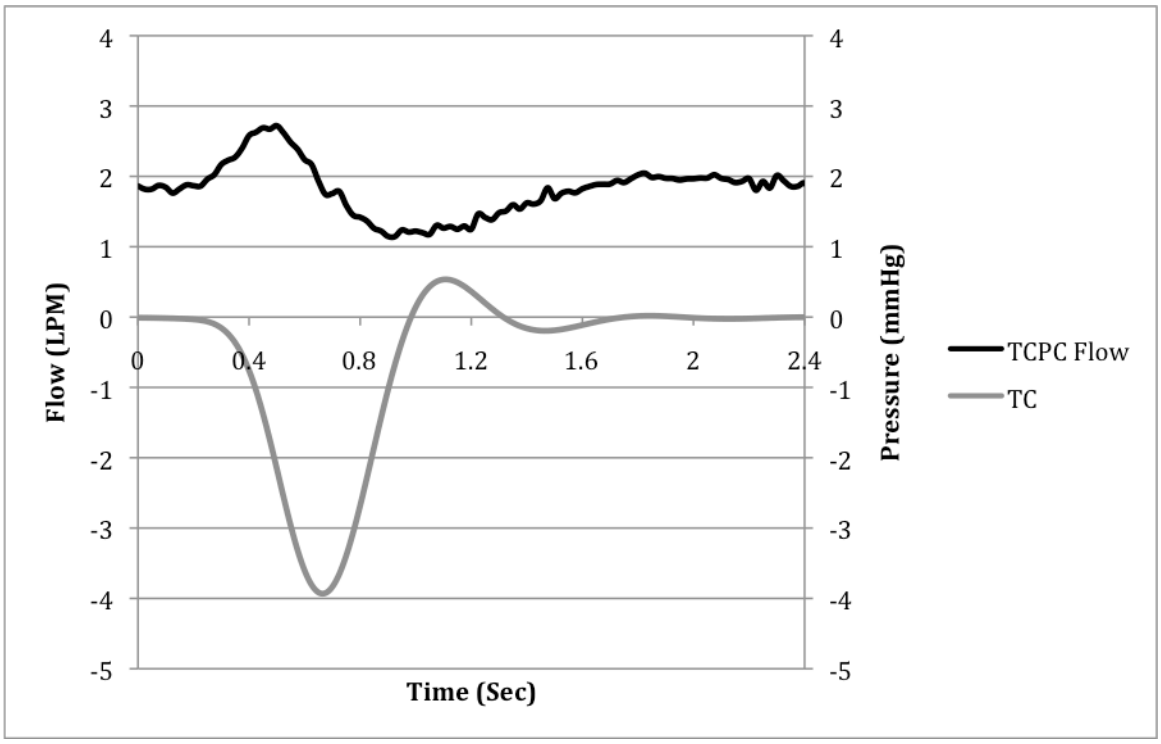

Figure 39: Sum of all flows into TCPC

The flow rate into the TCPC is higher during inspiration than expiration. A rigid TCPC was used for this study; therefore the relationship between flow into and out of the TCPC is governed by the mass balance. This implies that the flows into and out of the TCPC are equivalent. In this way, Figure 39 can also be interpreted as pulmonary artery flow during respiration, and thus is consistent with studies by Penny et al. (1991) (done on an APC patient) and Redington et al. (1990) observing flow rate to be higher during inspiration in the pulmonary artery. The Redington et al. (1990) study included echocardiographic pulmonary artery flow tracing on a TCPC patient, and is shown in Figure 40.

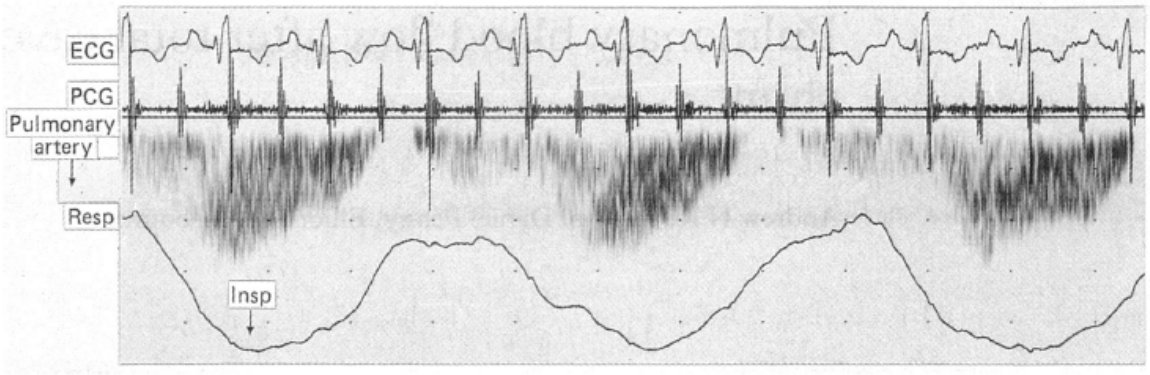

Figure 40: Clinical pulmonary artery flow measurements (Redington et al., 1990)

Figure 40 includes a pulmonary artery echocardiogram signal with respiration monitoring below. As in Figure 37, forward flow is indicated below the y-axis as a result of the ultrasound sensor orientation. The arrow indicating "Insp" on the diagram marks inspiration. The forward flow shows a sharp increase during inspiration, and slowly subsides during expiration. The respiration curve is not identical to that used in the mock circuit, but the pulmonary artery flow behavior appears similar to the mock circuit results in Figure 39, suggesting that the overall respiration – flow behavior is not dependent on the particular respiration waveform. This is a significant effect.

Particle Image Velocimetry (PIV)

Particle image velocimetry (PIV) is used to provide instantaneous full field two-dimensional velocity mappings of the TCPC flow. Each PIV velocity map frame corresponds to an instant in the respiratory cycle. A trigger is used as a reference for the timing of each frame. For this, the signal sent from the DAQ system to the vents to close (signaling the onset of inspiration) is used. The falling edge of this signal is used as the

reference value for time. This signal is shown in Figure 41, with corresponding respiration pressures. The time scale used in the forthcoming PIV images is consistent with that of Figure 41.

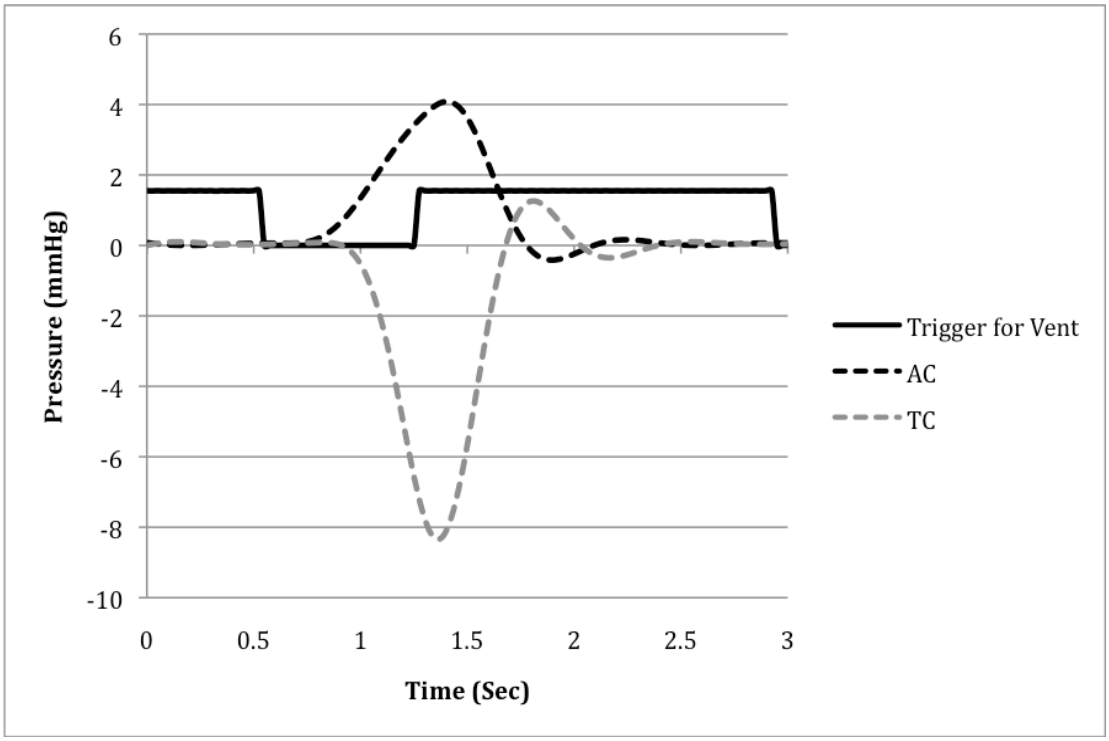

Figure 41: Trigger signal for PIV

Each individual velocity map is created from a double interrogation between two frames taken 500 μs apart. This interval is chosen because it allows the average particle to move about 5 pixels during this time. Each pixel represents 18 μm of real space. Initial images are subjected to a high-pass filter to correct non-uniformity in the laser sheet and remove scattering. The interrogation begins with a 128x128 pixel interrogation window and results in 64x64 interrogation cell resolution. A 50% overlap between windows is used, and results in a final resolution of 32x32 pixels for each interrogation window. This

process is repeated 15 times at the same instant in time relative to the respiration cycle. These 15 velocity maps are ensemble averaged to produce one velocity map at each point in the cycle. Ensemble averaged velocity maps are created at 50 ms intervals throughout the 2.4 second respiration cycle, resulting in 48 such maps. Figures 42-44 show an abbreviated series of these ensemble averaged velocity maps in 200 ms intervals. The field of view in these pictures is 37x37 mm of real space. The time stamp on the following PIV images (Figures 42-44) can be cross-referenced with Figure 41 to correspond with the respiration cycle.

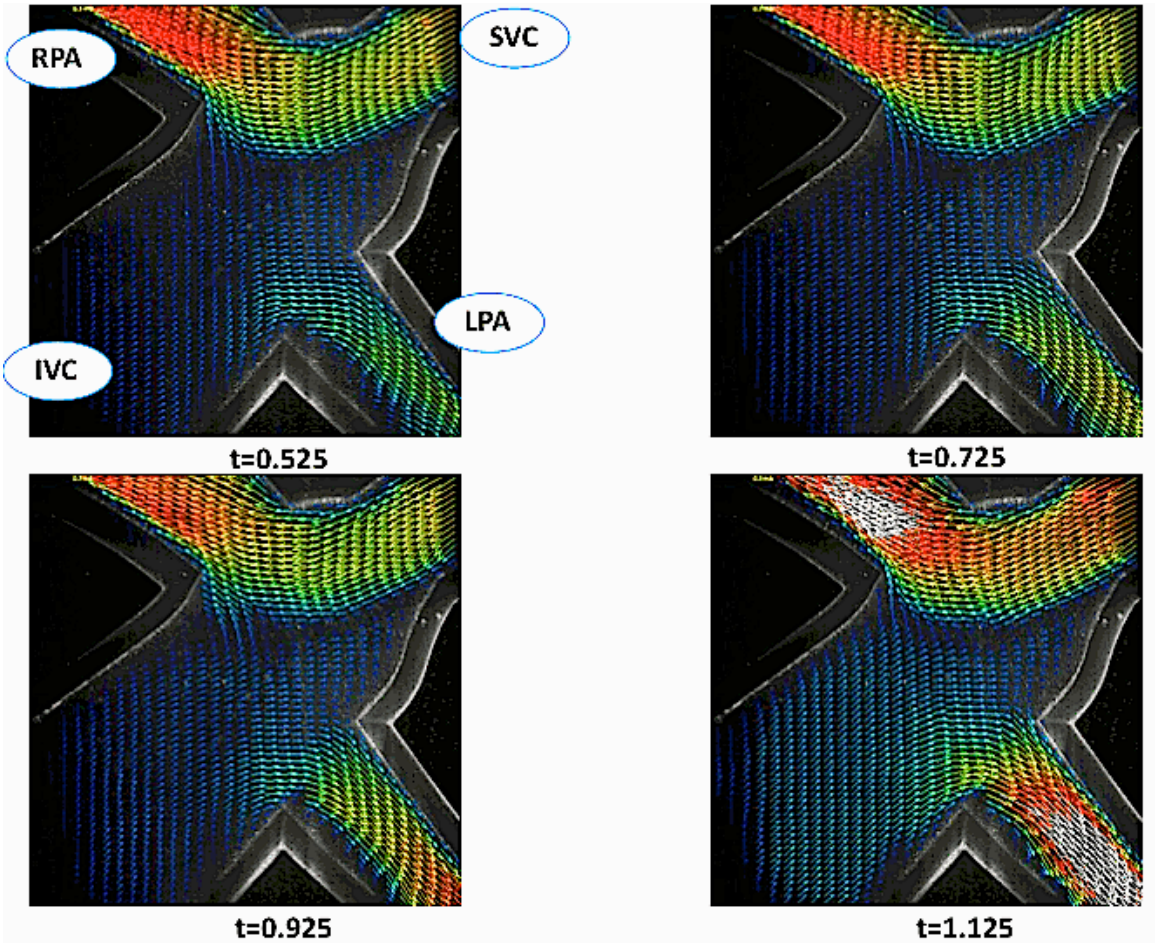

Figure 42: PIV images (start of inspiration)

Figure 42 shows the first four PIV images in the respiration cycle. Each map shows the Fontan junction and the four branches around it. Starting with the upper-left branch and continuing clockwise: right pulmonary artery, superior vena cava, left pulmonary artery, and inferior vena cava. Normal forward flow through the TCPC features flow entering from the SVC and IVC, and exiting through the pulmonary arteries. The first image (t=0.525) is taken just as the trigger signal is sent to the vents in the mock circulatory system to begin inspiration. The majority of the velocity comes from the SVC and

continues through RPA. The cranial branch has the highest flow rate in the small child model, and the SVC has a significantly smaller diameter than the IVC in this TCPC model. These two factors result in this branch having the highest velocity. Conversely, the IVC contains the lowest velocities in general because it has a large diameter and less flow rate going through hit. From Figure 41, inspiration begins around 0.7 seconds. The remaining images in Figure 42 above show increasing forward flow in all of the branches as time moves forward. This is consistent with the flow measurements that showed increasing flow during this time.

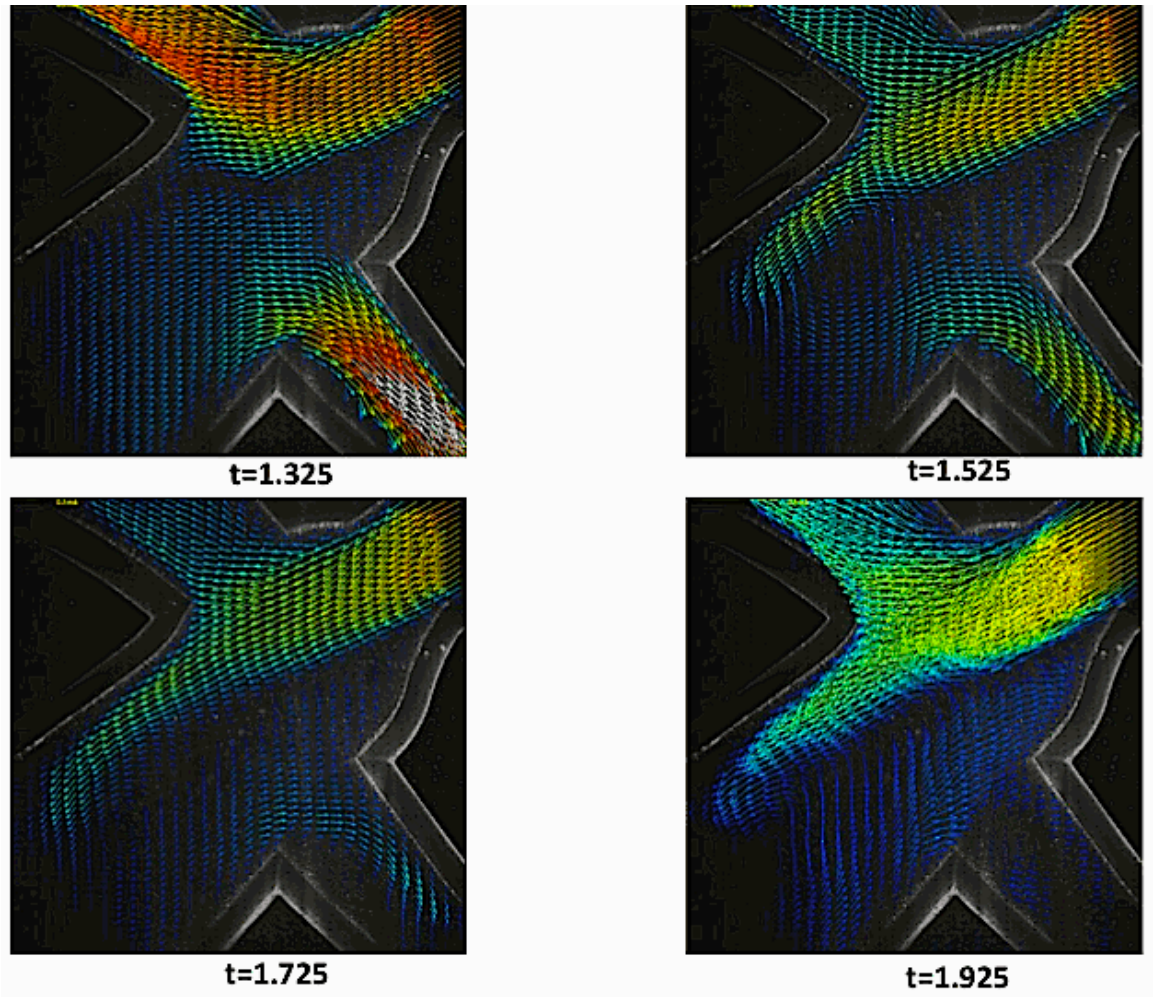

Figure 43: PIV images (end of inspiration to start of expiration)

From Figure 41, the transition from inspiration to expiration occurs at 1.4 seconds. Figure 43 shows the next four PIV images in the cycle. The first image (t=1.35) still shows strong forward flow at the very end of inspiration. The transition to expiration is reflected in the following three images. The forward flow is seen to decrease in each of the next three pictures; by the final image (t=1.925) all flows have decreased considerably. There appear to be regions of reverse flow in the IVC starting with the second image (t=1.525) and continuing until the second image (t=2.325) of Figure 44.

The LPA shows reverse flow as well in the last image (t=1.925) of Figure 43 and in the first image (t=2.125) of Figure 44.

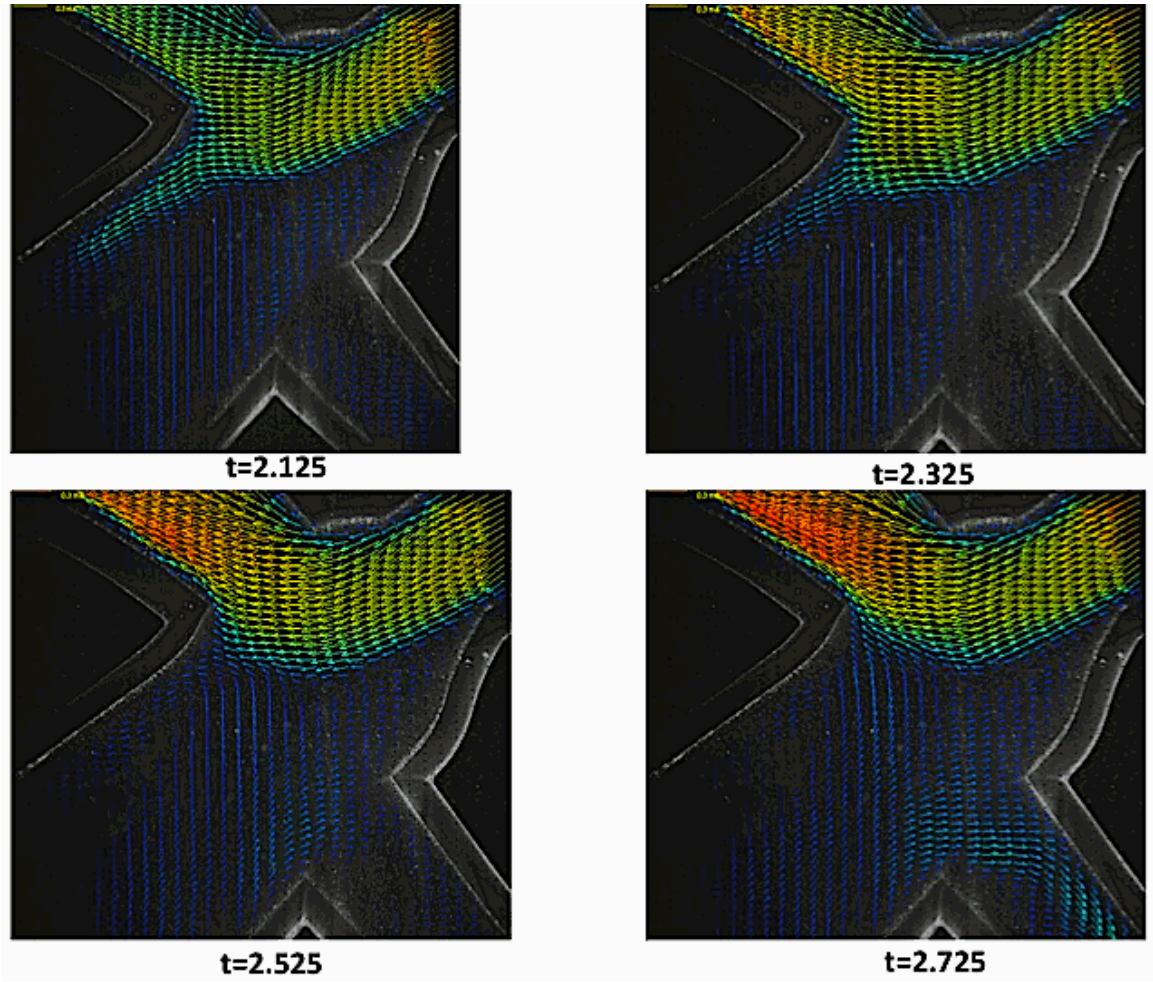

Figure 44: PIV images (end of expiration)

From Figure 41, expiration ends at 2 seconds. This is reflected in Figure 44 above. The first image (t=2.125) shows the TCPC just as expiration is ending. The resting period of the respiration cycle begins around this time. The forward flow increases with each image, as the depressed flow rates from expiration begin to come back up to their steady

state values. The last image (t=2.735) appears similar to the first image (t=0.525) in Figure 42. This is expected, as the respiration cycle is about to repeat itself.

The PIV images provide a better idea on flow patterns within the TCPC during respiration. It is interesting to note the majority of flow that the RPA receives. This is normal, as the right lung is always larger than the left in humans. However, this feature is likely exaggerated in this particular case due to the stenosis in the left pulmonary artery. The geometry of the SVC connection is also partly responsible, as the connection seems to guide the flow towards the RPA.

PIV results can also be used to generate shear stress and strain rate maps. These are especially important when dealing with a shear thinning non-Newtonian fluid such as blood. High levels of shear stress can lead to platelet activation or coagulation. This is vitally important when testing new devices that impact hemodynamic behavior. The strain rate maps corresponding to Figures 42-44 are given in the Appendix.

Pulmonary Vascular Resistance (PVR) Study

The mock circuit has been shown to replicate the effects of respiration upon the Fontan circulation in a way that provides realistic results. Of particular interest in this study is the examination of the splanchnic branch flow, as the reversal of flow here is thought to be troublesome to Fontan patients (Hsia et al., 2000) (Itatani et al., 2009). An experiment was created to examine the effects of increased pulmonary vascular resistance (PVR) on the splanchnic branch flow. The system is tuned to the small child model. Using this setup as a baseline, the PVR was increased by 20%. The added resistance was

applied in its entirety to either the pulmonary veins or arteries. For the case of increased PVR in the pulmonary veins, this models pulmonary hypertension, a condition often noted in adult Fontan patients and a sign of a failing circulation. Resistance was applied to the pulmonary veins using the valves shown in Figure 20 (#4). Resistance was applied to the pulmonary arteries by placing clamps in between the thoracic chamber and TCPC. The inset labels (#10 and #11) in Figure 19 show the approximate location of the clamps along the pulmonary arteries. Figure 45 shows the baseline splanchnic branch flow, along with the two cases of added resistance.

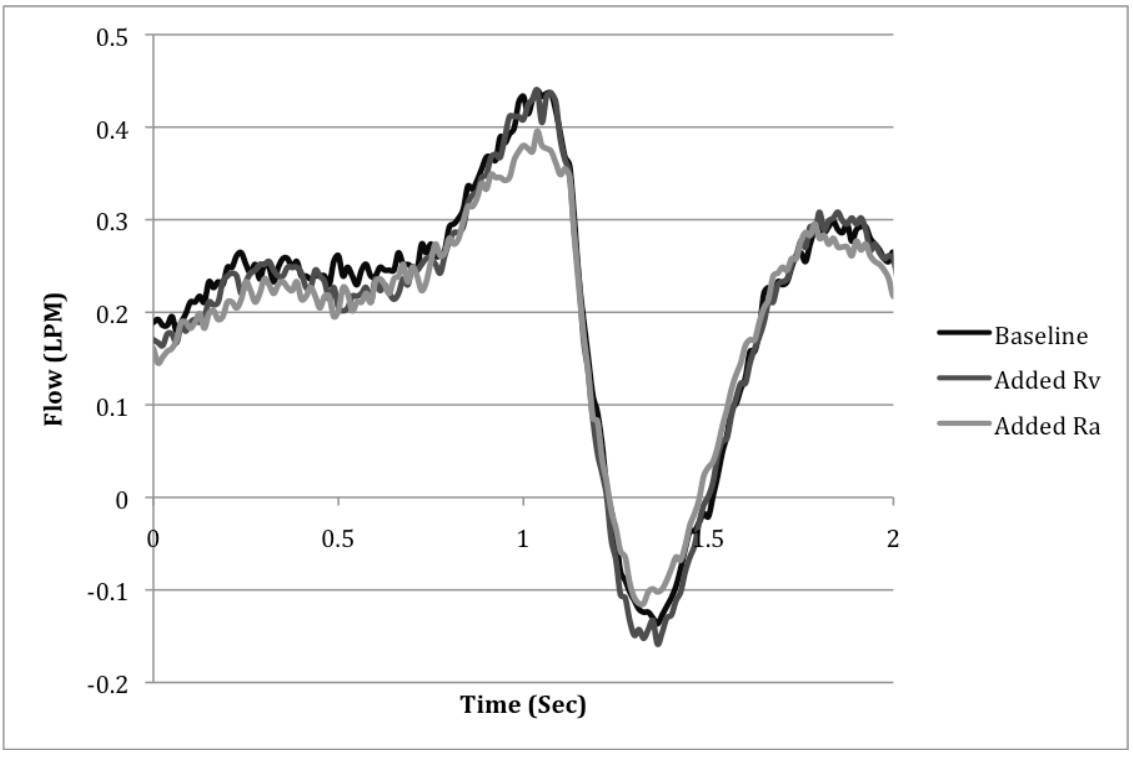

Figure 45: Effect of added PVR on splanchnic flow

Figure 45 shows that the splanchnic branch flow at baseline PVR is slightly higher than the elevated PVR cases before the respiration occurs, a consequence of adding resistance to the circuit. The highest measured reverse flow rate at baseline PVR was 0.14 LPM during expiration. When 20% additional PVR is added to the arteries, the influence of respiration upon the splanchnic flow appears to be weakened. The maximum reverse flow measured here was 0.12 LPM, a reduction of 15.4% from the baseline. Placing resistance in the pulmonary artery isolates the thoracic respiration somewhat, reducing the reverse flow. Conversely, adding 20% additional PVR to the veins increased reverse flow. The maximum reverse flow was 0.16 LPM, an increase of 16.2% from the baseline.

These results are consistent with the Kilner study, which examined reverse flow in the pulmonary artery as a function of resistance location. Kilner et al. (2008) reported higher reverse flow with resistance added away from the compliance. This condition was replicated in the mock system by adding pulmonary venous resistance, as the resistance lies on the other side of the compliance. As mentioned, the mock system saw an increase in reverse flow here. Kilner et al. (2008) also reported a decrease in reverse flow with resistance added proximal to the compliance. This condition was replicated in the mock system by adding the pulmonary arterial resistance, as it is between the flow measurement and the compliance. This setup resulted in decreased reverse flow.

It is important to see these results in light of the Cavalcanti et al. (2001) study of the failing Fontan circulation. That study compared healthy and failing Fontan circulations. Both groups demonstrated similar pulmonary artery pressures, but the

failing Fontan group demonstrated much higher pulmonary venous pressures (Cavalcanti et al., 2001). This leads to a prediction that pulmonary venous resistance is higher in failing Fontan patients, as this would elevate the pressures upstream in the pulmonary vein and artery. However, the pulmonary arterial pressures were similar between the two groups in the study. The only way this could occur is if the pulmonary arterial resistances were lower in the failing Fontan group. The lower resistances would bring the pulmonary artery pressures back down to a normal level. This is interesting in light of this study, because both of these conditions (higher pulmonary venous resistance, lower pulmonary arterial resistance) led to higher reverse flow in the mock circulatory system. Increased reverse flow exacerbates the chronic venous hypertension, a known symptom in the failing Fontan. In other words, the causes and effects of a failing Fontan circulation appear to be similar in both the body and in the mock circulatory system. This clinical observation has never before been modeled in an in vitro or numerical based system until now.

The mock circulatory system has shown to be a capable device that accurately portrays the effects of respiration upon the Fontan circulation in a laboratory environment. The respiration inputs to both the abdominal and thoracic chambers have been shown to give realistic amplitudes and shapes. The behavior within the three systemic branches is realistic and compares reasonably with clinical studies. The flow reversal seen clinically in the hepatic vein is also seen in the mock circulatory system in the analogous splanchnic branch. These results are evidence that the system accurately demonstrates the effects of respiration upon the flows and pressures within the Fontan

circulation. Also, it has been observed that adding 20% to the pulmonary vascular resistance (PVR) changes the flow reversal behavior in the splanchnic branch as a function of where the resistance is added.

CHAPTER FIVE

CLOSING

Conclusion

A multi-scale model of the Fontan circulation has been developed and constructed and includes the effects of respiration. The multi-scale model combines the 0-D scale of the patient's circulation in the lumped parameter model with a 3-D physiologically representative total cavopulmonary connection (TCPC) model. The 3-D model can be constructed based on patient specific clinical images and manufactured using rapid manufacturing methods. The rapid prototype model of the TCPC is then inserted into the system. The mock circulatory system is a physical realization of a model of the circulation, which has been simplified such that it can be realistically implemented in a laboratory setting. The parameters of the lumped parameter model can be adjusted to match those of any Fontan patient using data from the proper clinical measurements. The mock circulatory system is adjustable over a wide range of values from child to adult.

The system has been specifically tuned to a small child model, and has been coupled to a test section corresponding to this age. The behaviors in the systemic branches during respiration are comparable to what is seen in clinical studies. Flow increases throughout the system during inspiration and decreases during expiration. Flow reversal is seen during expiration in the splanchnic branch, analogous in this system to

the hepatic vein in the body. This is an important result as it has been observed clinically, and is thought to be a cause for liver failure in Fontan patients (Hsia, 2000).

The geometry of the TCPC has significant effects upon the flow and pressure behaviors of the system. These effects are studied more closely by mapping out the flow within the TCPC through particle image velocimetry (PIV). A transparent TCPC model was built and inserted into the system for this purpose. The PIV images show that forward flow increases through the TCPC during inspiration, and decreases during expiration. This is consistent with both the flow measurements in the mock circulatory system and clinical flow velocity measurements. Further, flow reversals within the IVC are seen during expiration. The hypothesis that a mock circulatory system can be used to simulate experimentally the effects of respiration upon the Stage 3 Fontan circulation has been verified.

A test reported here found that an increase in PVR equivalent to pulmonary hypertension affects the hepatic vein flow reversal. Added venous resistance increased reverse flow into the hepatic vein and may suggest a link to liver failure often associated with a failing Fontan circulation.

There are many possible uses for the system in the future, such as to provide quality validation data in the form of velocity maps and flow behaviors to test equivalent numerical models. Boundary condition requirements inherent in numerical modeling can be improved using flow and pressure tracings from the system. The system could also be used as a tool to carry out what-if scenarios of a full circulation, or as a calibration tool for quantitative MRI.

Recommendations for Future Research

This study has successfully demonstrated the capabilities of the system to produce clinically comparable results regarding the effect of respiration upon the Fontan circulation. However, there have been some limitations to this study. Many of these limitations can potentially be overcome in future research.

The mock circulatory system is highly adjustable, but the overall multi-scale model can be limited by the availability of MR image data. The scales of the lumped parameter model and test section must be matched in terms of patient age and size. The available MR image data during this study was limited to only a small child test section. For this reason, only results with the small child tuning are shown here. The system can be tuned for larger and older patients, but doing this correctly requires a TCPC model based on MR images from such a patient.

Another limitation of this study comes from the sodium iodide used to match the refractive indexes during PIV. Unfortunately, the density of this sodium iodide is nearly twice that of normal saline solution used in the system, which doubles all inertance in the system so that similarity operating conditions are needed. In addition, the refractive index match was very close but not exact. Use of diethyl phthalate (DEP) for refractive index matching is a promising alternative. All acrylic in the system would have to be replaced with polycarbonate and some other plastics would need to be replaced if DEP were to be used.

The compliant TCPC developed in this study had a compliance value that was low, 0.2 mL/mm Hg, relative to a more normal vasculature at 0.88 mL/mm Hg. One

means to increase compliance in the test model is to decrease its wall thickness. Indeed, Biglino et al. (2011) reports that compliance can be matched by varying wall thickness with the same materials used here. However, the compliant test section awaits the next study.

The flow signals are known to exhibit oscillation during the resting period of the respiration cycle in models with lower compliance. Adding resistance between these branches and their respective compliance elements effectively damps these oscillations. When this process is carried out, there are no quantitative criteria used to determine the amount of resistance applied. The resistance is added until these oscillations are smaller, and care is taken to preserve the original signal during respiration. Useful criteria concerning the cutoff frequency used for damping would eliminate any over or under-damping that may occur in method used here.

Some of the methods used to tune the respiratory compliances are time consuming. If this system is to be used to help make real-time decisions, faster turnarounds may be needed. The pulmonary and splanchnic compliances are tuned rigorously but slowly, using trial-and-error processes. The upside to this approach is that any value can be achieved with enough trials, but a faster method would improve turnaround time.

One limitation of this study has been that all simulations do not account for the gravitational effect upon the Fontan circulation. Acceleration due to gravity has been shown to have effects upon the Fontan circulation (Hsia et al., 2000) (Hsia et al., 2007) (de Leval, 2005). This effect has not been implemented into this mock circulatory

system. All measurements made in the mock circulatory system assume a supine position, which negates the gravity effect. Consequently, the clinical data to which the mock circulatory system results are compared also state that the patient was in the supine position. There is no problem with this, but the mock circuit results are limited to only these types of comparisons where gravity has little effect. Implementing the necessary changes to model gravity effects may involve another mock circuit entirely.

Finally, the mock circulatory system could be used to examine some potential solutions for improving the functional outcome of the Fontan circulation. Candidates for possible testing in the system may include assist devices, artificial pumps, or artificial valves. A fluid diode has been shown to reduce reverse flow in the pulmonary position (Figliola, 2007), and may potentially reduce reverse flow here. It has been postulated that a device decreasing venous pressures by as little as 5 mmHg will mitigate many of the problems associated with the Fontan circulation (de Leval, 2005). Hopefully these solutions will someday lead to better lives for these patients.

APPENDIX

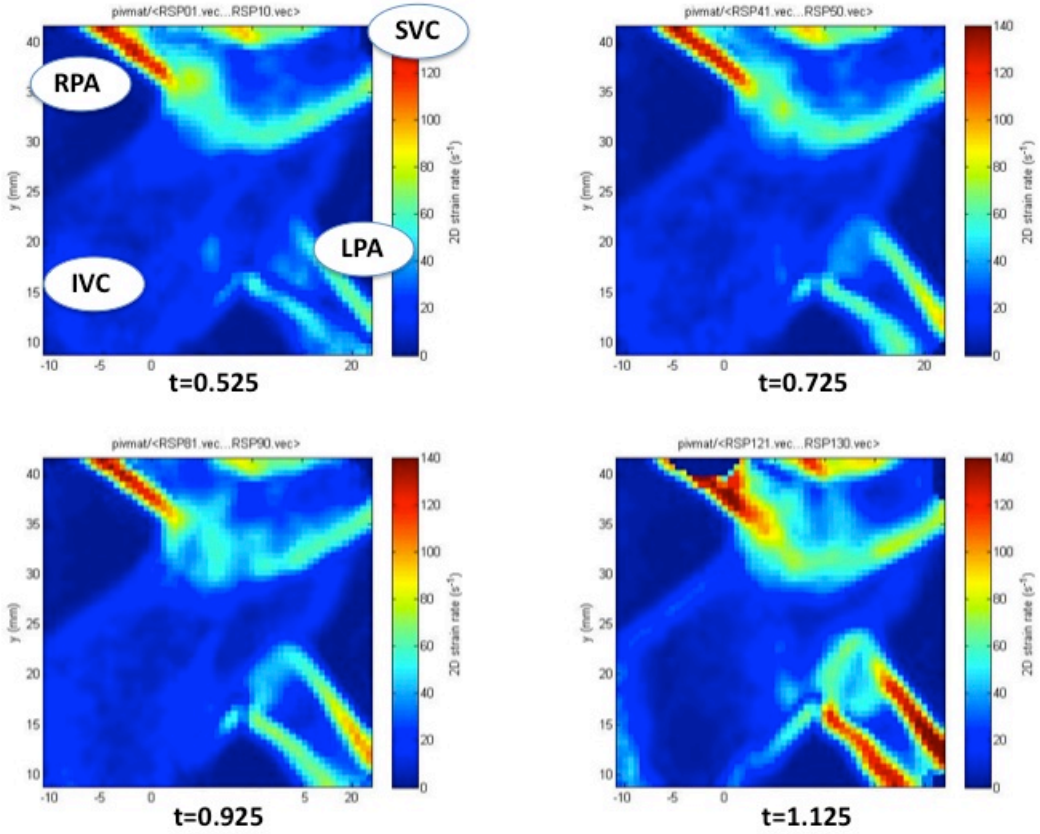

Figure A- 1: Strain rate maps (start of inspiration)

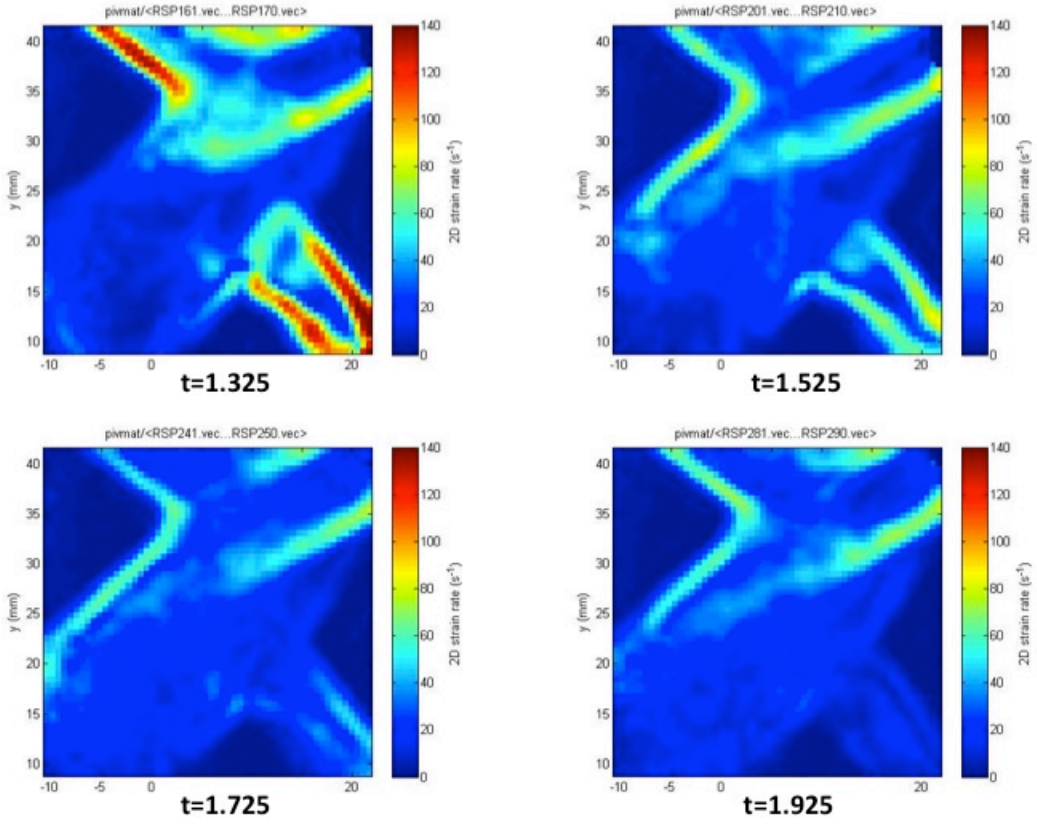

Figure A- 2: Strain rate maps (end of inspiration to start of expiration)

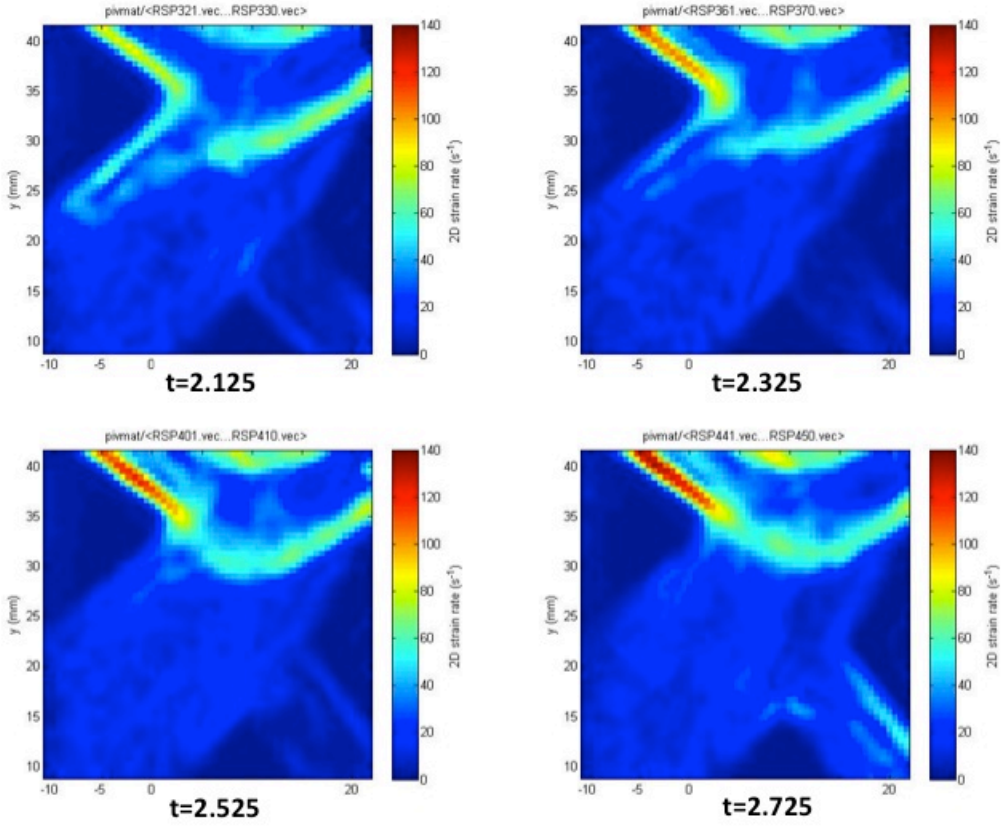

Figure A- 3: (end of expiration)

REFERENCES

1. Kilner PJ, et al, Pulmonary regurgitation: The effects of varying pulmonary artery compliance, and of increased resistance proximal or distal to the compliance, Int J Cardiol (2008), doi: 10.1016/j.ijcard.2008.06.078

2. Morimont, Philippe. "Effective arterial elastance as an index of pulmonary vascular load." *AJP - Heart Circ Physiol*. 294. (2008): H2736-H2742.

3. Manoliu, Vasile. "Considerations about the Lumped Parameter Windkessel Model Applicativity in the Cardiovascular System Structure." Politehnica Univiersity of Bucharest, n.d. Web. 21 August 2009. <snet.elth.pub.ro/snet2004/Cd/circ/circ_P16.pdf>.

4. Figliola, Richard. "In Vitro Study of Flow Regulation for Pulmonary Insufficiency." *ASME Journal of Biomechanical Engineering*. 129. (2007): 284-288. Print.

5. Baloa, L.A. "Elastance-Based Control of a Mock Circulatory System." *Annals of Biomedical Engineering*. 29. (2001): 244-251. Print.

6. Al-Jaafreh, Moha'med. "New Model to estimate mean blood pressure by heart rate with stroke volume changing influence." *EMBS Annual International Conference. 1-4244-0033-3/06*. (2006): 1803-1805. Print.

7. Cardis, Brian M. "Elastic Properties of Reconstructed Aorta in Hypoplastic Left Heart Syndrome." *Annals of Thoracic Surgery*. 81. (2006): 988-991. Print.

8. Khalil, Hassan A. "Continuous Flow Total Artificial Heart: Modeling and Feedback Control in a Mock Circulatory System." *ASAIO Journal*. 54. (2008): 249-255. Print.

9. McAlpine, James. "Modeling Fontan Circulation to Reduce Regurgitant Blood Flow to the Liver." Clemson University, 2009.

10. Adrian, Ronald J. "Particle-Imaging Techniques for Experimental Fluid Mechanics." *Annual Review of Fluid Mechanics*. 23. (1991): 261-304. Print.

11. Conover, Tim. "Design of the Mock Fontan Circulatory System." Clemson University, 2008.

12. Nayak, Sandeep. "The Fontan Circulation." *British Journal of Anasthesia*. 8.1 (2008): 26-30. Print.

13. DeGroff, C.G. "Modeling the Fontan Circulation: Where We Are and Where We Need to Go." *Pediatric Cardiol doi: 10.1007/s00246-007-9104-0*. (2007): Print.

14. Itatani, Keiichi. "Optimal Conduit Size of the Extracardiac Fontan operation based on Energy loss and Flow Stagnation." *45th Annual Meeting of the Society of Thoracic Surgeons. 0003-4975/09 doi:10.1016/j.athoracsur.2009.04.109*. (2009): Print.

15. Penny, D.J., and A.N. Redington. "Doppler Echocardiographic evaluation of pulmonary blood flow after the Fontan operation: the role of the lungs." *British Heart Journal*. 66. (1991): 372-374. Print.

16. Liu, Yingjie. "Design and Initial Testing of a Mock Human Circulatory Loop for Left Ventricular Assist Device Performance Testing." *Artificial Organs*. 29.4 (2005): 341-345. Print.

17. Hsia, Tain-Yen. "Effects of Respiration and Gravity on Infradiaphragmatic Venous Flow in Normal and Fontan Patients." *Journal of the American Heart Association 2000;102;III-148-III-153*. (2000): Print.

18. de Leval, Marc. "The Fontan Circulation: a challenge to William Harvey?." *Nature Clinical Practice: Cardiovascular Medicine*. 2.4 (2005): 202-208. Print.

19. Gewillig, Marc. "The Fontan Circulation." *Heart*, 2005;91;839-846. Doi:10.1136/hrt.2004.051789.

20. Slife, David M. "Pulmonary arterial compliance at rest and exercise in normal humans." *Am. J. Physiol. 258 (Heart Circ. Physiol. 27): H1823-H1828,1990.*

21. Hsia, Tain-Yen. "Subdiaphragmatic venous hemodynamics in patients with biventricular and Fontan circulation after diaphragm plication." *Journal of Thoracic and Cardiovascular Surgery*. 134.6 (2007): 1397-1405.

22. Redington, A.N., and D.J. Penny. "Pulmonary Blood Flow after total cavopulmonary shunt." *British Heart Journal*. 65. (1990): 213-7. Print.

23. Yun, Tae-Jin. "Pulmonary vascular compliance and pleural effusion duration after the Fontan procedure." *International Journal of Cardiology*. 133. (2009): 55-61.

24. Ovroutski, Stanislav. "Long-term cardiopulmonary exercise capacity after modified Fontan operation." *European Journal of Cardio-Thoracic Surgery doi:10.1016/j.ejcts.2009.06.053*. (2007): Print.

25. Dasi, Lakshmi. "Functional Analysis of Fontan energy Dissipation." *Journal of Biomechanics*. 41. (2008): 2246-2252. Print.

26. McElhinney, Doff. "Incorporation of the Hepatic veins into the cavopulmonary circulation in patients with heterotaxy and pulmonary atriovenous malformations after a Kawashima procedure.." *Annals of Thoracic Surgery*. 80. (2005): 1597-603. Print.

27. Ketner, M. "Energy Gains/Losses of normal and Fontan circulations in Lambs under varying respiration parameters." *0-7803-5674-8/99*. (1999): 249. Print.

28. Cavalcanti, Silvio. "Analysis by mathematical model of haemodynamic data in the failing Fontan circulation." *Institute of Physics Publishing: Physiol Meas.*. 22. (2001): 209-222. Print.

29. Kaulitz, R. "Instantaneous pressure-flow velocity relations of systemic venous return in patients with univentricular circulation." *Heart*. 82. (1999): 294-299. Print.

30. Pittaccio, Simone. "A Lumped parameter model for the study of the venous return in the total cavopulmonary connection." *2003 Summer Bioengineering Conference*. (2003): Print.

31. Conlon, Martin J. "Development of a Mathematical Model of the Human Circulatory System." *Annals of Biomedical Engineering*. 34.9 (2006): 1400-1413.

32. Pittaccio, Simone, and Francesco Migliavacca. "On the Use of computational methods for the quantitative assessment of surgery in congenital heart disease." *Anadolu Kardiyol Derg*. 5. (2005): 202-9.

33. Snyder, M.F., and V.C. Rideout. "Computer Simulation Studies of the Venous Circulation." *IEEE Transactions on Bio-Medical Engineering*. 16.4 (1969): 325-33.

34. Bull, Kate. "The Fontan Procedure: Lessons from the past." *Heart*. 79. (1998): 213-14.

35. Basnet, Narayan Bahadur. "Pulmonary arterial compliance in children with atrial and ventricular septal defect." *Heart Vessels*. 15. (2000): 61-69.

36. Kerner, Daniel R. "Solving Windkessel Models in MLAB." *Civilized Software, Inc.*. N.p., n.d. Web. 6 November 2009. <http://www.civilized.com/mlabexamples/windkesmodel.htmld/>.

37. Fontan, F., and E. Baudet. "Surgical Repair of tricuspid atresia." *Thorax*. 26. (1971): 240-8.

38. Takahashi, K. "Real-Time 3-dimensional echocardiography provides new insight into mechanisms of tricuspid valve regurgitation in patients with hypoplastic left heart syndrome." *Journal of the American Heart Association 2000;102;III-148-III-153*. 120. (2009): 1091-8.

39. Segers, Patrick. "Predicting systolic and diastolic aortic blood pressure and stroke volume in the intact sheep." *Journal of Biomechanics*. 34. (2001): 41-50.

40. Haque, M.A. "Investigation of the nonlinearity in the heart rate dynamcis." *Medical Engineering & Physics*. 23. (2001): 111-115.

41. Hirayama, H. "Analysis of Systemic Behavior of Circulatory System: Theoretical Study by Electrical Circuit Model." *SICE 1995. PR0001-3/95/0000-1425*.

42. Timms, Daniel. "A complete mock circulation loop for the evaluation of left,right, and biventricular assist devices." *Artificial Organs*. 29.7 (2005): 564-72.

43. Camp, T.A. "In Vitro Study of Flow Regulation for Pulmonary Insufficiency." *Journal of Biomechanical Engineering*. 129.4 (2007): 284-8.

44. Hjortdal, V.E. "Effects of Exercise and Respiration on Blood Flow in Total Cavopulmonary Connection." *Circulation*. 108. (2003): 1227-31.

45. Marcelletti C et al. (1990) Inferior vena cava–pulmonary artery extracardiac conduit. A new form of right heart bypass. J Thorac Cardiovasc Surg 100:228–232

46. Bove EL et al. (2003) Computational fluid dynamics in the evaluation of hemodynamic performance of cavopulmonary connections after the Norwood procedure for hypoplastic left heart syndrome. J Thorac Cardiovascular Surgery 126: 1040–1047

47. Fontan F et al. (1990) Outcome after a "perfect" Fontan operation. Circulation 81: 1520–1536

48. de Leval MR *et al.* (1988) Total cavopulmonary connection: a logical alternative to atriopulmonary connection for complex Fontan operations. Experimental studies and early clinical experience. *J Thorac Cardiovasc Surg* **96:** 682–695

49. Corsini C, Cosentino D, Hsia TY, Dubini G, Pennati G, and Migliavacca F., 2010, *Computational fluid dynamics multiscale models of the TCPC circulation.* 4th Southern California Symposium on Flow Physics, Irvine.

50. Hambley, Allan. *Electrical Engineering: Principles and Applications*. 4th ed. Upper Saddle River, NJ: Pearson Education, 2008.

51. White, Frank. *Fluid Mechanics*. 5th ed. New York, NY: McGraw-Hill Higher Education, 2003.

52. Pulmonary and caval flow dynamics after total cavopulmonary connection. Houlind K, Stenbøg EV, Sørensen KE, Emmertsen K, Hansen OK, Rybro L, *Hjortdal VE.* Heart 81:67-72, 1999

53. Flow during exercise in the total cavopulmonary connection measured by MR velocity mapping. Pedersen EM, Stenbøg EV, Freünd T, Houlind K, Kromann O, Sørensen KE, Emmertsen K*, Hjortdal VE*. Heart 87: 554-558, 2002

54. Caval Blood Flow during Supine Exercise in Normal and Fontan Patients *Hjortdal VE*, Christensen TD, Larsen SH, Emmertsen K, Pedersen EM Ann Thorac Surg 2008:85(2):599-603

55. Pedersen L, Pedersen T, Pedersen EM, Hoimyr H, Emmertsen K, *Hjortdal VE* Blood flow measured by magnetic resonance at rest and exercise after surgical bypass of aortic arch obstruction. Eur J CardioThorac Surg 37 (2010), pp. 658-661

56. Harris, R. Scott. "Pressure Volume Curves of the Respiratory System." *Respiratory Care*. 50.1 (2005): 78-99.

57. T.-Y. Hsia, S. Khambadkone, A.N. Redington and M.R. de Leval. Effect of fenestration on the sub-diaphragmatic venous hemodynamics in the total-cavopulmonary connection. *Eur J Cardiothorac Surg* 2001;19:785-79.

58. Tain-Yen Hsia, Sachin Khambadkone, John E. Deanfield, James F. N. Taylor, Francesco Migliavacca and Marc R. de Leval. Subdiaphragmatic venous hemodynamics in the Fontan circulation. *J Thorac Cardiovasc Surg* 2001;121:436-447.

59. Waite, Lee, and Jerry Fine. *Applied Biofluid Mechanics*. New York, NY: McGraw-Hill, 2007.

60. Kulakowski, Bohdan, John Gardner, and J. Lowen Shearer. *Dynamic Modeling and Control of Engineering Systems*. 3rd ed. New York, NY: Cambridge University Press, 2007. 219-43.

61. Chiulli, Kathy, and Richard Chiulli. Personal Interview by John Chiulli. 05 Apr 2011. 5 Apr 2011.

62. Schievano S, Migliavacca F, Coats L, Khambadkone S, Carminati M, Wilson N, Deanfield J, Bonhoeffer P, Taylor A. Percutaneous pulmonary valve implantation based on rapid prototyping of right ventricular outflow tract and pulmonary trunk from MR data. Radiology 2007;242(2):490-497

63. Schievano S, Sebire N, Robertson N, Taylor AM, Thayyil S. Reconstruction of fetal and infant anatomy using rapid prototyping of post-mortem MR images. Insights Imaging 2010;1(4): 281-286

64. Armillotta A, Bonhoeffer P, Dubini G, Ferragina S, Migliavacca F, Sala G, Schievano S. Use of rapid prototyping models in planning of percutaneous pulmonary valved stent implantation. Proc Inst Mech Eng [H] 2007;221(4):407-416 (MED Innovations Prize)

65. Migliavacca F, Balossino R, Pennati G, Dubini G, Hsia T-Y, de Leval MR, Bove EL. Multiscale modelling in biofluidynamics: application to reconstructive paediatric cardiac surgery. Journal of Biomechanics. 39(6): 1010-1020, 2006.

66. de Zélicourt D, Pekkan K, Kitajima H, Frakes D, Yoganathan A. Single-step stereolithography of complex anatomical models for optical flow measurements. Transactions of the ASME Journal of Biomechnical Engineering 2005; 127:204-7.

67. Armillotta A, P Bonhoeffer, G Dubini, S Ferragina, F Migliavacca, G Sala, and S Schievano. "Use of rapid prototyping models in the planning of percutaneous pulmonary valved stent implantation." *IMechE: Journal of Engineering in Medicine*. 221.Part H (2007): 407-16.

68. Lagana K, R Balossino, F Migliavacca, G Pennati, E Bove, M de Leval, and G Dubini. "Multiscale modeling of the cardiovascular system: application to the study of pulmonary and coronary perfusions in the univentricular circulation." *Journal of Biomechanics*. 38. (2005): 1129-41.

69. de Zélicourt D, K Pekkan, J Parks, K Kanter, M Fogel, and A Yoganathan. "Flow study of an extracardiac connection with persistent left superior vena cava." *Journal of Thoracic and Cardiovascular Surgery*. 131.4 (2006): 785-91.

70. de Zélicourt D, K Pekkan, L Wills, K Kanter, J Forbess, S Sharma, M Fogel, and A Yoganathan. "In vitro flow analysis of a patient-specific intraatrial total cavopulmonary conection." *Ann Thoracic Surgery*. 79. (2005): 2094-102.

71. Krishnankuttyrema R, L Dasi, K Pekkan, K Sundareswaran, and M Fogel. "Quantitative analysis of extracardiac versus intraatrial Fontan anatomic geometries." *Ann Thoracic Surgery*. 85. (2008): 810-7.

72. Hsia, T.Y. "Hepatic vein flow measurements." Message to John Chiulli. 04 Mar 2011.

73. Sondergaard L, Hoschtitzky A, Hsia T-Y, Deanfield JE, de Leval MR. Respiration synchronized flow quantification in total cavopulmonary connections. Circulation Suppl. II, 102(18):II-771. Nov. 2000. The 73nd Scientific Sessions of the American Heart Association, Nov. 2000, New Orleans, LA.

74. Biglino G, Giardini A, Baker C, Schievano S., Figliola RS. Quantification of TangoPlus FullCure 930 Compliance for Printing Patient-Specific Vascular Models, 57th ASAIO Conference , Washington, DC, June 2011.